



**University of
Zurich**^{UZH}

Hyperspectral leaf spectroscopy reveals the drought response of *Fagus sylvatica* seedlings from across the species' range.

GEO 511 Master's Thesis

Author

Dave Kurath
17-704-297

Supervised by

Dr. Sofia van Moorsel

Faculty representative

Prof. Dr. Meredith Schuman

29.01.2024

Department of Geography, University of Zurich



University of
Zurich ^{UZH}

Hyperspectral leaf spectroscopy reveals the drought response of *Fagus sylvatica* seedlings from across the species' range.

GEO 511 - Master Thesis

Supervised by	Submitted by
Dr. Sofia van Moorsel	Dave Kurath
Faculty representative	Mat. Nr. 17-704-297
Prof. Dr. Meredith C. Schuman	

January 29, 2024

Spatial Genetics, Remote Sensing Labs, Department of Geography, University of Zurich

Abstract

Europe is expected to experience increased numbers and intensified summer droughts due to climate change. The common European beech (*Fagus sylvatica*) is an important native tree species with a high ecological and economical value, which is sensitive to prolonged duration of droughts and anticipated to change its natural distribution range. Here, we conducted a common garden experiment with potted 180 two-year-old seedlings from 16 beech provenances across the species' range and simulated two drought periods by discontinuing irrigation (treatment). We combined empirical approaches (spectral indices) and a physically-based radiative transfer model (PROSPECT-D) on hyperspectral leaf spectroscopy data covering visible to short-wave infrared electromagnetic radiation to determine drought induced changes in leaf biochemical and functional traits and to assess the intraspecific response diversity. Findings from this experiment suggest that (i) spectroscopy is able to discern changes of a variety of leaf traits in drought treated seedlings, that (ii) spectral variation is higher in drought treated seedlings and associated uncertainties are negligible, and that (iii) there is no evidence of intraspecific variation in the response to drought in *F. sylvatica* leaf traits as it may be masked by variation on the individual level. We demonstrated that hyperspectral leaf spectroscopy is a useful tool to assess drought responses in leaf traits but must be complemented with further analysis on population structure to study intraspecific diversity and the persistence of *F. sylvatica*.

Keywords: hyperspectral leaf spectroscopy, drought, *fagus sylvatica*, response diversity, intraspecific diversity, common garden experiment, prospect, leaf optical properties, radiative transfer model

Acknowledgements

I would like to convey my appreciation for many people who have supported me during the time of my MSc-thesis. Each person mentioned herein have been instrumental to the process and completion of this thesis. First of all, I am thankful to Sofia for her dedication in supervising my thesis and providing competent feedback. Also, I would like to extend my appreciation to Merry for her helpful guidance. I also greatly appreciate the assistance from individuals in Spatial Genetics Group and the Remote Sensing Labs.

This endeavour would not have been possible without Jolanda, who designed the experiment and collected field data with me. Big thanks also go to Tis, who assisted me extensively during laboratory work under literally dark circumstances. I wish to express my appreciation for Guido for his proficient guidance throughout the lab work. In this context, lab technicians Yves and Barbara were of indispensable support by preparing and setting up the analysis. I thank everybody who was involved during the entire experiment: Linda for looking after the seedlings, Marylaure and Ewa for collecting the seeds, Marius for helping to transport steel grids, Mike for introducing to me the spectroscopy devices as well as Maarten for explaining the porometer, Marcel for helping to bury rooibos tea bags, Simone for helping to collect data, Nicole for collecting drone footage of the experiment and Matthias for maintaining the garden parcel at Irchel. This project is funded by the NOMIS foundation and I wish to thank this organisation.

I would like to thank my friends at the university for all the inspirational lunch and coffee breaks. Last but not least, I would like to express my sincere and deepest gratitude to my girlfriend and my family, who not only made my studies possible but also emotionally and tirelessly supported me at all times.

Acronyms

ANOVA	ANalysis Of VAriances
AU	Absorption Units
BV	Biological Variation
CV	Coefficient of Variation
DAD	Diode Array Detector
DF	Degrees of Freedom
DoT	Day of Treatment
EW	Epicuticular Wax
EWT	Equivalent Water Thickness
FWHM	Full Width at Half Maximum
HPLC	High-Performance Liquid Chromatography
HSD	Honestly Significant Difference
LMA	Leaf Mass per Area
LOP	Leaf Optical Properties
LRR	Log Response Ratio
MAP	Mean Annual Precipitation
NIR	Near InfraRed domain
NPQ	Non-Photochemical Quenching
NRMSE	Normalized Root-Mean-Squared Error
PSII	Photosystem II
RMSE	Root-Mean-Square Error
ROS	Reactive Oxygen Species
RT	Retention Time
RTM	Radiative Transfer Model
RU	Relative Uncertainty
SV	Spectral Variation
SWIR	Short-Wave InfraRed domain
TDT	Time-Domain Transmission
TMS	Temperature-Moisture-Sensors
VAZ	Violaxanthin, Antheraxanthin, Zeaxanthin (xanthophyll cycle pigments)
VIS	VISible domain
VNIR	Visible and Near InfraRed domain

Symbols

A	area
C_{ab}	chlorophyll a & b content
C_{ant}	anthocyanin content
C_{car}	carotenoid content
C_{chl}	chlorophyll content
C_m	dry matter content
$C_{pigment}$	pigment content
C_w	water content
dw	dry weight
fw	fresh weight
M	SPAD-502 readings
N	leaf structure parameter (N-plates)
n	sample size
R	reflectance
R_b	reflectance of black background
R_l	leaf reflectance
R_w	reflectance of white background
R^2	coefficient of determination
S_E	standard error
T	transmittance
T_b	target reflectance with black background
T_{mean}	mean temperature
T_w	target reflectance with white background
U_{abs}	absolute uncertainty
U_{rel}	relative uncertainty
v	volume
V_b	biological variation
V_s	spectral variation
\hat{Y}	dependent response variable
α	light incidence angle
β_0	intercept
β_1	slope
λ	wavelength (nm)
σ	standard deviation
Ψ	leaf water potential

Contents

1	Introduction	1
2	Material and Methods	6
2.1	Overview	6
2.2	Experimental design	6
2.2.1	Preparation	6
2.2.2	Common garden experiment	10
2.3	Chlorophyll content measurement	13
2.4	Spectral leaf measurement	13
2.4.1	Instruments	13
2.4.2	Measurement strategy	14
2.4.3	Spectral data preprocessing	15
2.5	Leaf trait retrieval with spectral indices	16
2.6	Leaf trait retrieval with PROSPECT-D inversion	18
2.7	Measurement uncertainties and biological variation	21
2.8	Validation of the PROSPECT-D inversion	22
2.8.1	Sample selection	23
2.8.2	Sampling leaf functional traits	23
2.8.3	Sequential pigment extraction	24
2.8.4	Chromatographic separation	24
2.8.5	Identification and quantification of pigment concentration	25
2.9	Data analysis	26
2.9.1	Statistical analyses	26
2.9.2	Log response ratios	27
2.9.3	Model accuracy assessment of PROSPECT-D inversion	28
3	Results	29
3.1	Lower soil moisture in drought treatment	29
3.2	Treatment had no effect on chlorophyll measured with SPAD.	31
3.3	Treatment effects on leaf traits derived from spectral indices	32
3.3.1	Leaf pigments	32
3.3.2	Leaf water potential and water content	32
3.3.3	Biomass and epicuticular wax	33

3.4	Treatment effects on leaf traits derived from the PROSPECT-D inversion	41
3.5	Uncertainties and biological variation	44
3.5.1	Absolute measurement uncertainties were small over the whole spectrum.	44
3.5.2	Spectral variation differed throughout the measurement period and across spectral domains.	45
3.5.3	Spectral variation differed between drought-treated and control group. . .	46
3.6	Comparison between spectral indices, leaf traits and validation data	49
3.6.1	Spectrally-derived indices correlate with leaf traits from PROSPECT-D. .	49
3.6.2	Measured leaf traits have a moderate to strong relationship with leaf traits from PROSPECT-D inversion.	53
4	Discussion	55
4.1	Drought stress impact on leaf traits	55
4.2	Using field spectroscopy to capture leaf trait variation	59
4.3	Intraspecific variation in drought stress responses	60
5	Conclusion	62
A	Supplementary Materials	82
A.1	Common garden experiment block design	82
A.2	Instrument configurations	83
A.3	Drought simulation	83
A.4	Wilting depending on length and provenance during the first drought period . . .	84
A.5	Post hoc analysis	85
A.6	Validation data from pigment extraction and HPLC	86

List of Tables

2.1	Summary of <i>F. sylvatica</i> provenances including sample sizes, elevation, coordinates and date of collection. Sample size is n . Mean temperature is T_{mean} and mean annual precipitation is MAP. Both MAP and T_{mean} were downloaded from WorldClim (Hijmans et al., 2005). No stated date of collection could indicate either no available information or the seeds were collected by collaborators. Seeds started to germinate last week of February 2021.	9
2.2	Summary of spectral indices including equation, author, and year of publication. R_λ indicates reflectance at wavelength λ	19
2.3	PROSPECT-D input parameters used for the computation of leaf reflectance and they display the natural occurring variation (Jacquemoud & Ustin, 2019). The units and the range of variation are listed.	20
3.1	One-way ANOVA table on linear model with C_{chl} measured with SPAD as dependent observation and length, treatment, provenance, and the interaction treatment \times provenance as independent factors during the first drought period. Significant values are in bold ($p \leq 0.05$).	32
3.2	One-way ANOVA table on linear model with chlorophyll spectral indices as dependent observation and length, group provenance and the interaction treatment \times provenance as independent factors during the first drought period. Significant values are in bold ($p \leq 0.05$).	34
3.3	One-way ANOVA table on linear model with carotenoid spectral indices as dependent observation and length, group provenance and the interaction treatment \times provenance as independent factors during the first drought period. Significant values are in bold ($p \leq 0.05$).	34
3.4	One-way ANOVA table on linear model with anthocyanin spectral indices as dependent observation and length, group provenance and the interaction treatment \times provenance as independent factors during the first drought period. Significant values are in bold ($p \leq 0.05$).	35
3.5	One-way ANOVA table on linear model with spectral indices related to water content as dependent observation and length, drought treatment, provenance and the interaction treatment \times provenance as independent factors during the first drought period. Significant values are shown in bold ($p \leq 0.05$).	35

3.6	One-way ANOVA table on linear model with spectral indices related to biomass and wax as dependent observation and length, group provenance and the interaction treatment \times provenance as independent factors during the first drought period. Significant values are in bold ($p \leq 0.05$).	36
3.7	One-way ANOVA table on linear model with inverse modelled traits as dependent observation and length, group provenance and the interaction treatment \times provenance as independent factors during the first drought period. Significant values are in bold ($p \leq 0.05$).	42
3.8	Summary of the measured (HPLC) and simulated (PROSPECT-D) leaf traits with each whole and optimal spectra input and corresponding accuracy parameters R^2 , RMSE, NRMSE. Sample size is n , intercept is β_0 and slope is β_1 . LMA and EWT are specified in $g.cm^{-2}$ while C_{ab} and C_{ab} are specified in $\mu g.cm^{-2}$. Significance code is as followed: $p \leq 0.001$ '***', $p \leq 0.01$ '**', $p \leq 0.05$ '*'.	54
A.1	Instrument configurations for ASD FieldSpec 4 during spectra acquisition.	83
A.2	Post-hoc Tukey's honest significance difference (HSD) test performed for C_{chl} (SPAD), NDLI and NDNI (spectral indices), and EWT (PROSPECT-D), which showed significant differences in their provenances based on ANOVA. Letters (a, ab, b) represent grouping of means and same letters are not significantly different from each other. Sample size is provided in brackets.	85
A.3	Method gradient for both eluents in the HPLC analysis.	87
A.4	Retention times, estimated compound, and absorbance maxima of each peak, which were observed in a chromatogram of one sample. (*) indicates global absorption maximum.	91

List of Figures

- 1.1 A typical leaf reflectance spectrum with simplified absorption features of various leaf traits. Grey areas mark spectral domains, which are used when referring to a specific spectral range. 3
- 2.1 Adapted European map depicting sampling locations and natural distribution range of *F. sylvatica* (EUFORGEN) (Caudullo et al., 2017). The first two letters in the abbreviations are country identifiers and the third letter is the site identifier. The map was created in ArcGIS Pro (v3.1) (ESRI Inc., 2023). 8
- 2.2 Drone footage showing the experiment shortly after the first drought. Some seedlings experienced visible drought stress symptoms. 10
- 2.3 Schematic illustration of the block arrangement, where (a) depicts the seedling height distribution in each block, where each shape and color represents a provenance and (b) illustrates the two drought scenarios with each arrangement of treatment and control groups. The letters (a-i) indicate the different blocks. . . . 11
- 2.4 The design of the rain cover featuring a) fixture of the pond foil on the seedling stem before the first stem node with laboratory film, b) three wooden sticks in regular distances stuck in the soil to elevate the cover, c) inverted pot tray, and d) north direction label. 12
- 2.5 Field spectral measurement strategy. a) The plant probe with a leaf clip used in this experiment. b) Flowchart of the measurement procedures. 14
- 2.6 Timeline of the field spectral measurements. We measured each block once before the drought, during recovery and after drought. During the drought phases, we repeatedly measured each block indicated in the timeline. Start of treatment indicate the day of installation of the cover. Day of treatment (DoT) indicates the number of days from the first application of the rain covers. 15
- 2.7 Flowchart of the retrieval of leaf traits with the PROSPECT-D inversion. 18
- 2.8 Flowchart of the validation of the PROSPECT-D inversion with sequential extraction and subsequent analysis. 22
- 3.1 Time series of a seedling (CHL) during the first drought simulation. The difference between each photograph is 3 days, with increasing number of rain-free days from left to right. 30
- 3.2 Time series of a seedling (BES) during the first drought simulation. There are no visual drought symptoms despite it undergoing drought treatment. 30

3.3	Weather conditions and soil moisture during the experiment. a) Soil moisture of control and treatment group specified in raw uncalibrated time-domain transmission (TDT) values and precipitation measured with the ATMOS 41. b) Temperature inside the covers measured by TMS-4, mean air temperature and relative humidity measured by ATMOS 41. Dashed lines indicate start and end of the drought periods.	30
3.4	Length of the seedlings measured before the first drought period against mean soil moisture values expressed as raw TDT values for treatment and control group. There was a negative association between soil moisture and tree length in both treatment ($R^2 = 0.420$) and control group ($R^2 = 0.521$).	31
3.5	Converted C_{chl} from SPAD values in treatment and control group during the first drought period.	31
3.6	The distribution of a) chlorophyll, b) carotenoid, and c) anthocyanin indices in treatment and control group during the first drought period. ANOVA significance code is as followed: $p \leq 0.001$ '***', $p \leq 0.01$ '**', $p \leq 0.05$ '*'.	37
3.7	The distribution of a) water potential index, b) water content indices, c) biomass indices, and d) wax index in treatment and control group during the first drought period. ANOVA significance code is as followed: $p \leq 0.001$ '***', $p \leq 0.01$ '**', $p \leq 0.05$ '*', $p \leq 0.1$ '.'.	38
3.8	a-h) LRRs during the first drought period for indices related to pigments (n=170). a-c) LRRs of indices related to chlorophyll, d-f) LRRs of indices related to carotenoids and g-h) LRRs of indices related to anthocyanin. Y-axis represents provenances arranged in ascending order of mean annual precipitation. X-axis are effect sizes $\pm 1\sigma$ (LRR).	39
3.9	a-d) LRRs during the first drought period of indices related to water potential and water content (n=170). a) LRRs of index related to moisture stress, b-c) LRRs of indices related to water content and d) LRRs of index related to water potential. Y-axis represents provenances arranged in ascending order of mean annual precipitation. X-axis are effect sizes $\pm 1\sigma$ (LRR).	40
3.10	a-d) LRRs of indices related to biomass and e) LRRs of index related to epicuticular wax (n=170). Y-axis represents provenances arranged in ascending order of mean annual precipitation. X-axis are effect sizes $\pm 1\sigma$ (LRR).	40
3.11	The distribution of PROSPECT-D inverse modelled leaf traits in treatment and control group during the first drought period. ANOVA significance code is as followed: $p \leq 0.001$ '***', $p \leq 0.01$ '**', $p \leq 0.05$ '*'.	43
3.12	The distribution of C_{ab}/C_{car} in treatment and control group during the first drought period. ANOVA significance code is as followed: $p \leq 0.001$ '***', $p \leq 0.01$ '**', $p \leq 0.05$ '*'.	43

3.13 a-f) LRRs during the first drought period for PROSPECT-D inverse modelled leaf traits (n=170). a-d) LRRs of pigment content, e) of EWT, and f) of LMA. Y-axis represents provenances arranged in ascending order of mean annual precipitation. X-axis are effect sizes $\pm 1\sigma$ (LRR).	44
3.14 Absolute uncertainties of the field spectrometer readings (n=1317) over the whole spectral range of 350 to 2500 nm. The spectral data from 350 to 400 nm were discarded due to high uncertainty. *Dashed line indicates $\mu = 400$ nm.	45
3.15 a-d) Spectral variation (SV) over the measurement period. a) SV over the entire measurement period (n=54) and SV for each b) June (n=18), c) July (n=18) and d) September (n=18). e-h) Biological variation (BV) and relative uncertainty (RU) over the entire measurement period. e) BV over the measurement period (n=54) and BV for each f) June (n=18), g) July (n=18) and h) September (n=18).	46
3.16 a-d) SV, BV and RU of the first drought period and e-l) SV, BV and RU of the second drought period. a-b) SV of each control (n=90) and treatment group (n=90) and c-d) BV and RU of control (n=90) and treatment (n=90) group. e-h) SV of each treatment group: control-control (CC) (n=18), control-treatment (CT) (n=72), treatment-control (TC) (n=18), treatment-treatment (TT) (n=72). i-l) BV and RU of each group: control-control (CC) (n=18), control-treatment (CT) (n=72), treatment-control (TC) (n=18), treatment-treatment (TT) (n=72).	48
3.17 a) C_{chl} from SPAD and chlorophyll related indices (NDSR, ChlNDI, Clre) against C_{ab} from PROSPECT-D. $R^2 (C_{chl}) = 0.488$, $R^2 (NDSR) = 0.118$, $R^2 (ChlNDI) = 0.962$, $R^2 (Clre) = 0.979$. b) Water potential (WABI) and water content related indices (NDWI, WI, MSI) against EWT from PROSPECT-D. $R^2 (NDWI) = 0.320$, $R^2 (WI) = 0.356$, $R^2 (MSI) = 0.781$, $R^2 (WABI) = 0.003$	50
3.17 (Continued). c) NDLMA index against LMA from PROSPECT-D. $R^2 (NDLMA) = 0.286$. d) Anthocyanin related indices (RGR, ARI) from before and after the drought periods against C_{ant} from PROSPECT-D. $R^2 (RGR (Pre)) = 0.294$, $R^2 (RGR (After)) = 0.665$, $R^2 (ARI (Pre)) = 0.547$, $R^2 (ARI (After)) = 0.864$	51
3.17 (Continued). e) Carotenoid related index (CARI) from before and after the drought periods against C_{car} from PROSPECT-D. $R^2 (CARI (Pre)) = 0.325$, $R^2 (CARI (After)) = 0.574$. f) Carotenoid related indices (CCI, PRI) from before and after the drought periods against C_{ab}/C_{car} derived from PROSPECT-D. $R^2 (CCI (Pre)) = 0.133$, $R^2 (CCI (After)) = 0.003$, $R^2 (PRI (Pre)) = 0.796$, $R^2 (PRI (After)) = 0.461$	52
3.18 Linear regression of measured (a) EWT, (b) LMA, (c) C_{ab} , and (d) C_{car} against their simulated values from PROSPECT-D inversion over the whole and optimal spectrum.	53
A.1 Randomized representative block design with provenances for the common garden experiment and location of TMS-4 sensors. North arrow indicates north direction.	82

A.2	Photos of visual drought symptoms photographed during the first drought period. Such symptoms include wilting and bleaching of the leaves.	83
A.3	Side view and bird's-eye view of the seedling with rain cover used to simulate the drought.	84
A.4	The length distribution of the seedlings (n=180) depending on provenances. Scatter points display the length value coloured by their corresponding wilting index value. The wilting indices do not show a specific pattern across the provenances and across lengths.	84
A.5	3D-cube plot depicting indices related to anthocyanin (RGR), chlorophyll (NDSR) and carotenoids (PRI), which were used for the selection of validation samples. Each color illustrates samples belonging to one of the five k-means clusters. The opaqueness of the data points display depth.	86
A.6	Leaf area estimation in ImageJ using the point tool and a known distance scale. .	86
A.7	Calibration curves from standards for the determination of pigment concentration including regression function and accuracy.	87
A.8	Pigment standards spectra with absorption maxima used for the identification of pigments. Note that lutein and xanthophyll are the same compound. Our xanthophyll standard was extracted from marigold and lutein was synthesized. . .	88
A.9	Spectra of pheophytin a and b sampled from a chromatogram when identifying unknown pigments.	88
A.10	Chromatogram of <i>Long red</i> special variety with corresponding wavelengths: 450 nm, 550 nm and 665 nm. <i>Long red</i> has seemingly high anthocyanin contents and are separable using the applied method.	89
A.11	Chromatogram of two leaf samples. Top: drought-treated leaf sample, bottom: control leaf sample. Y-axis depicts dimensionless absorption values and do not correspond to an absolute amount.	90

List of Equations

2.1	Polynomial transformation to estimate chlorophyll content with M	13
2.2	Mean of all scans per leaf	16
2.3	Set of i for R	16
2.4	Calculation of sample reflectance R_l per leaf measurement	16
2.5	Linear model to estimate leaf structure parameter N	20
2.6	Parameters to be estimated in the PROSPECT-D inversion	20
2.7	List of initial values for the inversion in PROSPECT-D	21
2.8	Calculation of absolute uncertainty U_{abs,R_l} of associated spectrum of a sample . .	21
2.9	Calculation of relative uncertainty U_{rel,R_l} of associated spectrum of a sample . . .	21
2.10	Calculation of spectral variation V_s	21
2.11	Calculation of biological variation V_b	22
2.12	Calculation of leaf mass per area (LMA)	23
2.13	Calculation of equivalent water thickness (EWT)	23
2.14	Normalization of pigment content per leaf area after peak integration from chromatograms	26
2.15	Formula used for $lm()$ and $anova()$	26
2.16	Equation for regression model	26
2.17	Calculation of log response ratios (LRRs)	27
2.18	Calculation of LRRS for series of negative values	27
2.19	Calculation of standard error S_E of LRR	27

Chapter 1

Introduction

Due to climate change, Europe will experience prolonged drought periods, which will threaten forest ecosystems and accelerate biodiversity loss (Cook et al., 2016; IPCC, 2023). These phenomena are caused by extended duration of local precipitation deficits and thus increase the risk of water stress and mortality for trees (Allen et al., 2010). A series of recent record-breaking summers in Northern Europe in 2003, 2018 and 2022 may only be the start of what is to come for Europe's forest ecosystems (Buras et al., 2020; Hermann et al., 2023; Millán, 2014; Sturm et al., 2022). To persist in these novel environments, sessile organisms such as trees, rely on phenotypic variation, i.e. the capacity to express diverse phenotypes in varying environmental conditions (Arnold et al., 2019; Benito Garzón et al., 2019; Whitman & Ananthakrishnan, 2009). There has been a significant amount of research aimed at understanding the role of intraspecific variation, which captures the diversity of phenotypes, in tree responses to droughts (e.g. *Fagus sylvatica*; Alvarez-Maldini et al., 2020; Baudis et al., 2014; Carsjens et al., 2014; Coccozza et al., 2016; Dounavi et al., 2016; González De Andrés et al., 2021; Leuschner, 2020; Schmeddes et al., 2023; Thom et al., 2023; Wang et al., 2021) to improve decision-making in forest management and enhance forest resilience to climate change.

The common European beech (*Fagus sylvatica*) is a dominant and widespread tree species native to many temperate European forests (Durrant et al., 2016) and is particularly sensitive to water deficit (Betsch et al., 2011; Leuschner, 2020; Walthert et al., 2021). Beech faces a disproportionate risk of habitat loss and growth decline, and may ultimately change its natural distribution on account of their reduced competitiveness (Aranda et al., 2015; Dittmar et al., 2003; Geßler et al., 2006; Kreyling et al., 2014; Leuschner, 2020; Martinez del Castillo et al., 2022; Rigling et al., 2019; Rose et al., 2009; Schmied et al., 2023). Due to their high potential to adapt to changing environments, they are regarded as a typical model late-successional tree species used for studying phenotypic diversity (Coccozza et al., 2016; Pluess et al., 2016).

Acclimation of trees to drought occur with a myriad of responses underpinned by an array of physiological adjustments and adaptations in leaf traits (Leuzinger et al., 2005; Pflug et al., 2018;

Rukh et al., 2023; Tognetti et al., 1995). As an immediate response, for example, plants close their stomata to prevent hydraulic failure. Long-term responses include photo-protection mechanisms such as increased ratio of xanthophyll cycle pigments (VAZ) to chlorophylls. Drought-stressed plants also show reversible down regulation of photosystem II (PSII), which results in a decrease of quantum yield and photosynthetic efficiency (Gallé & Feller, 2007; García-Plazaola & Becerril, 2000). Increasing carotenoid contents is another mechanism to respond to drought stress in plants to protect their photosynthetic apparatus (Baccari et al., 2020; Bacelar et al., 2007; Ben Abdallah et al., 2017).

Drought stress symptoms and acclimation are best understood by adopting interdisciplinary and multi-level analysis ranging from molecular to ecosystem levels (Leuschner, 2020; Rigling et al., 2019). Photosynthetic pigments such as chlorophyll *a* and *b* C_{ab} are key molecules involved in oxygenic photosynthesis by absorbing light and by initiating a series of biochemical reactions. Water deficits can degrade chlorophyll contents along with a decrease in photosynthetic capacity (Gai et al., 2023; Hu et al., 2023; Mafakheri et al., 2010; Wu et al., 2016). Carotenoids C_{car} , which consist of xanthophylls and carotenes, contribute to photosynthesis as accessory light-harvesting pigments and constitute the main photoprotective mechanism by their involvement in light absorption and their role as antioxidants removing reactive oxygen species (ROS) (Havaux, 2014; Sun et al., 2022). Thus, variation in total chlorophyll to carotenoid ratio C_{ab}/C_{car} may be a good indicator for drought stress in plants (Green & Durnford, 1996). Anthocyanins C_{ant} , which are responsible for the red coloration in senescent leaves, act as antioxidants and safeguard from environmental stressors as well (Gould, 2004). Drought stress increases the level of ROS inducing oxidative stress which which was observed to lead to higher anthocyanin accumulation (Li & Ahammed, 2023).

Water fluxes in *F. sylvatica* are strongly influenced by water availability and scarcity, which can lead to a decline in overall water content within the leaves (Betsch et al., 2011). Equivalent water thickness (EWT) is a mass of water content per leaf area and relates to drought resistance, photosynthetic activity and stomatal conductance (Lawlor & Cornic, 2002). Leaf water potential Ψ is also a major indicator for plant water stress, since it includes all energy gradients that move water such as turgor, osmotic and matrix potential. Quantitative thresholds of Ψ in *F. sylvatica* indicate various stress levels and different down regulations of physiological processes as Ψ decreases with progressing drought (Walthert et al., 2021). Another important leaf trait is the leaf mass per area (LMA) and is comparable to leaf dry mass composed of several constituents such as starch, sugars, and proteins. It is one of the most meaningful leaf trait used in ecological research as it is part of the leaf economic spectrum and connected to abiotic responses such as drought (De La Riva et al., 2016; Quero et al., 2006; Wellstein et al., 2017; Wright et al., 2004). However, a sudden withholding of water does not yield variation as the leaf structure hardly had time to change (Poorter et al., 2009). Other leaf structural traits are subject to drought responses: Lignin and cellulose, which are both found in the cell walls of plant and responsible for the overall stability of plant cells. Lignin biosynthesis in leaves is upregulated (Brinkmann

et al., 2003; Hu et al., 2009; Liu et al., 2018) while cellulose biosynthesis is down regulated due to limited availability of carbon (Hu et al., 2022).

Traditional techniques to characterize drought stress responses in plants include the measurement of gas exchange (e.g. photosynthesis systems) (Saathoff & Welles, 2021), leaf water potential such as the Scholander pressure chamber (Scholander et al., 1965), fluorescence (e.g. quenching analysis) (Maxwell & Johnson, 2000), and biochemical measurements. Determination of biochemical profiles commonly requires destructive sampling and wet chemistry analysis (e.g. HPLC, photometry) (Jacquemoud et al., 1996; Pflug et al., 2018). These are usually precise but time-consuming, logistically laborious and costly (Burnett et al., 2021b). Alternatively, remote sensing techniques such as portable hyperspectral field spectroscopy devices offer a relatively cost-effective, non-destructive and rapid solution for retrieving leaf traits (Féret et al., 2019; Jacquemoud & Baret, 1990). Spectroscopy on individual leaves, which is usually coupled with a leaf clip, exploits leaf optical properties (LOP), which describe how leaves physically interact with light. Since the biochemical and structural composition of the leaves determine how light reflects (Figure 1.1), transmits or is absorbed, the variation in LOP thus carries information about leaf traits across space and time (Cavender-Bares et al., 2017; Garonna et al., 2016; Jacquemoud & Ustin, 2019). Consequently, there is a growing body of literature in linking spectra to plant phenotypes and therefore plant trait variation (Cavender-Bares et al., 2016; Czyż et al., 2020; D’Odorico et al., 2023; Li et al., 2023).

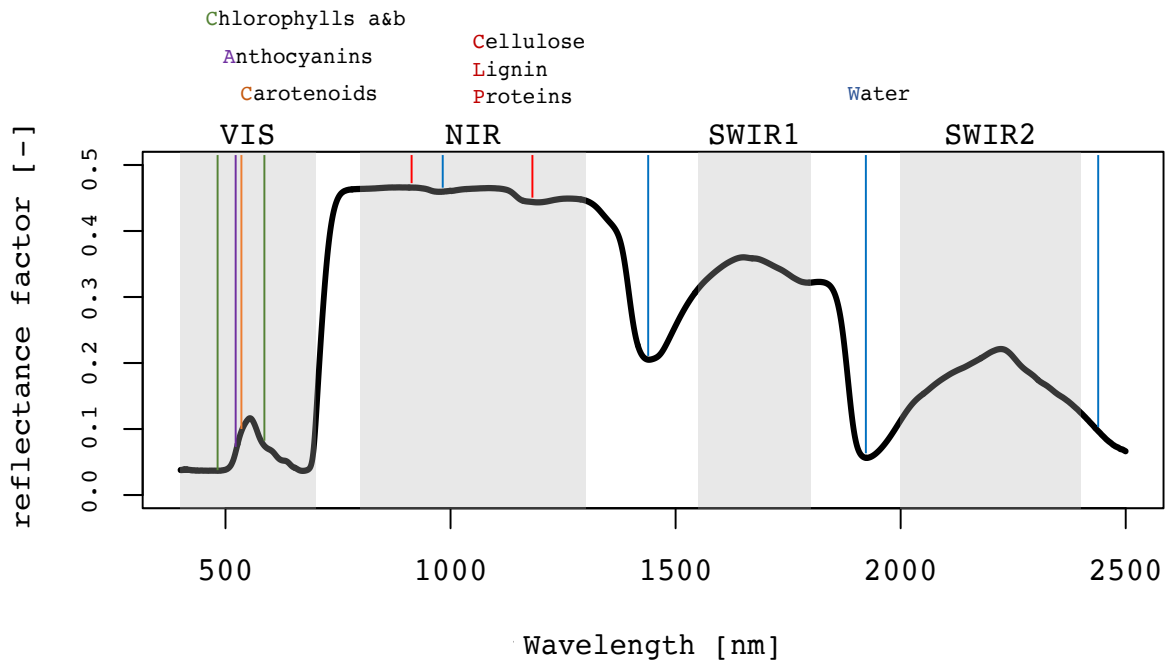


Figure 1.1: A typical leaf reflectance spectrum with simplified absorption features of various leaf traits. Grey areas mark spectral domains, which are used when referring to a specific spectral range.

Two main approaches exist for the estimation of leaf traits using leaf spectra, namely empirical and physically-based approaches (Féret et al., 2017). An empirical approach to derive leaf traits from spectral data is to combine reflectance values at different narrow bands, which are called spectral indices. This method relies on identifying two or more wavelengths in which the target of interest causes a relative absorption difference (Jacquemoud & Ustin, 2019; Verrelst et al., 2015). Other data-driven approaches are multivariate statistical models such as partial least squared regression (Burnett et al., 2021a) or machine learning (Féret et al., 2019). These approaches rely heavily on training data, which also depend on the quality of the data, and thus lack the ability for generalisation across species or sites. Nevertheless, indices have shown promising results in estimating relative abundance of traits such as photosynthetic activity (Gamon et al., 2016) and are computationally very efficient (Jacquemoud & Ustin, 2019). Physically-based approaches include radiative transfer models (RTMs) such as the extensively used open-source model propriétés spectrales (PROSPECT) (Boren et al., 2019; Jacquemoud & Baret, 1990; Jacquemoud & Ustin, 2019). The PROSPECT RTM relies on the physical properties of light interaction with matter such as absorption and scattering coefficients and is thus theoretically robust (Feret et al., 2008). In PROSPECT, leaves are represented as a generalized plate model with uniform layers (specifically air – cell wall interfaces) quantified with a structure parameter N (Allen et al., 1969; Spafford et al., 2021; Stokes, 1860), with which directional-hemispherical reflectance and transmittance between 400 nm and 2500 nm are simulated (Schaepman-Strub et al., 2006). One of the most recent PROSPECT developments is called PROSPECT-D(-ynamic). It allows C_{ab} , C_{car} , C_{ant} , brown pigments, N , EWT, and LMA as leaf trait parameter inputs to simulate leaf or canopy level spectral profiles, and it outperforms previous versions (Feret et al., 2008; Féret et al., 2017). The inversion of PROSPECT-D enables the retrieval of such leaf traits based on provided reflectance or transmittance. The inversion makes use of optimization algorithms with corresponding merit function (Jacquemoud et al., 1996; Tarantola, 2005). PROSPECT RTMs have been successfully applied across remote sensing and plant ecology research (Asner et al., 2014; Kothari & Schweiger, 2022; Serbin et al., 2014; Sun et al., 2018b; Zhao et al., 2014).

Common garden experiments are suitable to assess the plant trait responses to changing environmental conditions (Kreyling et al., 2014; Ramírez-Valiente et al., 2022; Rose et al., 2009; Schwinning et al., 2022; Stojnić et al., 2015). To study the intraspecific drought response of *F. sylvatica*, we thus conducted a common garden experiment on 180 two-year-old seedlings originating from 16 different provenances across the species’ range. Within one growing season, we simulated two drought periods by controlling for rain-free days with a duration of 14 days in early and late summer with an intermittent recovery period. We measured leaf reflectances with a field spectroradiometer before, during and after the drought periods to quantify spectral variation and derive leaf traits using both an empirical (spectral indices) and physically-based approach (PROSPECT-D inversion). In total, we computed 17 different indices and derived 6 different traits from PROSPECT-D. We also quantified chlorophyll content with SPAD measurements.

Following the recommendations of Petibon et al. (2021), we quantified reflectance associated uncertainties and biological variation of the spectral variation and validated the PROSPECT-D inversion with a novel sequential extraction and subsequent reversed-phase high-performance liquid chromatography (HPLC) method by Petibon and Wiesenberg (2022). In this thesis, we explored to what extent hyperspectral spectroscopy allows the detection of intraspecific drought stress responses in leaves. Specifically, we hypothesized that (i) drought-treated seedlings show different responses in spectral indices and simulated leaf traits compared to the control group. We anticipated that (ii) the biological variation is higher in drought-treated seedlings compared to their control group and (iii) relative uncertainty in the spectral variation remains negligible. We further aimed to test (iv) whether PROSPECT-D offers a robust quantification of leaf traits under simulated drought. Eventually, we hypothesized that (v) there is intraspecific variation in drought responses depending on the seedling's provenances aiming to identify the magnitude of the leaf trait responses to drought. Within the scope of this thesis, we were not able to conduct an extensive analysis on the intermittent recovery period and the second drought period to study adaptability and legacy effects.

Chapter 2

Material and Methods

2.1 Overview

To understand intraspecific drought responses using spectroscopy data and answer our hypotheses, we conducted a common garden experiment in one growing season. We simulated two drought periods each with a duration of 14 days. We had 180 *F. sylvatica* seedlings from 16 provenances arranged in a representative block design and we separated them into control and treatment group. To simulate the drought, we applied rain covers to control for irrigation (Section 2.2). During the experiment, we conducted several continuous measurements such as chlorophyll content (Section 2.3) and leaf spectral data with a field spectroradiometer (Section 2.4). The spectral data were then used to derive leaf traits using either indices (Section 2.5) or PROSPECT-D in inverse mode (Section 2.6) to then quantify differences in the response between the groups and provenances. Furthermore, we calculated the associated uncertainties of the spectral data and computed the biological variation (Section 2.7). We assessed the PROSPECT-D inversion with a validation dataset from extracted leaf traits with an extraction protocol (Section 2.8). Eventually, we conducted the data analysis with a one-way ANOVA and log response ratios of the first drought period, and a model accuracy assessment of the PROSPECT-D inversion (Section 2.9).

2.2 Experimental design

2.2.1 Preparation

2.2.1.1 Seed collection

The seeds were collected between 2020 and 2021. That year was a mast year, which typically occur in cycles of two- to five-year intervals (Drobyshv et al., 2010). The majority of seeds was sampled directly off the branches, since healthy and fertile seeds are frequently eaten or infested

by pathogens. We also conducted bulk sampling from the ground, however, when conditions were suitable. Seeds that appeared to be infertile were identified and removed. The seeds were released from the nuts and then stored in closed plastic bags sealed in plastic buckets to minimize the risk of cross contamination (de La Harpe & Schuman, 2021). The sampling campaign consisted of two field sampling batches and one per-post batch. The first batch consisted of populations from Italy (ITB, ITE, ITM), Belgium (BES) and France (FRM), while the second batch consisted of populations from Poland (PLB, PLW), Serbia (RSF), Croatia (HRP), Slovenia (SLK) and southern France (FRB). The third batch (Bosnia (HBV) and Romania (ROS)) was shipped in paper envelopes. Seeds from Switzerland (CHL) and Spain (ESM, ESP) were collected separately (de La Harpe & Schuman, 2021).

2.2.1.2 Drying and storage

The seeds were placed in boxes with nitrogen inlets and carefully monitored for moisture and temperature levels during the drying process. Worm larvae were removed, and mouldy seeds were washed with ethanol. Once dried, the seeds were preserved in hermetically sealed plastic bags and stowed in the refrigerator at 4°C to 5°C for a maximum of two months (de La Harpe & Schuman, 2021).

2.2.1.3 Germination

The seeds were sowed in a tree nursery in December 2020 and germinated in February 2021. Some seeds were rehydrated with water 24 hours in advance of the actual planting. The selected seeds were sowed in humus and wood chips mixed soils with no additional fertilizers, where a maximum of four seeds was put into a 5x5x20 cm pot. A wire grid was installed over the aligned pots and the flats were put outside and exposed to the environment. Additionally, damages to the dicotyledons were mitigated by bringing them inside a closed shelter when overnight temperatures outside descended to sub-zero temperatures (de La Harpe & Schuman, 2021).

2.2.1.4 Seedling care and cultivation

In October 2021 the seedlings were transported to the Hauenstein garden center in Rafz, Zurich, Switzerland (47°36'36"N, 8°32'35"E). The living individuals were transplanted into tall 4-liter pots filled with equally proportioned mixture of peat-free potting soil and low-organic matter sandy soil. The potting soil was enriched with Osmocote Exact Standard NPK (Mg) 12-14M (ICL Group, Tel Aviv-Jaffa, Israel) with micro-nutrients as fertilizer. The fertilizer contains 15% total nitrogen (N), 8% phosphorus pentoxide (P_2O_5), 11% potassium oxide (K_2O) and 2% total magnesium oxide (MgO) among other nutrients, which are composed of key elements for plants (ICL-SF, 2023). During the winter, the seedlings were in a winter tunnel, where the temperatures were maintained at circa 7°C. The seedlings were watered by an overhead

irrigation system as needed by assessment of soil moisture in the first one centimetre layer. Furthermore, Multikraft BB Start (Multikraft, Pichl/Wels, Austria) was used to treat the soil with ectomycorrhizal fungi. Inoculated effective microorganisms in the soil help to improve plant growth and root development (Joshi et al., 2019). This treatment was applied three times – once in the beginning, once after some weeks and again in the spring approximately during budburst. Once it was determined that the seedlings were no longer at risk of frost damage, the pots were moved outside the winter tunnel (de La Harpe & Schuman, 2021).

North direction was marked for each pot to ensure consistent sun exposure. In case of aphids, we sprayed NeemAzal-T/S (Andermatt Biogarten, Grossdietwil, Luzern, Switzerland) with a concentration of 3 ml/l in water directly onto the abaxial side of the leaf. This was repeated several times ad hoc under monitoring of the infestation. We conducted our experiment when the seedlings reached the age of 2 years. A total of 180 seedlings from 16 provenances across the natural distribution range (Figure 2.1 and Table 2.1) was considered in this experiment.

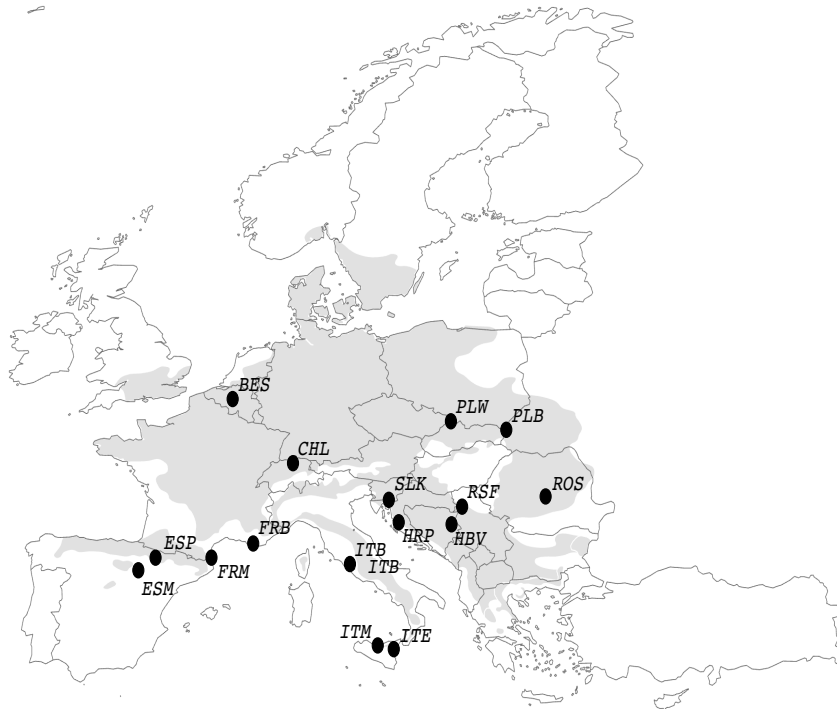


Figure 2.1: Adapted European map depicting sampling locations and natural distribution range of *F. sylvatica* (EUFORGEN) (Caudullo et al., 2017). The first two letters in the abbreviations are country identifiers and the third letter is the site identifier. The map was created in ArcGIS Pro (v3.1) (ESRI Inc., 2023).

Table 2.1: Summary of *F. sylvatica* provenances including sample sizes, elevation, coordinates and date of collection. Sample size is n . Mean temperature is T_{mean} and mean annual precipitation is MAP. Both MAP and T_{mean} were downloaded from WorldClim (Hijmans et al., 2005). No stated date of collection could indicate either no available information or the seeds were collected by collaborators. Seeds started to germinate last week of February 2021.

Label	Country	Locality	n	Lat./Lon.	Elevation (m.a.s.l.)	T_{mean} (°C)	MAP (mm)	Collection date
BES	Belgium	Zonian Forest	11	50.751/4.423	168	10.16	805	02.09.2020
CHL	Switzerland	Laegern	8	47.479/8.364	733	9.21	1137	07.08.2020
ESM	Spain	Moncayo	11	41.791/-1.810	1479	9.88	556	23.09.2020
ESP	Spain	San Juan de la Pena	31	42.508/-0.676	1200	10.88	720	24.09.2020
FRB	France	Sainte Baume	24	43.328/5.769	950	13.56	715	19.09.2020
FRM	France	Massane	6	42.491/3.032	722	14.20	604	25.08.2020
HBV	Bosnia	Vlasnica	9	44.168/18.919	1050	10.60	1216	-
HRP	Croatia	Paklenica National Park	18	44.360/15.467	924	7.82	1267	16.09.2020
ITB	Italy	Bracciano	2	42.174/12.156	584	13.70	234	21.08.2020
ITE	Italy	Etna	2	37.709/15.045	1721	11.41	699	17.08.2020
ITM	Italy	Madonie Park	2	14.042/37.858	1711	13.46	567	-
PLB	Poland	Bieszczadzski Park	2	49.232/22.472	893	6.01	933	11.09.2020
PLW	Poland	Wisla	19	49.669/18.860	662	7.19	925	09.09.2020
ROS	Romania	Sinca	8	45.654/25.164	865	9.80	1182	-
RSF	Serbia	Fruška Gora National Park	9	45.138/19.636	474	11.09	645	-
SLK	Slovenia	Pragozd Krokar	18	45.543/14.763	1178	7.71	1464	-
Total			180					

2.2.2 Common garden experiment

The seedlings were transported to the experiment site at the University of Zurich, Zurich, Switzerland (47°23'44"N, 8°33'05"E; elevation 509 m.a.s.l.). We implemented a 2 x 5 randomized block arrangement, in which each block formed a 3 x 6 grid (1.2 m x 1.4 m). Therefore, a block contained a total of 18 seedlings, which were placed in the slots of the steel grid with maximising distances to each other. Each block had a spacing of approximately 1 m to each block to avoid interaction between the blocks. Furthermore, the experiment was placed on black polypropylene fabric (MyPex) for weed control and the pots were stabilized to the steel grid with hemp cord (Figure 2.2). We installed an all-in-one weather station ATMOS 41 (METER Group, Pullman, WA United States) to measure local weather conditions such as precipitation, humidity and air temperature.

We employed a balanced approach between randomization and representation. We maximized the diversity of provenances within the blocks so each provenance is represented whenever possible. The placement of the seedling and the individuals within the blocks are randomized (Figure A.1). We measured the length of the primary shoot using a flexible tape measure from root collar to the highest point in its natural position. The distribution of seedling heights within the experiment was also accounted for by decreasing the discrepancies in heights between the blocks (Figure 2.3a).

For the two drought periods, we installed a different pair-wise control and treatment group arrangement. The groups in the first drought period were categorized into control (C) and treatment group (T) with equal sample sizes and the groups in the second drought period were categorized into four groups based on their previous group assignment: control-control (CC), control-treatment (CT), treatment-control (TC) and treatment-treatment (TT) with varying sample sizes (Figure 2.3b).



Figure 2.2: Drone footage showing the experiment shortly after the first drought. Some seedlings experienced visible drought stress symptoms.

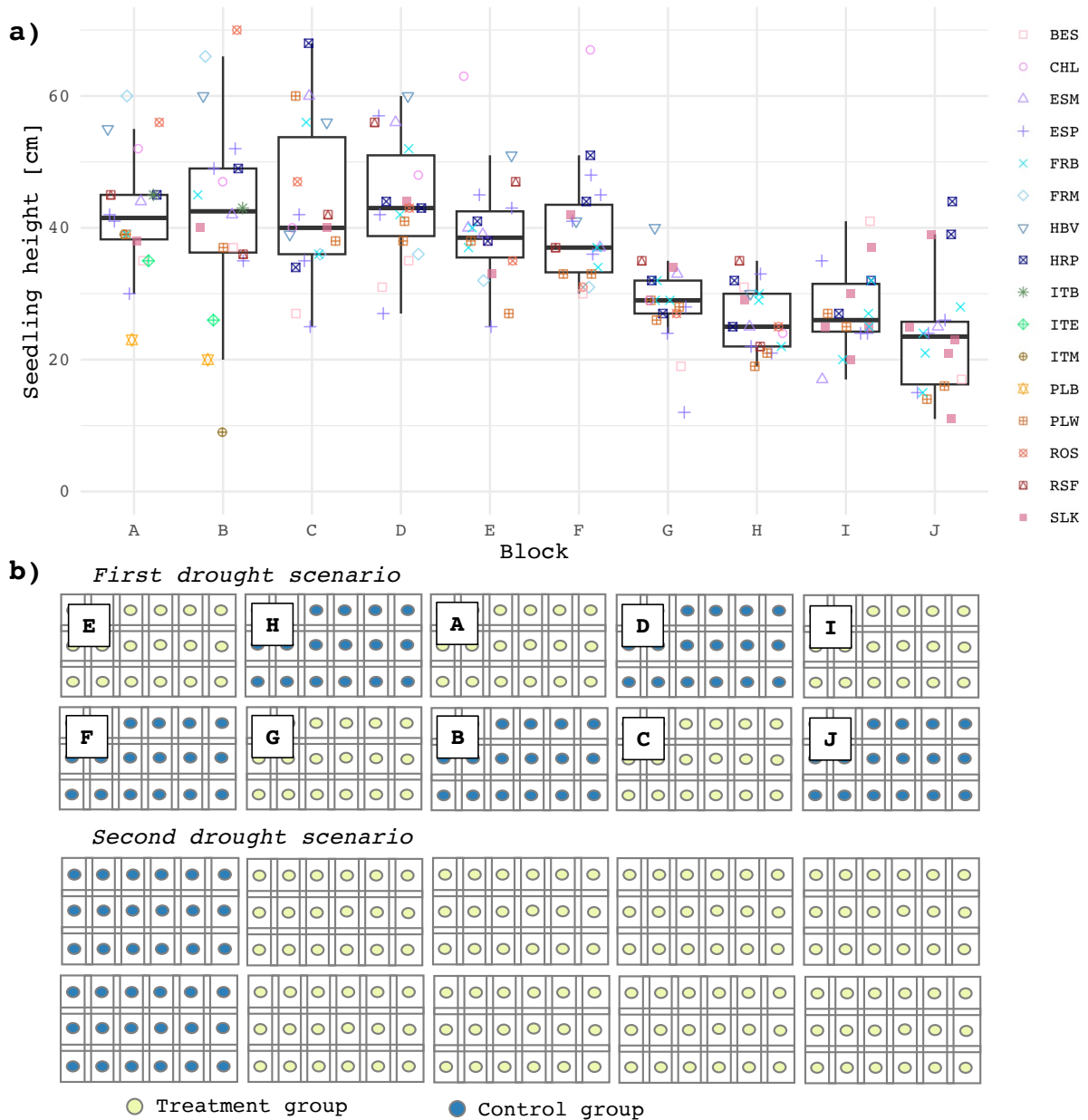


Figure 2.3: Schematic illustration of the block arrangement, where (a) depicts the seedling height distribution in each block, where each shape and color represents a provenance and (b) illustrates the two drought scenarios with each arrangement of treatment and control groups. The letters (a-i) indicate the different blocks.

2.2.2.1 Drought treatment

We carried out two drought scenarios, each for a duration of 14 days. We selected a duration of two weeks because Switzerland encounters an average of 11 consecutive rain-free days each year and it is anticipated that these dry periods may extend to as many as 19 days in the mid-term future (NCCS, 2018). During the drought periods the treatment group experienced rain-free days, whereas the control group was given plenty of water at regular intervals. We further implemented a 23-day-long recovery period with regular irrigation of all seedlings between the

two drought periods (Figure 2.6).

To simulate the rain-free days, we installed cone-shaped rain covers, which enclosed the entire pot. We installed the covers on both pots of the control and the treatment group, which allowed us to control for irrigation in both groups. Each cover had a diameter of 18 cm and a thickness of 0.5 mm, and was made of waterproof and UV-resistant PVC black pond foil (Heissner GmbH, Lauterbach, Hessen, Germany). The covers were fixed on the seedling stem with Parafilm (Pechiney Plastic Packaging Inc., Chicago, IL, United States) before the first stem node. Three thin wooden sticks were used to elevate the cover to leave a gap between the foil and the pot to enable air circulation. In addition, we inverted the pot trays in the treatment group to avoid the retention of water in the soil through capillary effects (Figure 2.4 and Figure A.3).

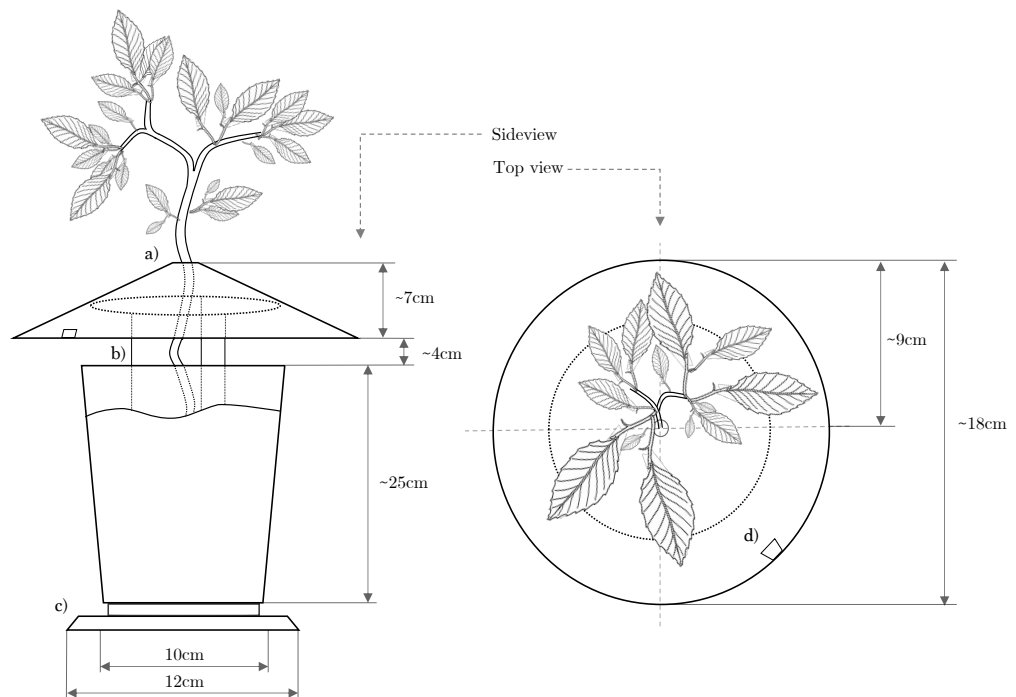


Figure 2.4: The design of the rain cover featuring a) fixture of the pond foil on the seedling stem before the first stem node with laboratory film, b) three wooden sticks in regular distances stuck in the soil to elevate the cover, c) inverted pot tray, and d) north direction label.

We prioritised tree survival by ad hoc irrigation of the drought-treated seedlings. When severe wilting was observed, we watered the seedlings with 600 ml water. Wilting was daily monitored and quantified by a wilting index. The wilting index, ranging from 0 to 4, was categorized into quartiles. A score of 0 denoted the absence of wilting, while scores 1-4 indicated wilting levels corresponding to $\leq 25\%$, $> 25\%$ to $\leq 50\%$, $> 50\%$ to $\leq 75\%$, and $> 75\%$ of leaves per seedlings respectively. Our aim was to avoid score 4, as such severe wilting would likely lead to seedling mortality.

To monitor soil moisture and air temperature, we selectively installed 20 TMS-4 probes (TOMST, Prag, Czech Republic) (Wild et al., 2019) in the pots from block A to F. The probes covered as many provenances as possible while capturing the entire range of plant heights within a single block (Figure A.1). The soil moisture and temperature were sampled in an interval of 15 minutes during the entire experiment.

2.3 Chlorophyll content measurement

For fast and repeated estimation of leaf chlorophyll content, we used a non-invasive hand-held chlorophyll meter SPAD-502 (Konica Minolta, Tokyo, Japan). The device is based on dual-wavelength absorbance which measures the transmittance of red (600 nm) and NIR (940 nm) and returns a relative value, which corresponds to the present chlorophyll or "greenness" in the leaf. We measured all seedlings across the whole growing season and during the two drought periods. We measured for each seedling a top, middle and bottom leaf to ensure a good representation. We measured adaxially and avoided any major leaf veins and took the mean of the three leaves per seedling.

SPAD readings are dimensionless values M and can be transformed to absolute chlorophyll exploiting their empirical relationships. Markwell et al. (1995) established non-linear relationships ($R^2 = 0.94$) of M with chlorophyll in maize and soybean leaves. To estimate the chlorophyll content C_{chl} in our samples, we adapted the polynomial transformation proposed by Markwell et al. (1995) and Buddenbaum et al. (2012):

$$C_{chl} = (10.6 + 7.39M + 0.144M^2) \times 0.09 \quad (2.1)$$

where C_{chl} denotes the estimated chlorophyll content specified in $\mu g.cm^{-2}$. The claimed accuracy of this SPAD device for M is ± 1.0 units (Minolta, 1989). To convert M to the same dimensions as the PROSPECT-D outputs, we applied a multiplication factor (0.09) based on the assumption that the molecular mass for chlorophyll $a+b$ is $900 g.mol^{-1}$.

2.4 Spectral leaf measurement

2.4.1 Instruments

Leaf spectral measurements were done with the ASD FieldSpec 4 Standard-Res device (serial N° 18,130; ASD Inc., Boulder, USA). This instrument has a total of 2151 bands covering the spectral range from 350 nm to 2500 nm. It has a spectral resolution (FWHM) of 3 nm at 700 nm and 10 nm resolution at 1400 nm and 2100 nm correspondingly. The discrepancy comes from

the inherent architecture of this device, as there are three individual sensors covering different optical domains. The VNIR (350-1000 nm) detector is a 521 element silicone array while both SWIR1 (1000-1800 nm) and SWIR2 (1800-2500 nm) are thermo-electrically cooled indium gallium arsenide photodiode detectors. The nominal spectral resolution is between 3 nm in VNIR and 10 nm in SWIR. The wavelength accuracy as stated by the production company is at 0.5 nm (Danner et al., 2015). We used a plant probe with a leaf clip (model A122317, serial N^o 455, ASD Inc., Boulder, USA) with a calibrated low-intensity halogen light source. The leaf clip allows the non-destructive handling of the leaves and the isolation of external illumination. The reflectances obtained are reflectance factors resulting from bi-directional measurement. Furthermore, we used the spectral acquisition software RS³ (ASD Inc., Boulder, CO, USA) with its respective instrument configurations (Table A.1) to capture leaf spectra throughout the entire measurement.

2.4.2 Measurement strategy

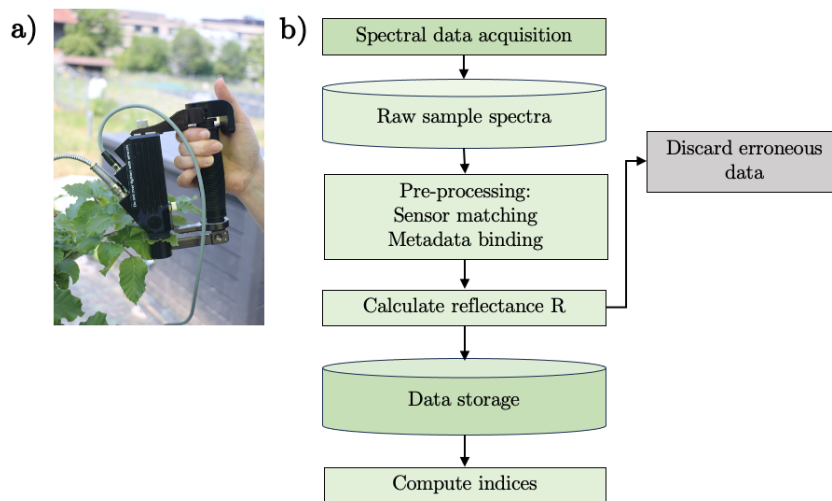


Figure 2.5: Field spectral measurement strategy. a) The plant probe with a leaf clip used in this experiment. b) Flowchart of the measurement procedures.

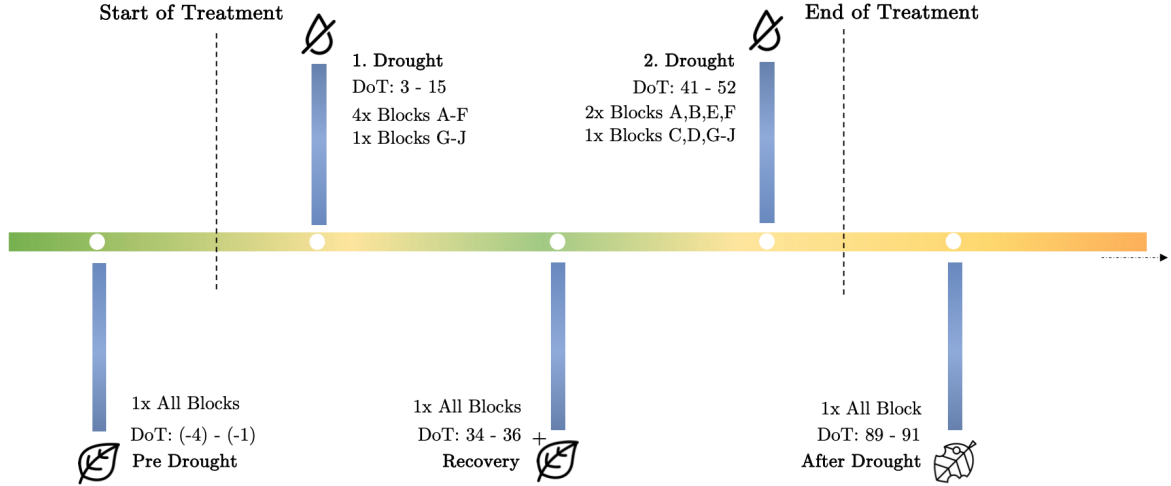


Figure 2.6: Timeline of the field spectral measurements. We measured each block once before the drought, during recovery and after drought. During the drought phases, we repeatedly measured each block indicated in the timeline. Start of treatment indicate the day of installation of the cover. Day of treatment (DoT) indicates the number of days from the first application of the rain covers.

For each sampling day, we constrained the measurement time to ± 3 hours from solar noon to account for consistency in circadian oscillation (Creux & Harmer, 2019). Before taking the measurements, the ASD Fieldspec was warmed up in-situ for at least 30 minutes to decrease measurement errors due to variation in ambient and internal temperatures (Hueni & Bialek, 2017). Field spectral measurements consisted of four successive measurements for each leaf: the white reference R_w , the white reference with target leaf T_w , the black reference R_b , and the black background reference with target leaf T_b . We gathered 5 readings per scan, totalling 20 scans per leaf. For each seedling, we measured two random sun-exposed top-of-canopy leaves. Thus, each seedling underwent a total of 40 scans. We placed the leaf clip on the leaf adaxial surface preferentially with large enough surface and avoiding the midrib. Following the recommendations for spectral in-situ measurements with the leaf clip from Petibon et al. (2021), we systemically recorded metadata such as measurement protocol and environmental conditions. We measured different spots of the samples over the whole experiment due to possible chemical alterations in the leaf by prolonged exposure to light and quantified the measurement uncertainties in relation to the overall spectral variation. We also recalibrated the sensors with the RS³ software against the white reference background of the leaf clip after measuring 10 seedlings.

2.4.3 Spectral data preprocessing

To process the spectral data, we employed the R statistical software (v4.3.1) (R Core Team, 2023) with the *spectrolab* package (v0.0.18) (Meireles & Schweiger, 2020). We first conducted a visual inspection with ViewSpec Pro (v6.20) (ASD Inc., Boulder, CO, USA) to identify artifacts

in the captured raw spectra. Any erroneous data such as reflectance values clearly above 1 or wrong measurement types were discarded. We then spliced the bands at sensor transitions, and interpolated the sliced bands using the `match_sensor()` function. Due to the low signal:noise ratio and higher absolute uncertainty in the 350-400 nm region (Figure 3.14), we only used the spectral range spanning from 400 to 2500 nm (Petibon et al., 2021).

To calculate the total reflectance of each leaf, we first took the mean of the five scans for each measurement:

$$\bar{R}_i = (R_{i,1} + R_{i,2} + R_{i,3} + R_{i,4} + R_{i,5})/5 \quad (2.2)$$

where

$$i = \{R_w, R_b, T_w, T_b\} \quad (2.3)$$

The mean reflectance values were then used to calculate the leaf sample reflectance R_l based on the equation by Petibon et al. (2021) and Miller et al. (1992). The result indicates a dimensionless ratio between 0 and 1, where 0 is no reflectance and 1 is complete reflectance:

$$R_l = \frac{T_b \times R_w - T_w \times R_b}{R_w - R_b} \quad (2.4)$$

We processed a total of 2634 spectra spanning the entire duration of the experiment. The calculated R_l were used to retrieve indices and used as input parameter for the PROSPECT-D inversion described in Sections 2.5 and in 2.6, respectively.

2.5 Leaf trait retrieval with spectral indices

We derive information about leaf traits by calculating indices with the measured reflectance spectra. We used previously published spectral indices that correlate with leaf biochemical traits and functional traits:

1. **Chlorophylls:** Chlorophylls characteristically show strong absorption in blue and red regions of VIS capturing light for photosynthesis, while maximal absorbance occurs around 670 nm. Due to spectral interference in blue with carotenoids as well as anthocyanins in green, many empirical models use reflectances in the 700 nm regions (Buschmann & Nagel, 1993; Datt, 1999; Lichtenthaler et al., 1996). We

used **NDSR** based on Sims and Gamon (2002), which considers R from the centre of the broad range bands of the typically used normalized difference vegetation index (NDVI) in remote sensing. We also calculated **ChlNDI** developed by Gitelson and Merzlyak (1994), which is directly proportional to chlorophyll content. Furthermore, we estimated **CIRE**, which is based on the transitional wavelength position between low reflectance in red and high reflectance in NIR. Both ChlNDI and the red edge parameter are rather insensitive to the saturation effect (Jacquemoud & Ustin, 2019; Sims & Gamon, 2002).

2. **Carotenoids:** It is technically more difficult to estimate carotenoid content through indices because of the overlap between chlorophyll and carotenoid absorption peaks. Estimating the ratio of carotenoid to chlorophylls for relative carotenoid content are consequently more successful. Therefore, we used **CCI** developed by Gamon et al. (2016) for tracking seasonal dependent photosynthetic rates. Similarly, we estimated **PRI** as proxy for photosynthetic light use efficiency based on Sims and Gamon (2002). Both are carotenoid-sensitive indices and practical tools to monitor photosynthetic activity (Sasagawa et al., 2022). A novel index **CARI** developed by Zhou et al. (2017) showed increased correlations for carotenoid estimation in large synthetic dataset simulated in PROSPECT.
3. **Anthocyanins:** Similar to carotenoids, the absorption of anthocyanins with a peak absorption at around 550 nm coincides with chlorophyll absorption, leading to comparable challenges in their estimation (Sims & Gamon, 2002). Thus, we used **RGR** based on the red:green ratio by Gamon and Surfus (1999), which was capable of estimating the anthocyanin to chlorophyll ratio. We used **ARI** developed by Gitelson et al. (2001), allowing the accurate estimation of anthocyanin accumulation in stressed leaves.
4. **Leaf water potential Ψ and moisture stress:** Ψ is an indicator of the whole plant water status and measure how a plant may respond to water stress (Rodriguez-Dominguez et al., 2022). We used **WABI**, a spectral index used for proximally tracking water status changes in grapevines (Rapaport et al., 2017) and we used **MSI** developed by Hunt Jr. and Rock (1989), which is correlated to relative water content to infer to moisture stress.
5. **Equivalent water thickness (EWT):** EWT is associated with leaf-level water status and thus sensitive to dryness stress. EWT can be calculated either by directly measuring the variables (Equation 2.13) or estimated with indices (Féret et al., 2019). We also used the semi-empirical **WI** from Datt (1999) and **NDWI** to estimate water content and are widely used across the remote sensing community (Gao, 1996; Xu, 2006).

6. **Biomass:** Comparable to EWT, LMA can be directly calculated (Equation 2.12) or estimated with indices. We used the **NDLMA** developed by Lemaire et al. (2008) on leaf canopy biomass and tested by Féret et al. (2011) with equally fair results on synthetic datasets of PROSPECT simulations. Foliar nitrogen and foliar lignin concentration are usually estimated when assessing ecosystem processes such as growth and decomposition. They have an absorption peak at 1510 nm and 1754 nm respectively. We hence computed **NDNI** and **NDLI** based on Serrano et al. (2002), who assessed nitrogen and lignin in shrub vegetation. The **CAI** was used to estimate cellulose absorption by exploiting the absorption peak caused by cellulose and lignin at around 2100 nm. This index was developed by Daughtry et al. (2004), who found a correlation between crop residue and CAI.

7. **Epicuticular wax (EW):** EW in plants may be considered as the first line of protection against biotic and abiotic stressors. It is also associated with resilience to drought stress and heat (Guo et al., 2016). The extraction, however, comes with difficulties as EW absorption peaks overlap with those associated with photosynthesis and water. We used **EWI** as the most accurate narrow-band index developed by Camarillo-Castillo et al. (2021) to estimate EW.

To retrieve the leaf traits, we applied the equations summarized in Table 2.2 on the respective R_λ , where λ indicates the wavelength. Depending on the type of index, we calculate dimensionless simple ratio values or dimensionless normalized difference values.

2.6 Leaf trait retrieval with PROSPECT-D inversion

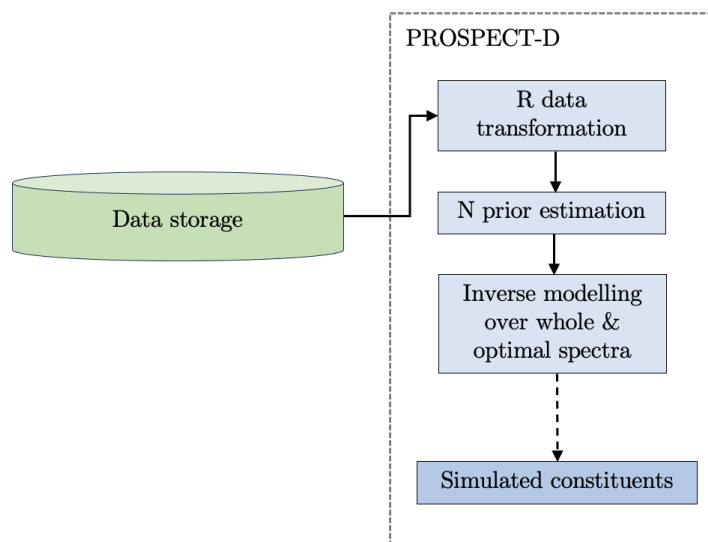


Figure 2.7: Flowchart of the retrieval of leaf traits with the PROSPECT-D inversion.

Table 2.2: Summary of spectral indices including equation, author, and year of publication. R_λ indicates reflectance at wavelength λ .

Trait	Index	Short	Formula	Reference
Chlorophyll	Normalized Difference Simple Ratio	NDSR	$(R_{800} - R_{680}) / (R_{800} + R_{680})$	Sims and Gamon (2002)
Chlorophyll	Chlorophyll Normalized Difference Index	ChlNDI	$(R_{750} - R_{705}) / (R_{750} + R_{705})$	Gitelson and Merzlyak (1994)
Chlorophyll	Red-Edge Chlorophyll Index	CIre	$(R_{783} / R_{704}) - 1$	Gitelson (2005)
Chl/Car	Chlorophyll/Carotenoid Index	CCI	$(R_{528} - R_{665}) / (R_{528} + R_{665})$	Gamon et al. (2016)
Chl/Car	Photochemical Reflectance Index	PRI	$(R_{531} - R_{570}) / (R_{531} + R_{570})$	Sims and Gamon (2002)
Carotenoid	Carotenoid Index	CARI	$(R_{720} / R_{8521}) - 1$	Zhou et al. (2017)
Anthocyanin	Red:Green Ratio	RGR	$\frac{Red}{Green} = \frac{\sum_{i=600}^{699} R_i}{\sum_{i=500}^{599} R_i}$	Gamon and Surfus (1999)
Anthocyanin	Anthocyanin Reflectance Index	ARI	$R_{550}^{-1} - R_{700}^{-1}$	Gitelson et al. (2001)
Ψ	Water Balance Index	WABI	$(R_{1490} - R_{531}) / (R_{1490} + R_{531})$	Rapaport et al. (2015)
Water	Moisture Stress Index	MSI	R_{1600} / R_{820}	Hunt Jr. and Rock (1989)
Water	Water Index	WI	R_{900} / R_{970}	Datt (1999)
Water	Normalized Difference Water Index	NDWI	$(R_{860} - R_{1240}) / (R_{860} + R_{1240})$	Gao (1996)
LMA	Normalized Difference Leaf Mass Area	NDLMA	$(R_{1368} - R_{1722}) / (R_{1368} + R_{1722})$	Lemaire et al. (2008)
Nitrogen	Normalized Difference Nitrogen Index	NDNI	$\frac{\log(R_{1510}^{-1}) - \log(R_{1680}^{-1})}{\log(R_{1510}^{-1}) - \log(R_{1680}^{-1})}$	Serrano et al. (2002)
Lignin	Normalized Difference Lignin Index	NDLI	$\frac{\log(R_{1754}^{-1}) - \log(R_{1680}^{-1})}{\log(R_{1754}^{-1}) - \log(R_{1680}^{-1})}$	Serrano et al. (2002)
Cellulose	Cellulose Absorption Index	CAI	$0.5 \times (R_{2000} + R_{2200}) - R_{2100}$	Daughtry et al. (2004)
EW	Epicuticular Wax Index	EWI	$(R_{625} \times (R_{739}^{-1} - R_{832}^{-1}))$	Camarillo-Castillo et al. (2021)

To run PROSPECT-D, we employed the *prospect* package (v1.3.0) by Féret et al. (2017) in the R statistical software (v4.3.1) (R Core Team, 2023). To use the inversion and thus to estimate the output parameters, we called the function *Invert_PROSPECT()*, which uses the iterative optimization algorithm in the *fmincon()* function included in the *pracma* package (v2.4.2). We used the root-mean-squared error (RMSE) merit function, which minimizes the RMSE between the simulated and measured properties. We used PROSPECT version D over previous versions because of its improved trait parametrization over a larger database and the inclusion of relevant traits such as anthocyanin content (Jacquemoud & Ustin, 2019). Table 2.3 summarizes the input parameters and their variable ranges in PROSPECT-D.

Table 2.3: PROSPECT-D input parameters used for the computation of leaf reflectance and they display the natural occurring variation (Jacquemoud & Ustin, 2019). The units and the range of variation are listed.

Parameter	Range of Variation	Unit
N	1-4	-
C_{ab}	0-100	$\mu g.cm^{-2}$
C_{ant}	0-40	$\mu g.cm^{-2}$
C_{car}	0-40	$\mu g.cm^{-2}$
C_m	0-0.05	$g.cm^{-2}$
C_w	0-0.05	$g.cm^{-2}$

We followed the recommendations of Spafford et al. (2021) to obtain prior information on the leaf structure parameter N when only R is measured. N is estimated simultaneously with other traits otherwise. Their study found significantly improved estimations of leaf traits when N is determined a priori particularly when only R is measured. We determined N using the integrated function *Get_Nprior()*, which computes N when R is measured over the full spectral range with the following linear model:

$$N_R = 1.83 \times \frac{R_{1131}}{1 - R_{1131}} + 0.0711 \quad (2.5)$$

Spafford et al. (2021) further found improved performance when optical subdomains are used. This means only a certain range of wavelengths are used for the retrieval of certain traits (i.e., 700-720 nm and 520-560 nm for C_{ab} and C_{car} , or 1700-2400 nm for C_m and C_w). We ran the inversion for both whole spectra and optical subdomains with the function *Invert_PROSPECT_OPT()* after prior estimation of N . We estimated the following traits:

$$c(C_{ab}, C_{ant}, C_{car}, C_m, C_w) \quad (2.6)$$

with the defined input parameters as initial values for the optimization:

$$c(C_{ab} = 40, C_{ant} = 0, C_{car} = 8, C_m = 0.01, C_w = 0.01, \alpha = 40, N = N_R) \quad (2.7)$$

Hereby, leaf surface roughness and anisotropic structure is imitated with assessing the incident radiation expressed as α . $N = N_R$ is the prior estimated N for each iteration. C_m and C_w are different expressions for LMA and EWT respectively (Spafford et al., 2021). Based on the post hoc accuracy assessment (Table 3.8), we used the more accurate spectral input for our dataset (whole spectrum: C_{ab} , C_{car} , LMA; optimal spectrum: C_{ant} , EWT).

2.7 Measurement uncertainties and biological variation

Optical measurements come with inherent measurement uncertainties due to characteristics of the measurement device (i.e., field spectroradiometer, leaf clip). Experimental conditions are also a source of uncertainty. Thus, both contribute to the total spectral variation (Hueni & Bialek, 2017). When assessing species trait variation through spectral measurements, it is crucial to quantify the associated uncertainties within spectral variation (Petibon et al., 2021).

To calculate the absolute measurement uncertainty U_{abs,R_l} , we employed the following equation from Li et al. (2023), which is derived from Petibon et al. (2021) and Miller et al. (1992). σ signifies the standard deviation and n the scan sample size:

$$U_{abs,R_l}^2 = \left(\frac{R_b \times (T_w - T_b)}{(R_w - R_b)^2} \right)^2 \left(\frac{\sigma_{R_w}}{\sqrt{n}} \right)^2 + \left(\frac{R_b}{R_w - R_b} \right)^2 \left(\frac{\sigma_{T_w}}{\sqrt{n}} \right)^2 + \left(\frac{R_w \times (T_w - T_b)}{(R_w - R_b)^2} \right)^2 \left(\frac{\sigma_{R_b}}{\sqrt{n}} \right)^2 + \left(\frac{R_w}{R_w - R_b} \right)^2 \left(\frac{\sigma_{T_b}}{\sqrt{n}} \right)^2 \quad (2.8)$$

The relative uncertainty U_{rel,R_l} in % can then be computed as a ratio of U_{abs,R_l} and R_l :

$$U_{rel,R_l} = \frac{U_{abs,R_l}}{R_l} \times 100 \quad (2.9)$$

To calculate the spectral variation V_s in %, which is also defined as the coefficient of variation (CV) in Petibon et al. (2021), we used the following equation:

$$V_s = \frac{\sigma}{R_l} \times 100 \quad (2.10)$$

From which we then calculate the biological variation V_b for each wavelength as %:

$$V_b = V_s - U_{rel, R_l} \quad (2.11)$$

V_b quantifies the variation in the spectrum that is caused by differences in LOPs such that we can infer to variation depending on the measurement period and treatment groups.

2.8 Validation of the PROSPECT-D inversion

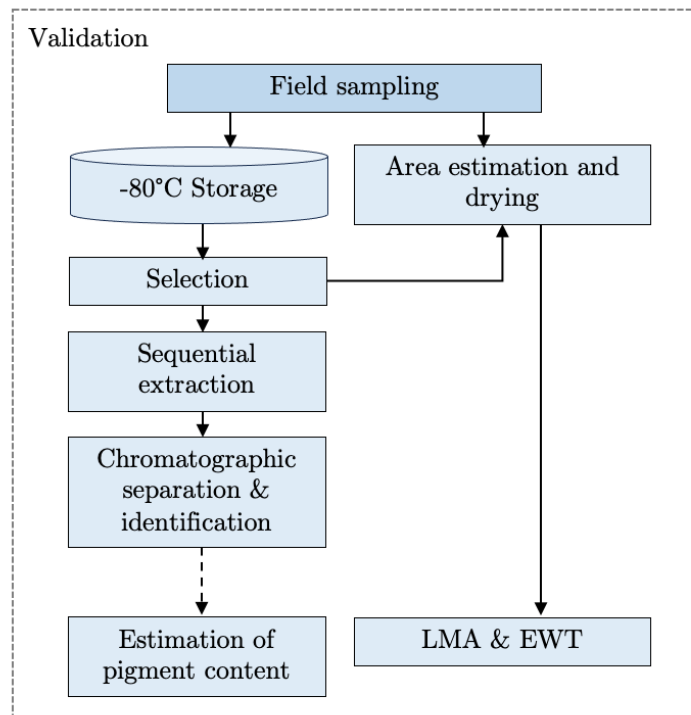


Figure 2.8: Flowchart of the validation of the PROSPECT-D inversion with sequential extraction and subsequent analysis.

To ensure the reliability of this model, we conducted a validation process with a validation dataset based on an established pigment extraction protocol by Petibon and Wiesenberg (2022). They developed a validated methodology for sequential extraction and subsequent high-performance liquid chromatography analysis (HPLC) of pigments in *F. sylvatica* among other European deciduous species.

In this section, we detail the approach (Figure 2.8) to validate the PROSPECT-D output for both optical subdomains and whole spectra for each leaf trait and assess their accuracy.

2.8.1 Sample selection

We collected leaves ($n=55$) across the control and treatment group in June before and during the first drought simulation from which we used a subset for the pigment extraction. The leaf samples were stored in non-transparent plastic bags immediately after their spectral measurement and transported to a deep-freezer at -80°C to prevent degradation of the pigments.

To ensure a robust representation of our data, we first calculated the three indices RGR, NDSR and PRI (Table 2.2), which surrogated for relative anthocyanin, chlorophyll, and carotenoid content respectively for all the collected samples. Secondly, we clustered the calculated indices based on k-means in python (v3.9.7) (Figure A.5) from the *sklearn* library (v1.3.2) from Pedregosa et al. (2012). We took a total of 20 samples which represents the full range of the pigments for the subsequent extraction.

2.8.2 Sampling leaf functional traits

Before the pigment extraction, we measured the leaves for their fresh weight fw using a semi-microscale balance (0.015 mg repeatability) and area A_{leaf} using the point tool and a known distance (Figure A.6) in the image analysis program ImageJ (v1.38) (Schneider et al., 2012). The leaves were then freeze-dried overnight using the lyophilizer Alpha 2-4 LD plus (Martin Christ, Osterode am Harz, Germany) and weighed again for their dry weight dw . In addition to the selected HPLC samples, we took additional samples ($n=55$) for their fw and A_{leaf} . The fresh leaves were stored in paper bags and directly put into an oven at 70°C for 72 h, after which we weighed the dry leaves for dw .

To calculate LMA for both sampling batches, we applied the following equation adapted from Féret et al. (2019), where dw indicates oven-dry weight and A_{leaf} the one-sided leaf area. The result is specified in mg.cm^{-2} :

$$\text{leaf mass per area} = \frac{dw}{A_{\text{leaf}}} \quad (2.12)$$

We calculated EWT specified in mg.cm^{-2} using the following equation by Féret et al. (2019), where fw refers to fresh leaf weight:

$$\text{equivalent water thickness} = \frac{fw - dw}{A_{\text{leaf}}} \quad (2.13)$$

2.8.3 Sequential pigment extraction

For the extraction we used the following solvents: acetone ($\geq 99.9\%$, Carl Roth, Karlsruhe, Germany) and n-hexane ($\geq 95\%$, Carl Roth, Karlsruhe, Germany), which were UltraGrade. Isopropanol ($\geq 99.9\%$, Sigma-Aldrich, Steinheim, Germany) is LC grade. We modified the previously published protocol by Petibon and Wiesenberg (2022).

All procedures were done under subdued light to avoid pigment degradation by light exposure. We prepared the dried leaf samples by carefully removing the mid-vein and manually grounding the leaf in liquid nitrogen to homogenized leaf powder with a mortar and a pestle. We then filled each amber glass vials with 17-22 mg of ground leaf powder. The vials and the solvents were stored in the freezer at -20°C for later use.

We performed a sequential extraction with the following solvents in this order:

1. acetone:water(deion.) (85:15, v/v)
2. acetone (100%)
3. isopropanol:n-hexane (2:1, v/v)

We added ≈ 0.8 ml of cooled solvent to the leaf powder vial and then agitated the solution with a vortex stirrer. We left the solution to settle before filtering it on a $1\ \mu\text{m}$ glass-fiber filter (Macharey-Nagel, Dueren, Germany) and transferring it to a 10 ml amber vial, which was kept cool. We repeated this procedure three times for each solvent. We then concentrated the eluate, first by nitrogen evaporation with a sample concentrator (Cole-Parmer, Vernon Hills, USA) and steel needle inlets under a steady stream of N_2 and secondly with a concentrator plus centrifuge (Vaudaux-Eppendorf, Basel-Land, Switzerland) under vacuum. Before chromatographic separation, we redissolved the eluate and transferred it to a 1.5 ml autosampler vial with inserts.

2.8.4 Chromatographic separation

We used the following reagents as eluents: Ultrapure water deionised with Milli-Q Advantage A10 purification (Merck, Darmstadt, Germany). Both methanol (99.9%, Carl Roth, Karlsruhe, Germany) and ethyl acetate ($\geq 99.8\%$, Merck, Darmstadt, Germany) were hypergrade LC-MS. Formic acid ($\geq 98\%$, Sigma-Aldrich, Steinheim, Germany) was used as well.

The chromatographic separation was performed on the Agilent 1290 Infinity UHPLC system (Agilent Technologies, Santa Clara, USA) with integrated binary pump (Agilent G4220A) and autosampler (Agilent G4226A) with tray cooler kept at 4°C . The column oven was equipped with a InfinityLab Poroshell 120SB – C_{18} (4.6 x 150 mm, particle size of $2.7\ \mu\text{m}$, Agilent) column and kept at 10°C . The detection was done with a diode array detector (DAD) (Agilent VL+G1315C).

For the HPLC analysis, we used the following eluents:

- Eluent A: water:formic acid (500:1, v/v , pH 2.5)
- Eluent B: methanol:ethyl acetate (68:32, v/v)

Directly before the HPLC measurement, we redissolved the samples in a known volume of 50 μl of isopropanol:n-hexane (2:1, v/v) and 250 μl of acetone:water (85:15, v/v). Injection volume per sample was 15 μl and the flow rate for the chromatographic separation was 0.5 ml per minute. The total run time of the chromatographic separation was 44 min. The method gradient with eluent A and eluent B can be found in Table A.3.

2.8.5 Identification and quantification of pigment concentration

We used the following analytical standards to derive the calibration curves: Chlorophylls: chlorophyll *a* ($\geq 95.0\%$, HPLC) and chlorophyll *b* ($\geq 95.0\%$, HPLC). Carotenoids: α -carotene ($\geq 97.0\%$, HPLC), β -carotene ($\geq 95.0\%$, HPLC), xanthophyll (marigold), lutein ($\geq 96.0\%$, HPLC), neoxanthin ($\geq 97.0\%$, HPLC), and zeaxanthin ($\geq 96.0\%$, HPLC). Anthocyanins: delphinidin chloride ($\geq 95.0\%$, HPLC), cyanidin chloride ($\geq 98.0\%$, HPLC), and pelargonidin chloride. All standards were purchased from Sigma-Aldrich (Steinheim, Germany). Due to different polarities, we used different solvents for the analytical standards. The derived calibration curves are found in Figure A.7.

We identified the main pigments based on the absorption spectra and retention time (RT) of the analytical standards (Figure A.8). We categorized chlorophylls at the 665 nm and carotenoids at the 450 nm chromatograms, which is based on one of their absorption maxima. The global absorption maxima does not always convey accurate readings due to over saturation at the respective wavelength. Other compound peaks, for which we do not have analytical standards, were identified based on the decision tree provided by Petibon and Wiesenberg (2022) as either derivatives or unknown compounds. We categorized peaks with small absorption (< 5 mAU) in combination with low signal:noise ratio as unknown. Moreover, due to their relatively high absorption contribution in the chromatograms, we identified pheophytin *a* and pheophytin *b*, which are demetallized chlorophyll *a* and chlorophyll *b* based on their unique absorption spectra respectively (Figure A.9) (Petrovic et al., 2012).

For peak area integration, we used the OpenLAB CDS ChemStation software by Agilent (Santa Clara, USA). Quantification was based on the compound peak areas A_{peak} as absorption units specified in mAU in their predefined wavelength and the regression function of their calibration curves $x = (y - b)/a$, where x is the pigment concentration specified in $\mu g.ml^{-1}$ (Figure A.7). Given the known solvent volume (0.3 ml), the previously determined ground leaf weight m_g , dw and the leaf area (A_{leaf}), we normalized the pigment per area C_{pigment} specified in $g.cm^{-2}$:

$$C_{\text{pigment}} = \left(\frac{A_{\text{peak}} - b}{a} \right) \times 0.3 \times m_g^{-1} \times dw \times A_{\text{leaf}}^{-1} \quad (2.14)$$

This calculation has been performed for each identified compound for which we had analytical standards. We did not include any derivatives into the peak area integration because of the lack of their standard spectra. The normalized outputs of the HPLC analysis were then summarized in either C_{ab} or C_{car} and were used to validate leaf traits from the PROSPECT-D inversion and assessed for accuracy.

2.9 Data analysis

2.9.1 Statistical analyses

Since we measured two leaves per seedling, we took the arithmetic mean of the indices and the model outputs. The statistical analysis was conducted using the statistics software R (v4.3.1) (R Core Team, 2023).

To meet the model assumptions, we removed some outliers. We did a visual inspection of the histogram using *hist()*, residuals versus fits and QQ-plot using *qqPlot()* to identify outliers. We discovered that by excluding all seedlings which exhibited strong wilting (wilting index ≥ 2) and NDWI < 0 , we were able to meet the model assumptions. The outliers (n=12) contained seedlings from multiple provenances but all belonged to the drought treatment.

We performed a one-way analysis of variance (ANOVA) for the first drought period to assess the significance of different sources of variation in the model. We used the multiple regression function *lm()* of the *stats* package (v3.6.2) to fit the model and subsequently conducted the one-way ANOVA with the function *anova()* on the model. We set out the following formula:

$$\hat{Y} \sim \text{length} + \text{treatment} * \text{provenance} \quad (2.15)$$

which converts to this regression model:

$$\hat{Y} = \beta_0 + \beta_1 \cdot \text{length} + \beta_2 \cdot \text{group} + \beta_3 \cdot \text{provenance} + \beta_4 \cdot (\text{treatment} \times \text{provenance}) + \epsilon \quad (2.16)$$

where \hat{Y} is the dependent response variable (such as C_{chl} , index, or modelled trait) which is regressed over the predictor variables length, treatment, provenance, and the interaction treat-

ment \times provenance. For the ANOVA, we assume randomness in the observations, homogeneous variances in each group and normality in the response variable. We considered $p \leq 0.05$ as our significance threshold.

When there were significant differences in provenances and the interaction group \times provenance, we applied the Tukey’s honestly significant difference (HSD) post hoc test with the function *HSD.test()* of the *agricolae* package (v.1.3.7) (Felipe de Mendiburu & Muhammad Yaseen, 2020) to determine which specific provenances differ significantly from each other.

2.9.2 Log response ratios

Ecological research may resort to log response ratio (LRR, or RR) to compute outcomes of ecological experiments. This metric for effect size quantifies the log-proportional change of the mean of the treatment and the control group (Lajeunesse, 2016). A strength of this method is that it linearizes its metric, treating the deviations in the numerator and denominator in the same way. To calculate the LRR and to subsequently compute the variations of a leaf trait between the provenances we adapted the following equation from Hedges et al. (1999) and Bakbergenuly et al. (2020):

$$\hat{\lambda}_i = \ln(\bar{X}_T/\bar{X}_C) \quad (2.17)$$

where $\hat{\lambda}_i$ indicates the LRR and \bar{X} denotes the observed means of each treatment (T) and control (C) group. Since the logarithm is only defined for positive values and some indices show a series of negative and positive values, we apply an offset transformation by adding a constant c , where c equals to 1 except for ARI, where c equals to 3:

$$\hat{\lambda}_i = \ln(\bar{X}_T + c/\bar{X}_C + c) \quad (2.18)$$

Following, the standard error S_E can then be computed as:

$$S_{E_{\hat{\lambda}_i}} = \sqrt{\frac{s_T^2}{n_T \bar{X}_T^2} + \frac{s_C^2}{n_C \bar{X}_C^2}} \quad (2.19)$$

where s denotes standard deviations and n the sample sizes of the groups. We incorporated the outliers in the computation and visualization of the LRR, however, we did not calculate LRR for a subset of provenances where sample sizes were too small to compute standard errors (i.e., ITM, ITE, ITB, and PLB).

2.9.3 Model accuracy assessment of PROSPECT-D inversion

To assess the accuracy of the PROSPECT-D inversion, we performed a linear model for LMA, EWT, C_{ab} , and C_{car} between the measured and simulated values each over the whole and optimal spectral range. We used the function $lm()$ of the *stats* package (v3.6.2) to build the model. We then quantified the intercept β_0 , the slope β_1 , and the coefficient of determination R^2 , which measures the percentage of variance explained by the correlation between the measured and simulated values. We also calculated the RMSE and the normalized RMSE (NRMSE) to assess the accuracy of the regression model. Both RMSE and NRMSE represent error measures, where RMSE shows the average magnitude of the residuals and NRMSE scales the RMSE with the range of the observed values.

Chapter 3

Results

3.1 Lower soil moisture in drought treatment

Using TMS-4 probes, we tracked soil moisture and air temperature for 20 pots throughout the experiment (Figure 3.3a). During the first drought, the mean raw time-domain transmission (TDT) value was 1913 units for the control group and 1578 units for the treatment group. In the second drought, the mean raw TDT value was 1971 units for the control group and 1582 units for the treatment group. Control and treatment group thus showed differences in soil moisture during both drought periods but were comparable (mean control: 2009 units, mean treatment: 2125 units) during the recovery phase. This implies that the treatment group had less soil water available during both drought periods. Jumps in soil moisture readings are due to the targeted irrigation of the control group. Furthermore, we found an inverse relationship between soil moisture and tree length for both control and treatment group, implying that longer seedlings tended to have less soil moisture in their pots (Figure 3.4).

Weather conditions, such as local air temperature, precipitation and relative humidity, were measured throughout the experiment with ATMOS 41 (Figure 3.3a-b). During the first drought period, mean temperature measured by the TMS-4 probes was 21.6°C (ranging from 8.9°C to 35.1°C) and the local air temperature measured by ATMOS 41 was 20.5°C. This discrepancy could have been due to the black rain covers absorbing the sunlight and thus warming up the soil temperature. Mean relative humidity was 63% and there were 6 days with precipitation accumulating a total of 36 mm of rain. During the second drought period, mean air temperature between TMS-4 probes was 21.1°C (ranging from 10.5°C to 37.9°C) and differed also from ATMOS 41 (19.7°C). Mean relative humidity was 76% and there were 11 days with precipitation accumulating a total of 25 mm of rain. The second drought period was characterized by cloudy conditions and spontaneous precipitation.

Morphological changes such as leaf wilting, bleaching, or defoliation gave us an insight into the seedling's current health (Figure A.2). We monitored the seedlings each day. Some seedlings

seemingly showed visual drought symptoms (Figure 3.1, while most of the seedlings did not (Figure 3.2). If needed, we reacted by giving a predefined amount of water to prevent tree mortality. All seedlings survived.



Figure 3.1: Time series of a seedling (CHL) during the first drought simulation. The difference between each photograph is 3 days, with increasing number of rain-free days from left to right.



Figure 3.2: Time series of a seedling (BES) during the first drought simulation. There are no visual drought symptoms despite it undergoing drought treatment.

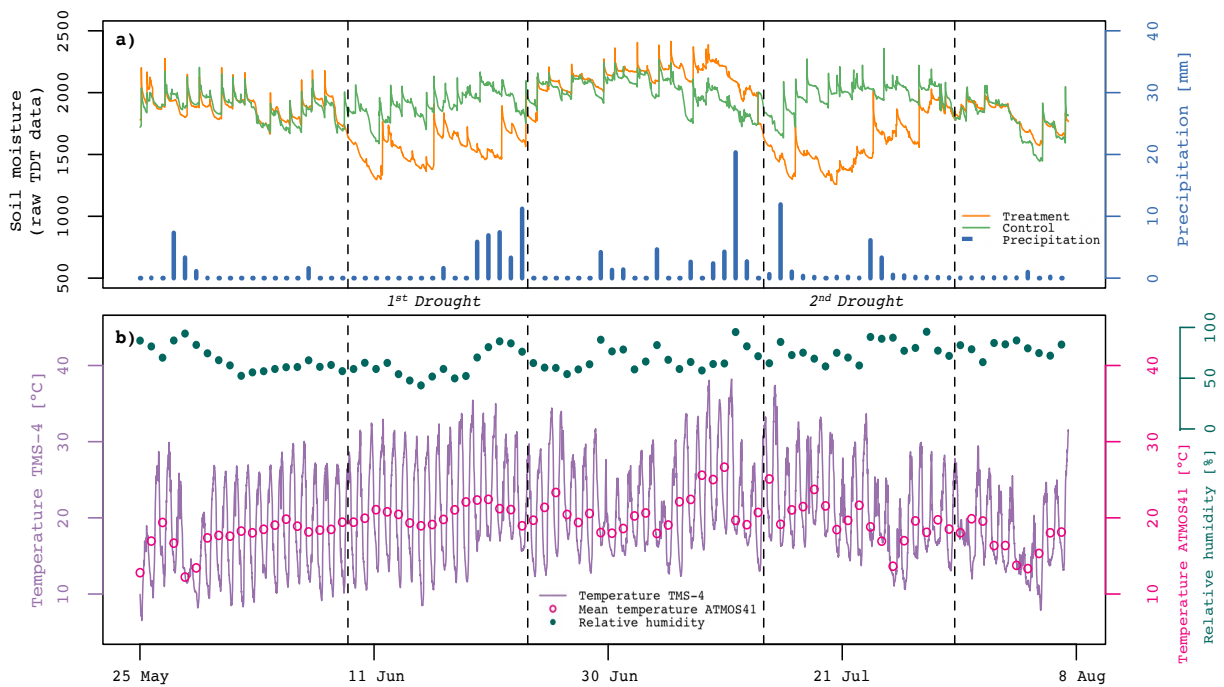


Figure 3.3: Weather conditions and soil moisture during the experiment. a) Soil moisture of control and treatment group specified in raw uncalibrated time-domain transmission (TDT) values and precipitation measured with the ATMOS 41. b) Temperature inside the covers measured by TMS-4, mean air temperature and relative humidity measured by ATMOS 41. Dashed lines indicate start and end of the drought periods.

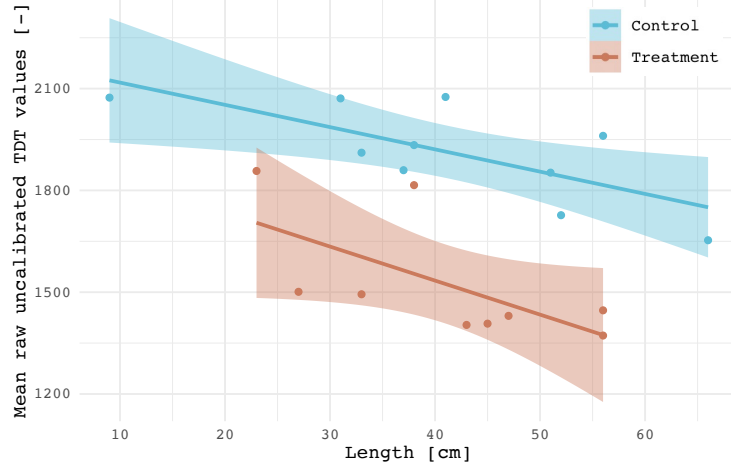


Figure 3.4: Length of the seedlings measured before the first drought period against mean soil moisture values expressed as raw TDT values for treatment and control group. There was a negative association between soil moisture and tree length in both treatment ($R^2 = 0.420$) and control group ($R^2 = 0.521$).

3.2 Treatment had no effect on chlorophyll measured with SPAD.

We looked at the response of C_{chl} from SPAD to seedling length, treatment, provenance, and the interaction drought treatment \times provenance during the first drought period. The one-way ANOVA revealed that there was no statistically significant difference in C_{chl} between drought treatment and control ($F(1,134) = 0.03$, $p = 0.866$) (Figure 3.5) but a statistical difference between provenances ($F(15,134) = 2.20$, $p = 0.009$) (Table 3.1). Tukey's HSD post hoc test revealed grouping of the means in which ITE and ITB were significantly different to the other provenances, however, sample sizes in these two provenances were small (Table A.2).

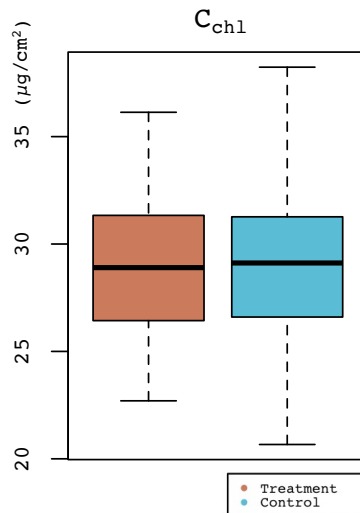


Figure 3.5: Converted C_{chl} from SPAD values in treatment and control group during the first drought period.

Table 3.1: One-way ANOVA table on linear model with C_{chl} measured with SPAD as dependent observation and length, treatment, provenance, and the interaction treatment \times provenance as independent factors during the first drought period. Significant values are in bold ($p \leq 0.05$).

Index	Factor	DF	F value	p value
C_{chl}	Length	1	1.98	0.162
	Treatment	1	0.03	0.866
	Provenance	15	2.20	0.009
	Treatment \times Provenance	15	1.08	0.379
	Residuals	134		

3.3 Treatment effects on leaf traits derived from spectral indices

3.3.1 Leaf pigments

We ran linear models for nine spectral indices relating to leaf pigments, using seedling length, treatment, provenance, and the interaction treatment \times provenances as fixed effects from the first drought period in the one-way ANOVA. For chlorophyll indices NDSR, ChINDI and CIre, we found a statistically significant difference between control and treatment with a lower index value in the treatment group (Figure 3.6a). Furthermore, length was significant for ChINDI and CIre (Table 3.2). Similar to chlorophyll, carotenoid related indices were significantly decreased between treatment and control: CCI ($F(1,135) = 16.49$, $p < 0.001$), CARI ($F(1,132) = 33.54$, $p < 0.001$) and PRI ($F(1,135) = 33.49$, $p < 0.001$) (Figure 3.6b). For PRI we found that the length was significantly different (Table 3.3). In both indices related to anthocyanin, namely RGR and ARI, we found increased values in the treatment group in contrast to the control group (Figure 3.6c). Additionally, length was significant for ARI (Table 3.4). Provenance was never significant and neither was the interaction treatment \times provenance for chlorophyll, carotenoid, and anthocyanin related indices. We thus observed variation between control and treatment, but not between provenances and their response to drought.

Figure 3.8 shows the log response ratios (LRRs) of indices related to pigments. The general direction of the effect sizes was negative for chlorophyll and carotenoid indices, demonstrating the decrease of the index value as a response to the drought treatment. We observed the opposite in anthocyanin indices, which had a positive effect size. Provenances such as RSF showed a higher magnitude as a response compared to other provenances.

3.3.2 Leaf water potential and water content

We further ran a linear model on four indices related to water potential and water content on length, treatment, provenance and the interaction treatment \times provenance in the one-way ANOVA during the first drought period. Water content indices WI and NDWI did not differ

significantly between the control and treatment groups as opposed to water potential index WABI, which had decreased index values, and moisture stress index MSI, which had increased index values (Figure 3.7a-b, Table 3.5). WABI and WI had significant differences in length. We did not find any significant differences for the interaction drought treatment \times provenance for water potential and water content related indices (Table 3.5)

There was no general direction of the effect sizes for the moisture stress and water content related indices (Figure 3.9a-c) and effect sizes were small in general. Only the water potential index exhibited positive and negative responses (Figure 3.9d).

3.3.3 Biomass and epicuticular wax

None of the biomass (NDLMA, NDNI, NDLI, CAI) and epicuticular wax (EWI) indices showed any significant differences between control and treatment (Figure 3.7c-d) in the ANOVA. NDLMA, CAI, and EWI were significantly influenced by seedling length. Furthermore, we found a significant effect of provenance for NDLI and NDNI (Table 3.6). Tukey's HSD post hoc analysis in NDLI revealed that ITB and ITE were significantly different to the other provenances. Similarly, NDNI also showed significant differences in provenances ITE, ITM, and PLB. However, these provenances had small sample sizes (Table A.2). We did not find any significant differences in the interaction treatment \times provenance for biomass and wax related indices (Table 3.6). Similar to water content indices, there was no general direction of the effect sizes for the biomass and wax related indices as most of the LRRs were located around zero (Figure 3.10a-e).

Table 3.2: One-way ANOVA table on linear model with chlorophyll spectral indices as dependent observation and length, group provenance and the interaction treatment \times provenance as independent factors during the first drought period. Significant values are in bold ($p \leq 0.05$).

Index	Factor	DF	F value	p value
NDSR	Length	1	0.86	0.356
	Treatment	1	26.99	< 0.001
	Provenance	15	1.02	0.438
	Treatment \times Provenance	14	0.30	0.993
	Residuals	127		
ChlNDI	Length	1	10.01	0.002
	Treatment	1	33.54	< 0.001
	Provenance	15	1.09	0.374
	Treatment \times Provenance	15	0.66	0.819
	Residuals	132		
CIre	Length	1	6.76	0.010
	Treatment	1	33.49	< 0.001
	Provenance	15	1.20	0.278
	Treatment \times Provenance	13	0.55	0.887
	Residuals	129		

Table 3.3: One-way ANOVA table on linear model with carotenoid spectral indices as dependent observation and length, group provenance and the interaction treatment \times provenance as independent factors during the first drought period. Significant values are in bold ($p \leq 0.05$).

Index	Factor	DF	F value	p value
CCI	Length	1	3.87	0.0512
	Treatment	1	16.49	< 0.001
	Provenance	15	0.64	0.839
	Treatment \times Provenance	14	0.85	0.611
	Residuals	135		
CARI	Length	1	2.48	0.117
	Treatment	1	15.05	< 0.001
	Provenance	15	1.55	0.096
	Treatment \times Provenance	14	1.34	0.191
	Residuals	132		
PRI	Length	1	6.83	0.010
	Treatment	1	34.89	< 0.001
	Provenance	15	1.24	0.249
	Treatment \times Provenance	13	0.96	0.503
	Residuals	135		

Table 3.4: One-way ANOVA table on linear model with anthocyanin spectral indices as dependent observation and length, group provenance and the interaction treatment \times provenance as independent factors during the first drought period. Significant values are in bold ($p \leq 0.05$).

Index	Factor	DF	F value	p value
RGR	Length	1	0.56	0.455
	Treatment	1	30.33	< 0.001
	Provenance	15	0.59	0.877
	Treatment \times Provenance	14	0.46	0.949
	Residuals	133		
ARI	Length	1	12.87	< 0.001
	Treatment	1	5.69	0.019
	Provenance	15	1.55	0.831
	Treatment \times Provenance	14	1.34	0.832
	Residuals	131		

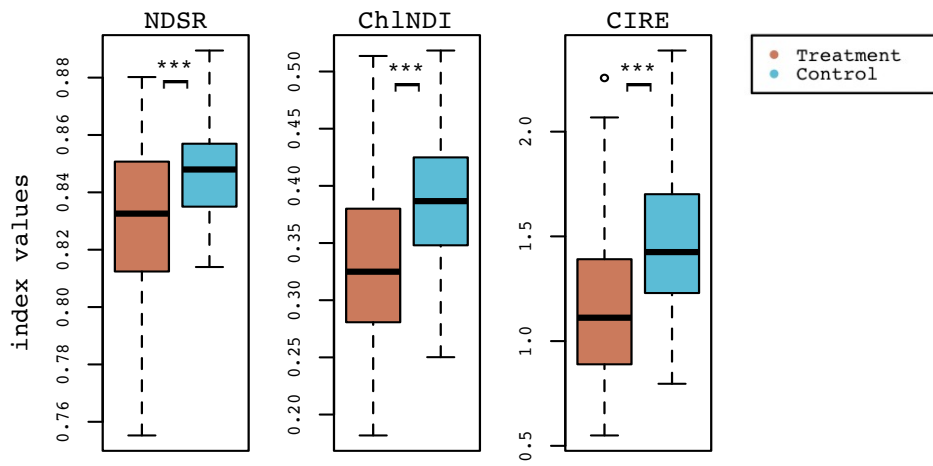
Table 3.5: One-way ANOVA table on linear model with spectral indices related to water content as dependent observation and length, drought treatment, provenance and the interaction treatment \times provenance as independent factors during the first drought period. Significant values are shown in bold ($p \leq 0.05$).

Index	Factor	DF	F value	p value
WABI	Length	1	5.34	0.022
	Treatment	1	26.23	< 0.001
	Provenance	15	1.15	0.321
	Treatment \times Provenance	15	1.19	0.287
	Residuals	132		
MSI	Length	1	2.48	0.117
	Treatment	1	15.05	< 0.001
	Provenance	15	1.55	0.096
	Treatment \times Provenance	14	1.34	0.191
	Residuals	132		
WI	Length	1	4.46	0.037
	Treatment	1	3.04	0.083
	Provenance	15	0.67	0.807
	Treatment \times Provenance	14	0.32	0.990
	Residuals	133		
NDWI	Length	1	3.22	0.075
	Treatment	1	3.63	0.059
	Provenance	15	0.63	0.848
	Treatment \times Provenance	14	0.41	0.969
	Residuals	134		

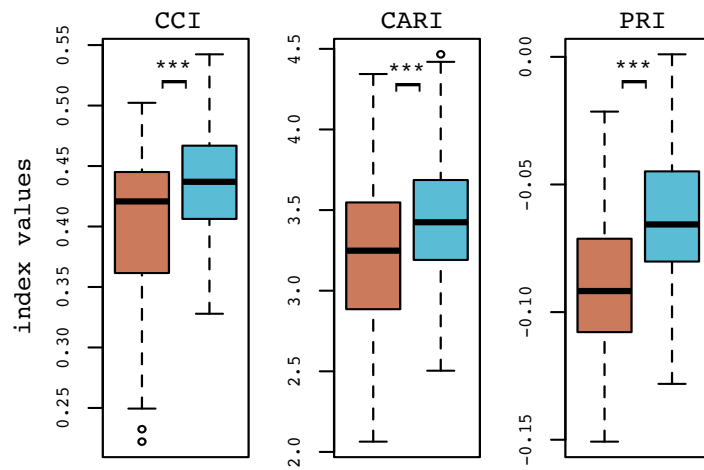
Table 3.6: One-way ANOVA table on linear model with spectral indices related to biomass and wax as dependent observation and length, group provenance and the interaction treatment \times provenance as independent factors during the first drought period. Significant values are in bold ($p \leq 0.05$).

Index	Factor	DF	F value	p value
NDLMA	Length	1	9.28	0.003
	Treatment	1	0.21	0.646
	Provenance	15	1.17	0.300
	Treatment \times Provenance	14	1.07	0.394
	Residuals	133		
NDNI	Length	1	1.58	0.211
	Treatment	1	0.18	0.670
	Provenance	15	1.95	0.024
	Treatment \times Provenance	15	0.74	0.737
	Residuals	135		
NDLI	Length	1	0.33	0.569
	Treatment	1	3.80	0.053
	Provenance	15	2.25	0.007
	Treatment \times Provenance	15	0.91	0.555
	Residuals	135		
CAI	Length	1	37.80	< 0.001
	Treatment	1	1.63	0.204
	Provenance	15	1.26	0.237
	Treatment \times Provenance	15	0.82	0.654
	Residuals	134		
EWI	Length	1	27.19	< 0.001
	Treatment	1	0.88	0.349
	Provenance	15	0.84	0.637
	Treatment \times Provenance	14	0.91	0.548
	Residuals	134		

a) Chlorophyll



b) Carotenoid



c) Anthocyanin

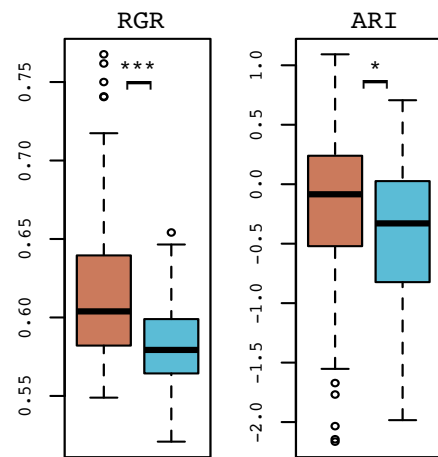


Figure 3.6: The distribution of a) chlorophyll, b) carotenoid, and c) anthocyanin indices in treatment and control group during the first drought period. ANOVA significance code is as followed: $p \leq 0.001$ '***', $p \leq 0.01$ '**', $p \leq 0.05$ '*'.

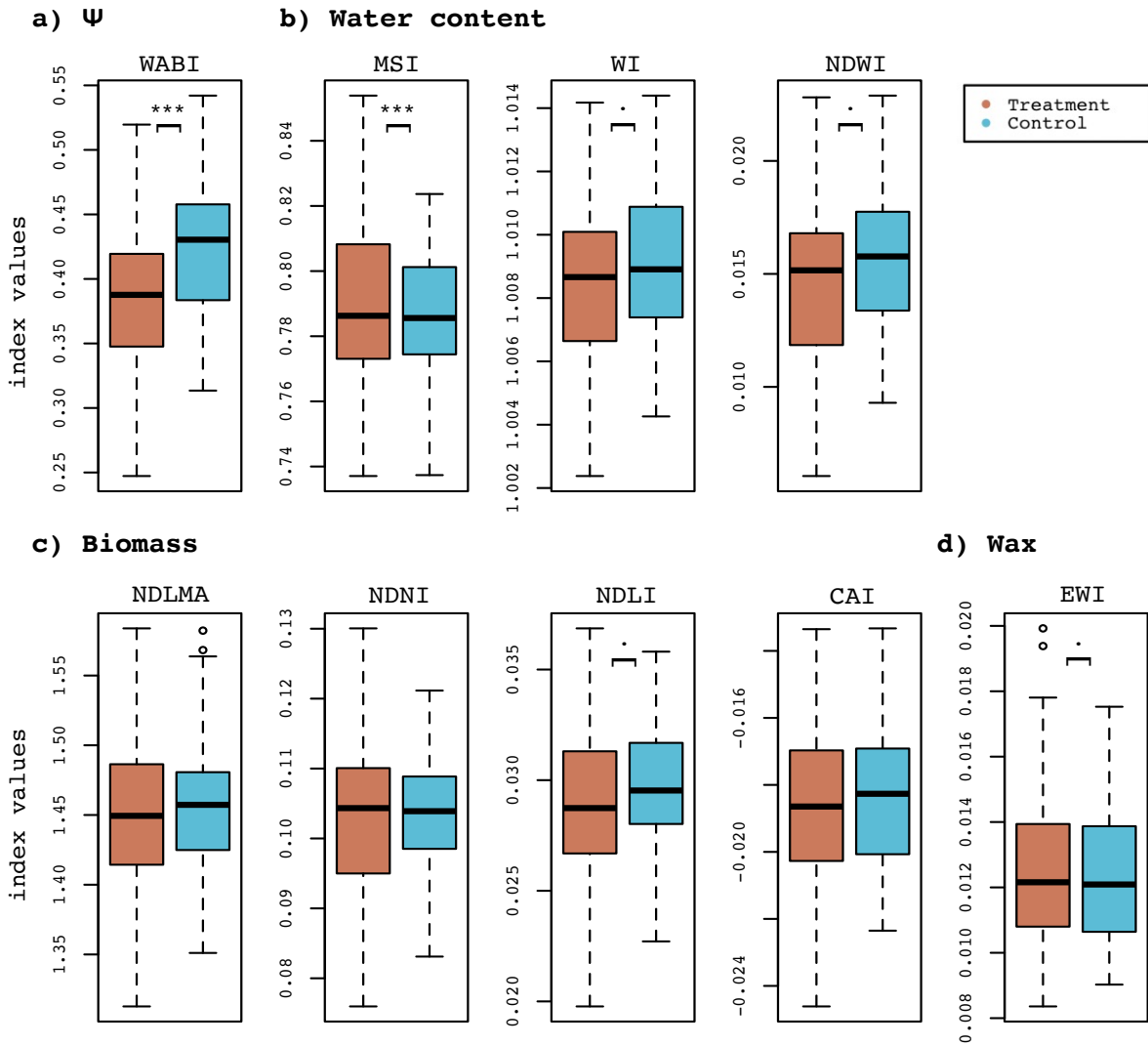


Figure 3.7: The distribution of a) water potential index, b) water content indices, c) biomass indices, and d) wax index in treatment and control group during the first drought period. ANOVA significance code is as followed: $p \leq 0.001$ '***', $p \leq 0.01$ '**', $p \leq 0.05$ '*', $p \leq 0.1$ '.'.

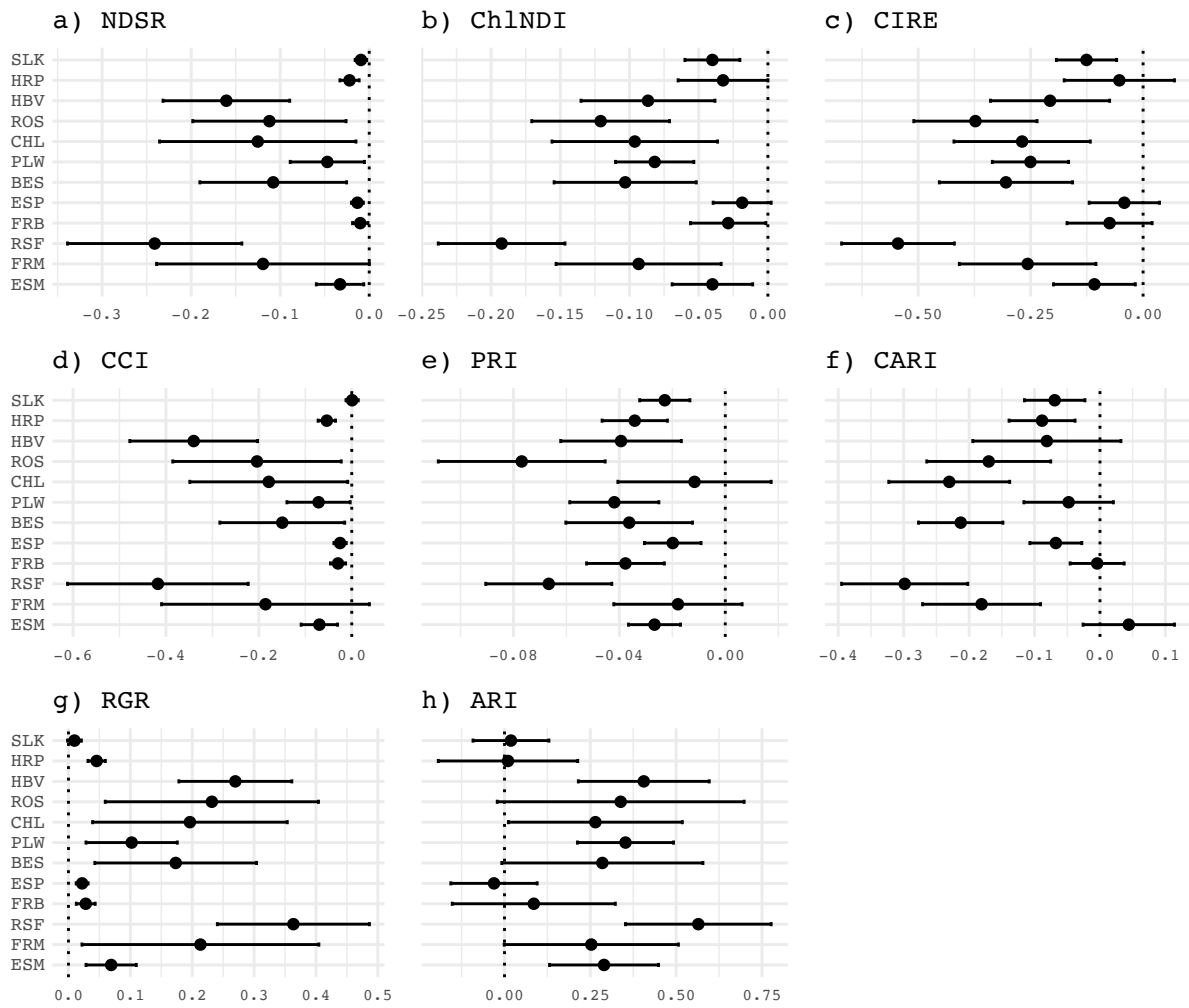


Figure 3.8: a-h) LRRs during the first drought period for indices related to pigments (n=170). a-c) LRRs of indices related to chlorophyll, d-f) LRRs of indices related to carotenoids and g-h) LRRs of indices related to anthocyanin. Y-axis represents provenances arranged in ascending order of mean annual precipitation. X-axis are effect sizes $\pm 1\sigma$ (LRR).

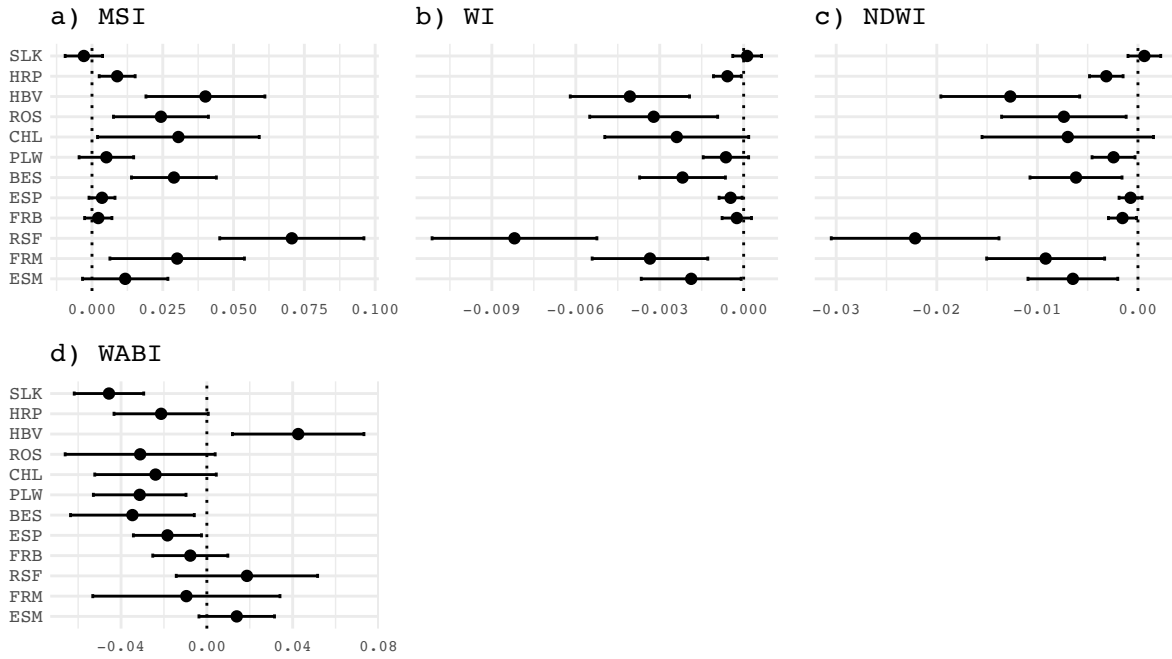


Figure 3.9: a-d) LRRs during the first drought period of indices related to water potential and water content (n=170). a) LRRs of index related to moisture stress, b-c) LRRs of indices related to water content and d) LRRs of index related to water potential. Y-axis represents provenances arranged in ascending order of mean annual precipitation. X-axis are effect sizes $\pm 1\sigma$ (LRR).

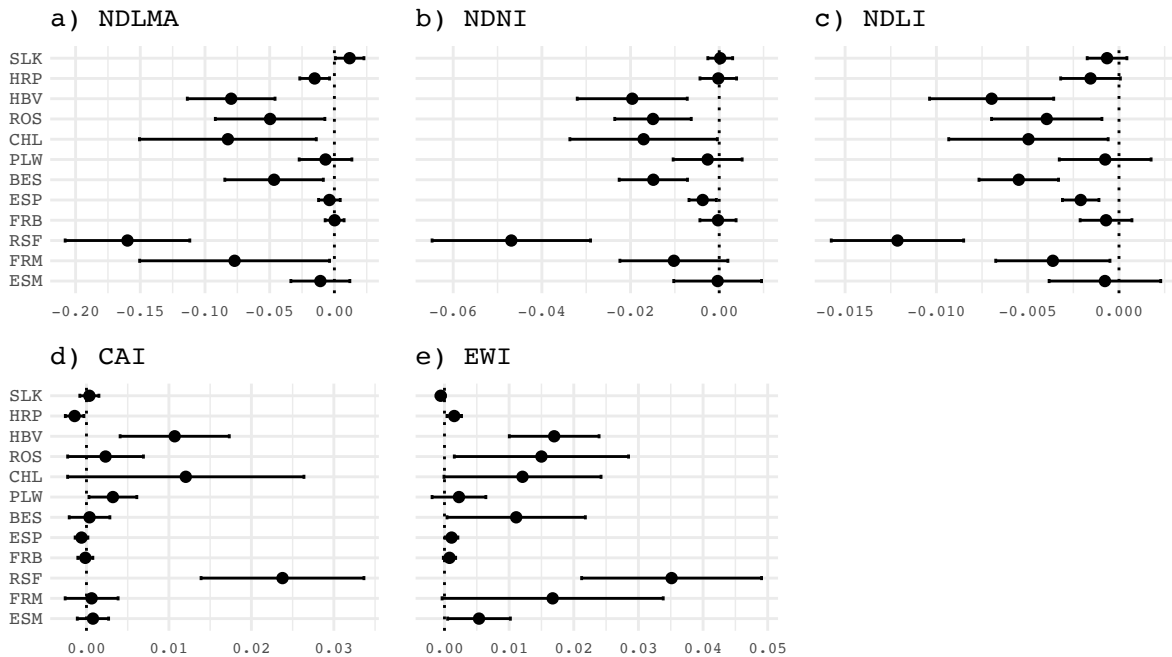


Figure 3.10: a-d) LRRs of indices related to biomass and e) LRRs of index related to epicuticular wax (n=170). Y-axis represents provenances arranged in ascending order of mean annual precipitation. X-axis are effect sizes $\pm 1\sigma$ (LRR).

3.4 Treatment effects on leaf traits derived from the PROSPECT-D inversion

We regressed six PROSPECT-D inverse modelled traits on length, treatment, provenance and the interaction treatment \times provenances and applied one-way ANOVA during the first drought period. C_{ab} was significantly decreased in the treatment group, while C_{car} and ratio C_{ab}/C_{car} also showed a decrease (Figure 3.11 and Figure 3.12). We found a significant effect of length for C_{ab} and for C_{ab}/C_{car} . There was no significant differences for EWT and LMA between control and treatment group. However, we found an effect of provenance for EWT with the mean grouping summarized in Table A.2. We did not find any significant differences for the other traits in the provenance and the interaction treatment \times provenance (Table 3.7).

Figure 3.13 shows the LRRs of the PROSPECT-D-derived leaf traits during the first drought period. We observed a general negative direction for all provenances in C_{ab} and C_{car} and their ratio (Figure 3.13a-b,d). This implied a decrease in both chlorophyll and carotenoid content, however, the corresponding magnitude was low. C_{ant} showed a positive direction in most provenances but a few showed negative responses, implying a decrease in anthocyanin content in only some provenances (Figure 3.13c). The LRRs of EWT and LMA further showed no general direction as many provenances and their standard deviations were located around zero (Figure 3.13e-f). There was no general direction of the effect sizes for the moisture stress and water content related indices (Figure 3.9a-c). However, the water potential index had slightly positive and negative responses (Figure 3.9d).

Table 3.7: One-way ANOVA table on linear model with inverse modelled traits as dependent observation and length, group provenance and the interaction treatment \times provenance as independent factors during the first drought period. Significant values are in bold ($p \leq 0.05$).

Index	Factor	DF	F value	p value
C_{ab}	Length	1	8.00	0.005
	Treatment	1	46.60	< 0.001
	Provenance	15	1.62	0.766
	Treatment \times Provenance	15	0.89	0.573
	Residuals	129		
C_{car}	Length	1	3.23	0.975
	Treatment	1	17.32	< 0.001
	Provenance	15	1.49	0.118
	Treatment \times Provenance	15	0.93	0.53
	Residuals	133		
C_{ant}	Length	1	4.14	0.044
	Treatment	1	0.58	0.448
	Provenance	15	0.65	0.828
	Treatment \times Provenance	15	0.71	0.753
	Residuals	129		
EWT	Length	1	0.63	0.430
	Treatment	1	1.03	0.312
	Provenance	15	1.77	0.046
	Treatment \times Provenance	15	0.76	0.718
	Residuals	134		
LMA	Length	1	0.77	0.381
	Treatment	1	0.47	0.493
	Provenance	15	1.44	0.139
	Treatment \times Provenance	14	0.75	0.726
	Residuals	134		
C_{ab}/C_{car}	Length	1	17.01	< 0.001
	Treatment	1	34.04	< 0.001
	Provenance	15	1.15	0.320
	Treatment \times Provenance	14	1.44	0.146
	Residuals	125		

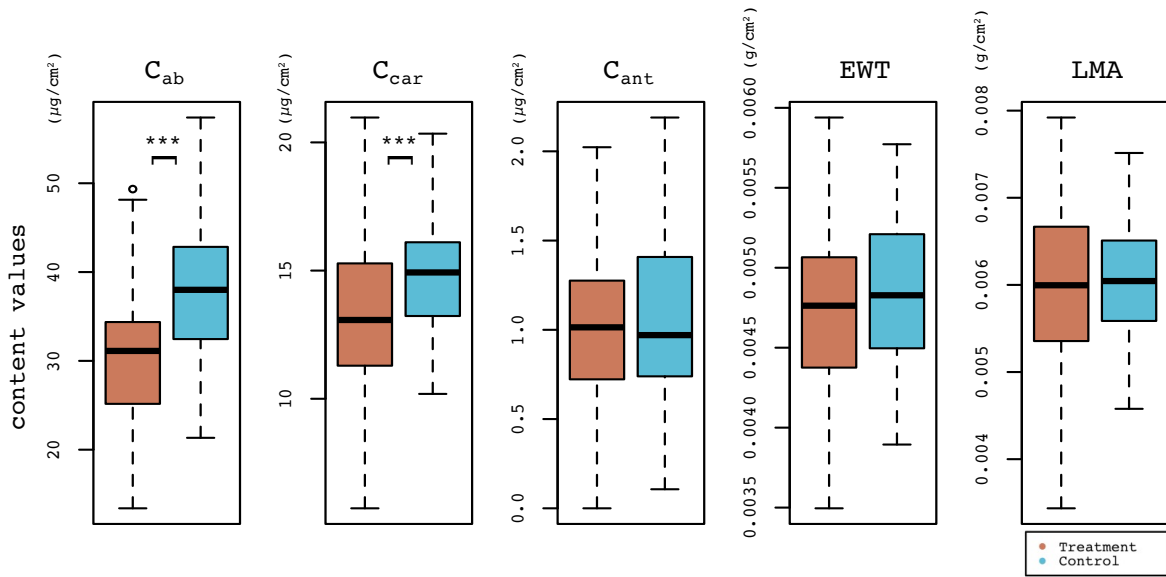


Figure 3.11: The distribution of PROSPECT-D inverse modelled leaf traits in treatment and control group during the first drought period. ANOVA significance code is as followed: $p \leq 0.001$ '***', $p \leq 0.01$ '**', $p \leq 0.05$ '*'.

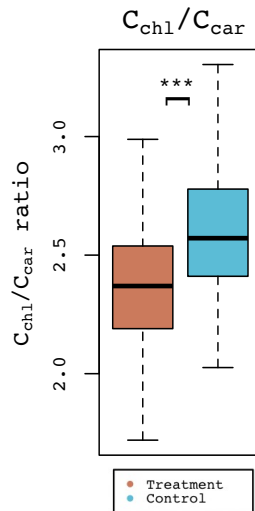


Figure 3.12: The distribution of C_{ab}/C_{car} in treatment and control group during the first drought period. ANOVA significance code is as followed: $p \leq 0.001$ '***', $p \leq 0.01$ '**', $p \leq 0.05$ '*'.

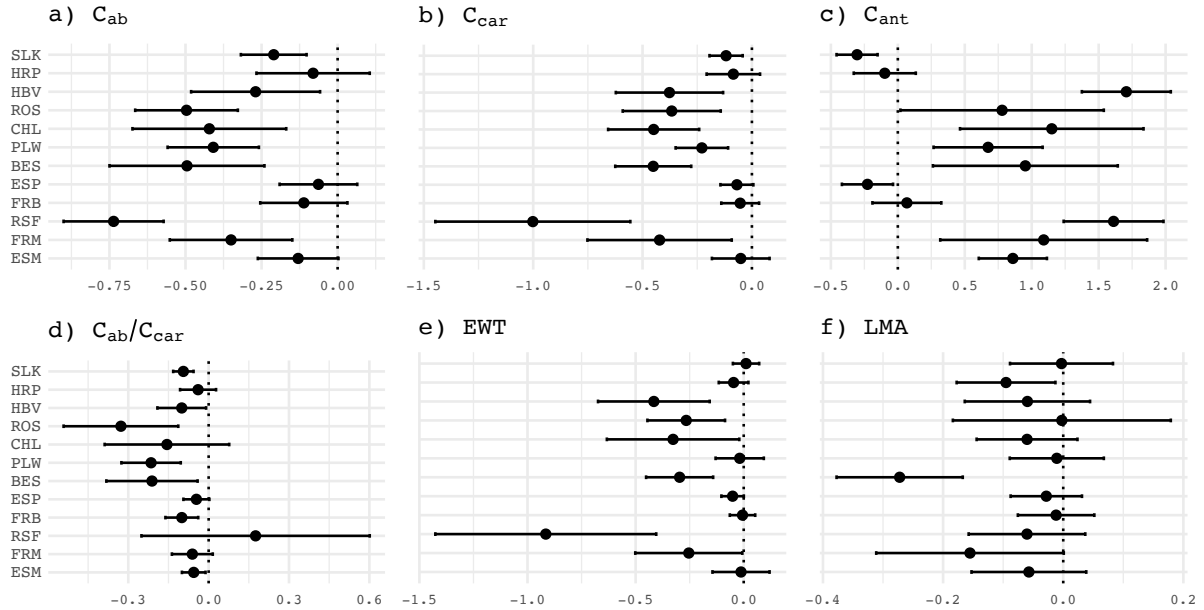


Figure 3.13: a-f) LRRs during the first drought period for PROSPECT-D inverse modelled leaf traits ($n=170$). a-d) LRRs of pigment content, e) of EWT, and f) of LMA. Y-axis represents provenances arranged in ascending order of mean annual precipitation. X-axis are effect sizes $\pm 1\sigma$ (LRR).

3.5 Uncertainties and biological variation

3.5.1 Absolute measurement uncertainties were small over the whole spectrum.

We quantified the absolute measurements uncertainties associated with the leaf clip over repeated reflectance measurements throughout the whole experiment. Over the entire spectral range, we found several mean uncertainty maxima at 350 nm, 750 nm, 1400 nm, 1880 nm, and 2500 nm. The 350 nm global maximum and the 2500 nm maximum corresponded to sensor limits, the 750 nm maximum was located on the red-edge while the 1400 nm and 1880 nm maxima were near to water absorption regions. The highest uncertainty was found in the 350 to 400 nm region with the maximum of $\approx 0.0052 \pm 0.0020$ reflectance units. The noise in this region was due to the low quantum efficiency of the VNIR detector in combination with the halogen lamp (Petibon et al., 2021). Mean absolute uncertainty across all wavelengths without the 350 to 400 nm region was 0.0003 ± 0.0002 (Figure 3.14).

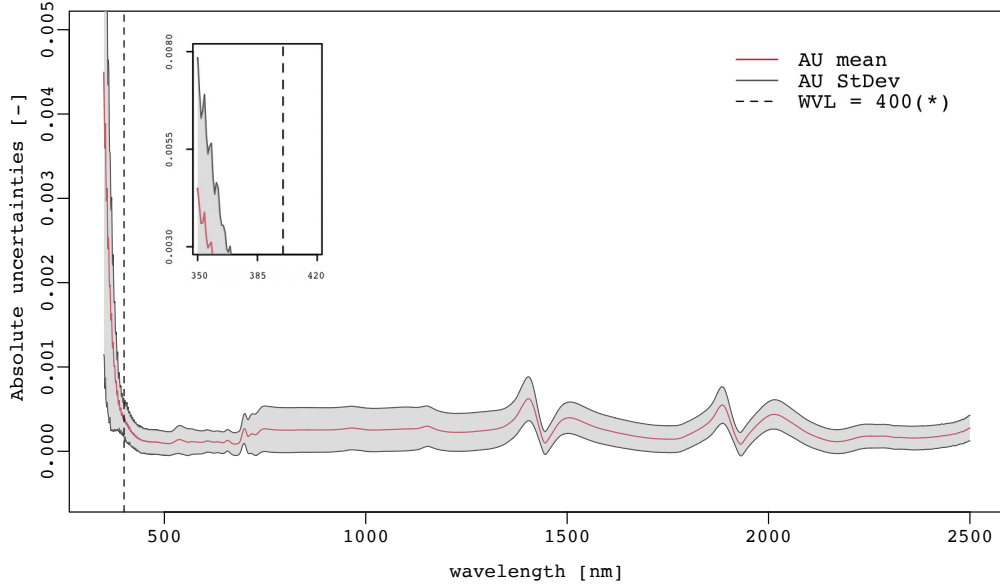


Figure 3.14: Absolute uncertainties of the field spectrometer readings ($n=1317$) over the whole spectral range of 350 to 2500 nm. The spectral data from 350 to 400 nm were discarded due to high uncertainty. *Dashed line indicates $\mu = 400$ nm.

3.5.2 Spectral variation differed throughout the measurement period and across spectral domains.

We calculated the spectral variation V_s from measurements done in June, July, and September using a control block consisting of 18 seedlings. These seedlings did not experience any treatment and naturally expressed phenology. The mean standard deviation for R of all wavelengths during the measurement period was 0.031 reflectance units. They varied across June (0.031), July (0.013) and September (0.043) (Figure 3.15a-d). This indicates that the July measurements exhibited the smallest variation, whereas September measurements had the highest variation. The biological variation V_b exhibited similar patterns. Mean V_b of all wavelengths during the measurement period was 15.45% and varied across June (15.19%), July (5.85%) and September (18.28%). Mean U_{rel} of all wavelengths during the measurement period was $0.096 \pm 0.048\%$ and remained similar throughout the measurements: June ($0.096 \pm 0.048\%$), July ($0.101 \pm 0.045\%$) and September ($0.089 \pm 0.045\%$). The U_{rel} across all wavelengths represented $0.83 \pm 0.66\%$ of the V_s on average with a maximum of 7.24% during the measurement period and also varied across June ($0.83 \pm 0.66\%$, max. 7.48%), July ($1.8 \pm 1.26\%$, max. 11.81%) and September ($0.59 \pm 0.53\%$, max. 6.29%) (Figure 3.15e-h). We found several maxima of V_b which roughly corresponded to the maxima of U_{rel} , namely around 680 nm, 1420 nm and 1920 nm. Nevertheless, the global maximum of V_b across the spectrum might vary. These maxima indicated spectral domains in which the variation is governed by V_b where V_b could reach up to 54.90% (680 nm) in June, 20.10% (680 nm) in July, and 65.75% (1920 nm) in September. The month of July generally displayed the lowest spectral variation.

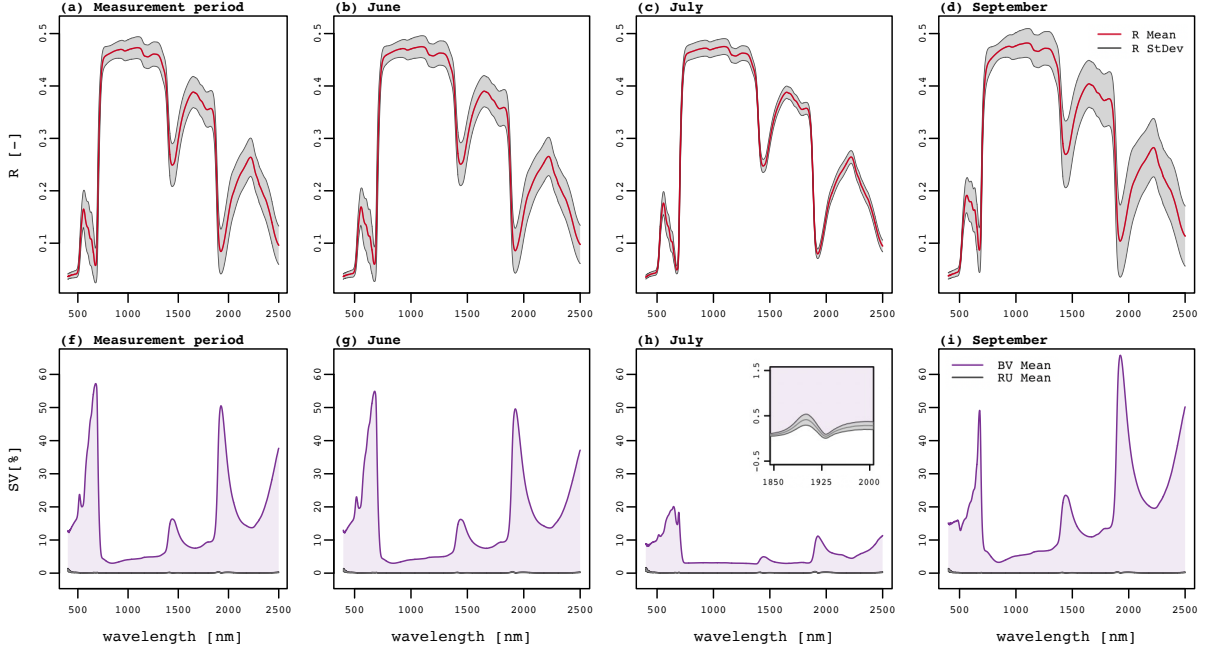


Figure 3.15: a-d) Spectral variation (SV) over the measurement period. a) SV over the entire measurement period ($n=54$) and SV for each b) June ($n=18$), c) July ($n=18$) and d) September ($n=18$). e-h) Biological variation (BV) and relative uncertainty (RU) over the entire measurement period. e) BV over the measurement period ($n=54$) and BV for each f) June ($n=18$), g) July ($n=18$) and h) September ($n=18$).

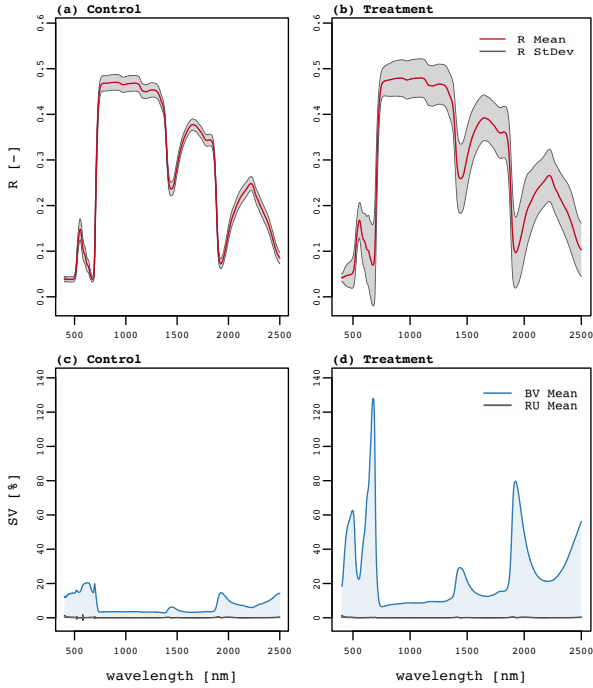
3.5.3 Spectral variation differed between drought-treated and control group.

We then calculated the spectral variation for both drought periods by treatment groups. The samples consisted of one measurement round of all seedlings ($n=180$) towards the end of the drought periods. In the first drought, the mean standard deviation for R of all wavelengths was 0.014 reflectance units for the control group and 0.054 reflectance units for the treatment group (Figure 3.16a-b), spectral variation was thus greater in the treatment group. Mean V_b of both group varied. The control group exhibited 7.23% and the treatment group 26.71% of V_b , which is greater than during the measurement period. Mean U_{rel} were consistent in both control group ($0.115 \pm 0.061\%$) and treatment group ($0.110 \pm 0.068\%$). The U_{rel} represented $0.18 \pm 0.96\%$ of the V_s on average with a maximum of 7.27% during the first period and differed with the treatment group ($0.51 \pm 0.34\%$, max. 4.49%) (Figure 3.16c-d). We located the V_b and U_{rel} maxima at the same spectral domains as in the measurement periods (680 nm, 1420 nm, 1920) (Figure 3.15e-h). Nevertheless, we found an additional maximum at around 500 nm in the treatment group. The V_b global maximum was substantially higher in the treatment group (128.11% at 680 nm) compared to the global maximum in the control group (20.37% at 680 nm) and substantially higher to the global maxima in the measurement period.

(Figure 3.16e-l) illustrates the spectral variation for the second drought period with four treatment groups. The mean standard deviation for R of all wavelengths were as followed: CC group:

0.013 reflectance units, CT group: 0.047 reflectance units, TC group: 0.065 reflectance units, and TT group: 0.036 (Figure 3.16a-b). Mean V_b in CC group (6.22%) is considerably lower than in the CT (19.97%), TC (27.39%) and TT (16.58%) group. Mean U_{rel} in CC group is $0.14 \pm 0.16\%$, while it was consistent between CT group ($0.10 \pm 0.09\%$), TC group ($0.10 \pm 0.06\%$), and TT group ($0.14 \pm 0.05\%$). The U_{rel} represented $2.34 \pm 1.24\%$ of the V_s on average with a maximum of 12.36% for the CC group. It was consistent in the other groups: CT ($0.58 \pm 0.52\%$, max. 6.90%), TC ($0.45 \pm 0.44\%$, max. 5.83%), and TT ($0.74 \pm 0.61\%$, max. 7.22%) (Figure 3.16i-l). The same maxima location for U_{rel} and V_b were found as in the first drought. CC group exhibited the lowest global maximum with 21.41% (680 nm) in V_b compared to the relatively consistent CT group (99.29% at 680 nm), TC group (113.00% at 680 nm) and TT group (76.04% at 680 nm).

First Drought



Second Drought

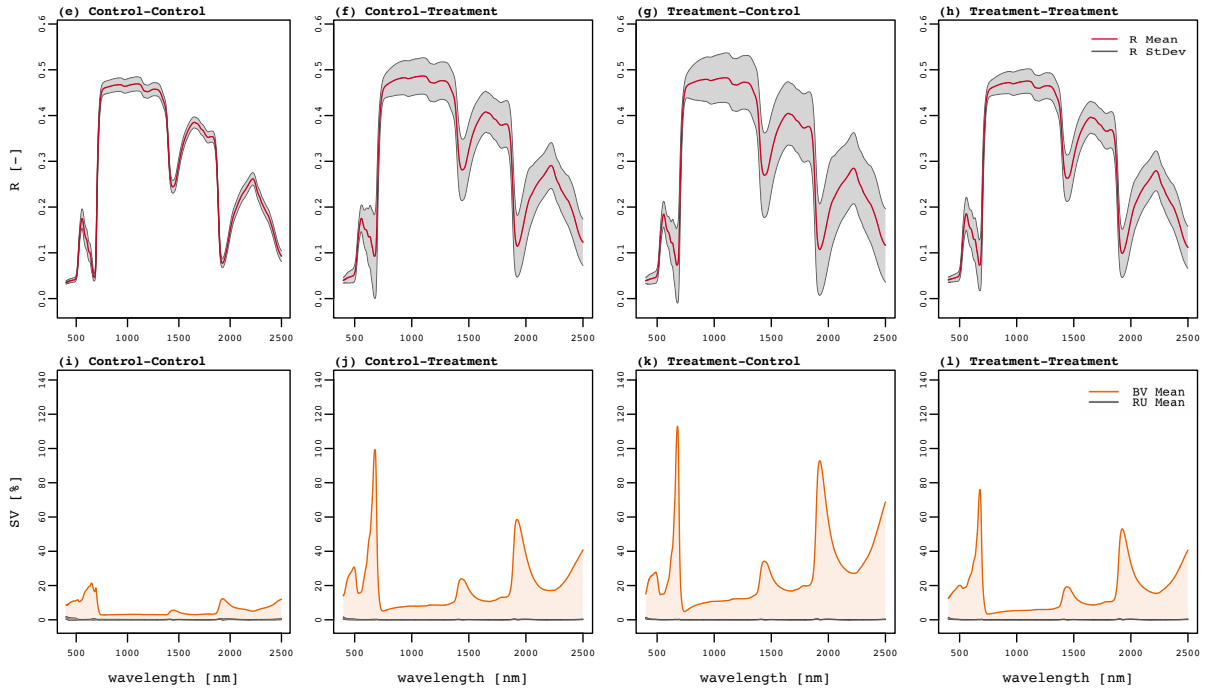


Figure 3.16: a-d) SV, BV and RU of the first drought period and e-l) SV, BV and RU of the second drought period. a-b) SV of each control (n=90) and treatment group (n=90) and c-d) BV and RU of control (n=90) and treatment (n=90) group. e-h) SV of each treatment group: control-control (CC) (n=18), control-treatment (CT) (n=72), treatment-control (TC) (n=18), treatment-treatment (TT) (n=72). i-l) BV and RU of each group: control-control (CC) (n=18), control-treatment (CT) (n=72), treatment-control (TC) (n=18), treatment-treatment (TT) (n=72).

3.6 Comparison between spectral indices, leaf traits and validation data

3.6.1 Spectrally-derived indices correlate with leaf traits from PROSPECT-D.

Figure 3.17 shows the relationship between leaf traits from the PROSPECT-D inversion and spectral indices used to estimate the relative presence of leaf traits. For C_{ab} , EWT, and LMA, we used one measurement round of all seedlings (n=180) before the first drought period while we used a dataset before (mid-June) and after the drought periods (mid-September) for C_{ant} , C_{car} and the ratio C_{ab}/C_{car} to estimate the indices' performance at different time stamps. We estimated C_{chl} with the polynomial transformation of M values measured with SPAD, which correlated fairly with the modelled C_{ab} ($R^2 = 0.488$). From the three indices related to chlorophyll, we found that CIre ($R^2 = 0.979$) performed slightly better than ChlNDI ($R^2 = 0.962$) and NDSR performed poorly ($R^2 = 0.118$) (Figure 3.17a).

We used four different indices which are related to water content to estimate their relationship to PROSPECT-D-derived EWT. WABI performed poorly ($R^2 = 0.003$), which is due to the fact that it does not stand as a proxy for water content per se but for water potential. MSI, which is an index related to moisture stress, showed the strongest relationship with EWT ($R^2 = 0.781$) while NDWI ($R^2 = 0.320$) and WI ($R^2 = 0.356$) showed fair relationships with EWT (Figure 3.17b). Furthermore, NDLMA had a mediocre relationship with $R^2 = 0.286$ to LMA (Figure 3.17c).

Anthocyanin content as expressed by C_{ant} increased from before and after the drought periods, which is also reflected in both anthocyanin related indices RGR and ARI. RGR performed comparatively poorly before the drought ($R^2 = 0.294$) than after the drought periods ($R^2 = 0.665$). ARI generally performed better than RGR and ARI has a fair relationship before the drought ($R^2 = 0.547$) as opposed to a stronger relationship after the drought periods ($R^2 = 0.864$) with anthocyanin (Figure 3.17d). CARI, which is an index related to carotenoid, and C_{car} showed both a decrease in index value and carotenoid content respectively from before the drought to after the drought periods. CARI performed better after the drought periods ($R^2 = 0.574$) than before the first drought period ($R^2 = 0.325$) (Figure 3.17e). PRI and CCI are both indices related to the ratio of chlorophyll to carotenoid C_{ab}/C_{car} . The ratio decreased in both CCI and PRI after the drought periods suggesting an asymmetric decrease of chlorophylls to carotenoids. PRI performed generally better before ($R^2 = 0.796$) and after ($R^2 = 0.461$) the drought periods compared to the poorly performing CCI before ($R^2 = 0.133$) and after ($R^2 = 0.003$) the drought periods. (Figure 3.17f).

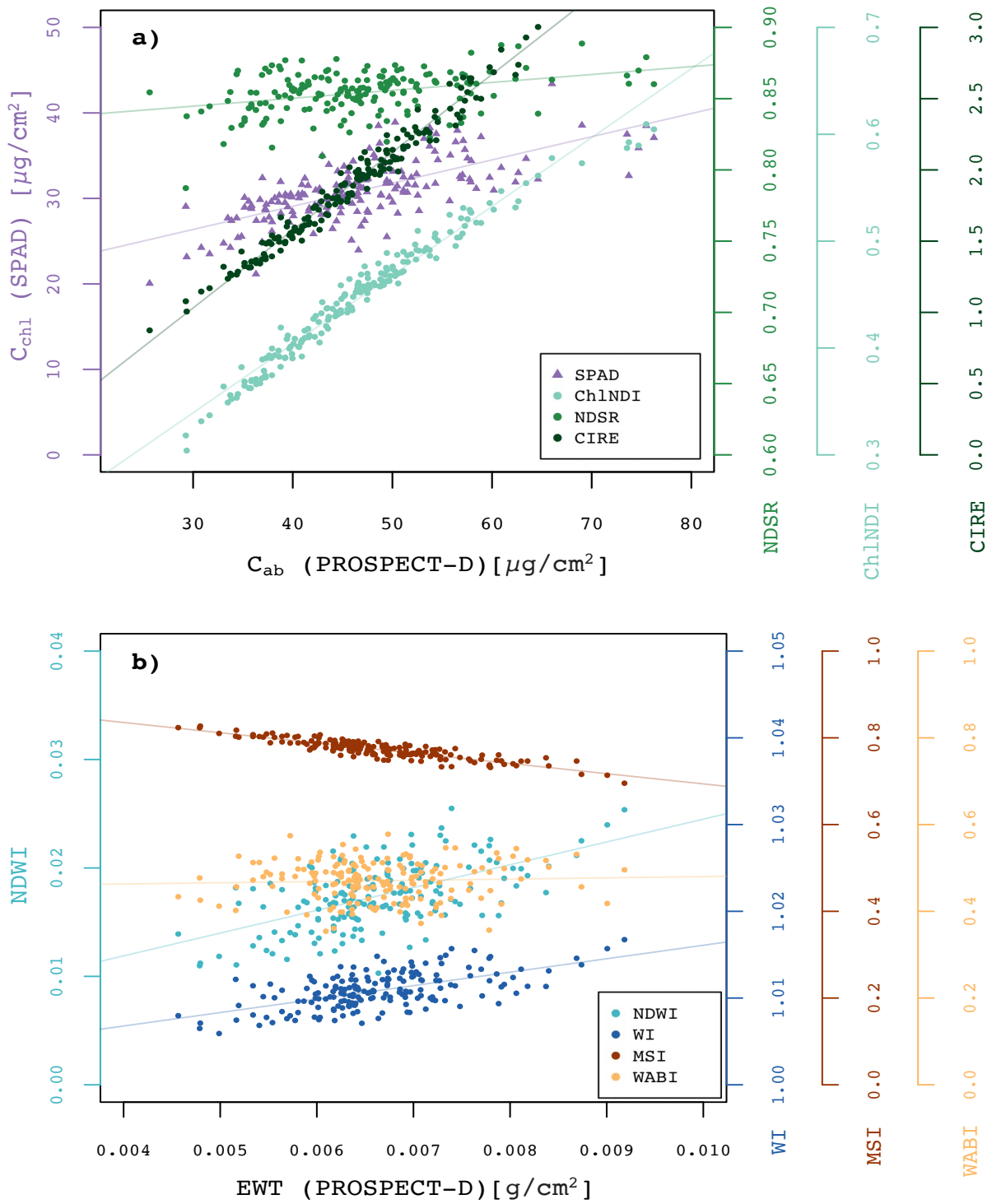


Figure 3.17: a) C_{chl} from SPAD and chlorophyll related indices (NDSR, ChlNDI, CIre) against C_{ab} from PROSPECT-D. $R^2(C_{chl}) = 0.488$, $R^2(\text{NDSR}) = 0.118$, $R^2(\text{ChlNDI}) = 0.962$, $R^2(\text{CIre}) = 0.979$. b) Water potential (WABI) and water content related indices (NDWI, WI, MSI) against EWT from PROSPECT-D. $R^2(\text{NDWI}) = 0.320$, $R^2(\text{WI}) = 0.356$, $R^2(\text{MSI}) = 0.781$, $R^2(\text{WABI}) = 0.003$.

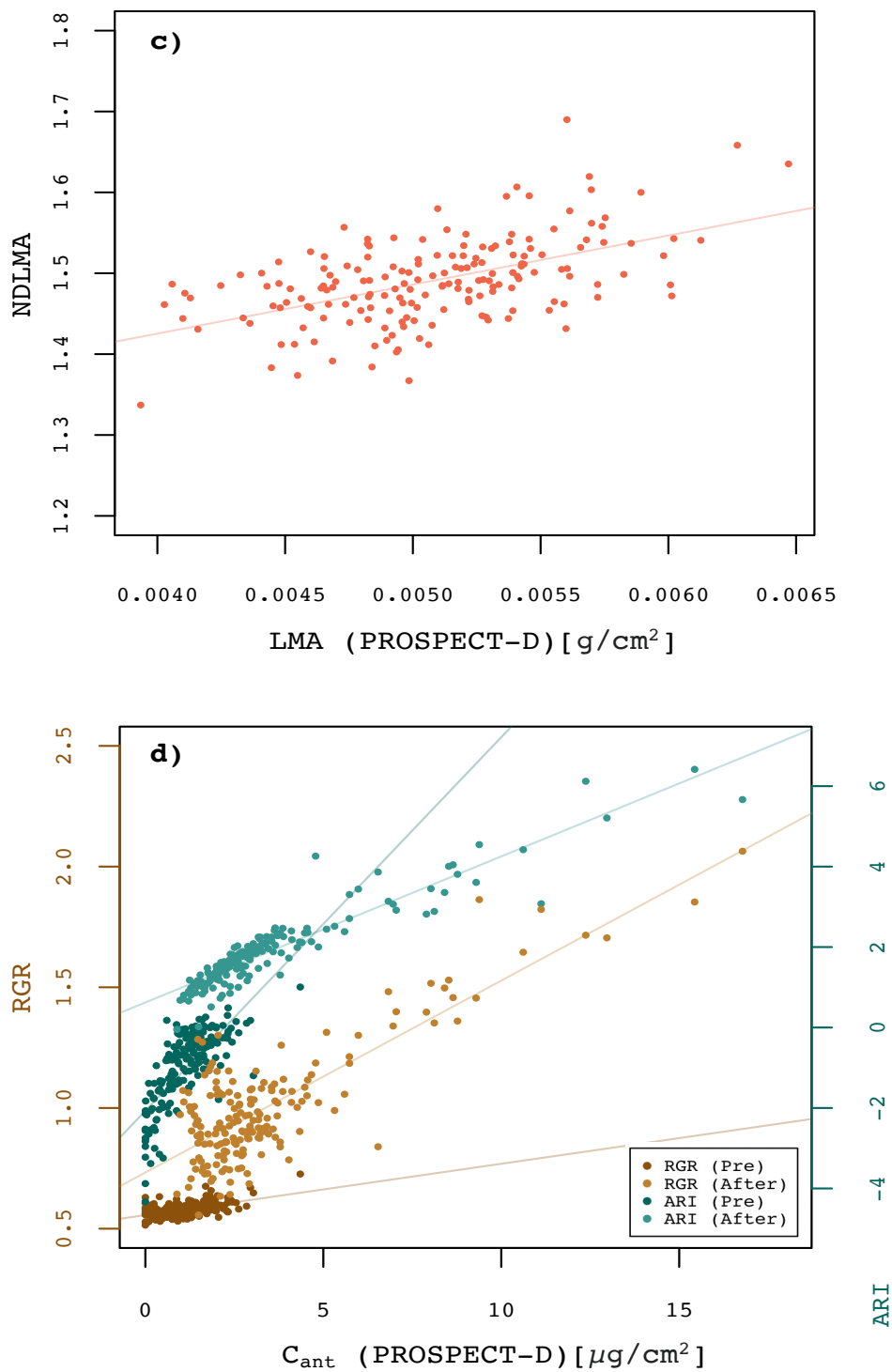


Figure 3.17: (Continued). c) NDLMA index against LMA from PROSPECT-D. R^2 (NDLMA) = 0.286. d) Anthocyanin related indices (RGR, ARI) from before and after the drought periods against C_{ant} from PROSPECT-D. R^2 (RGR (Pre)) = 0.294, R^2 (RGR (After)) = 0.665, R^2 (ARI (Pre)) = 0.547, R^2 (ARI (After)) = 0.864.

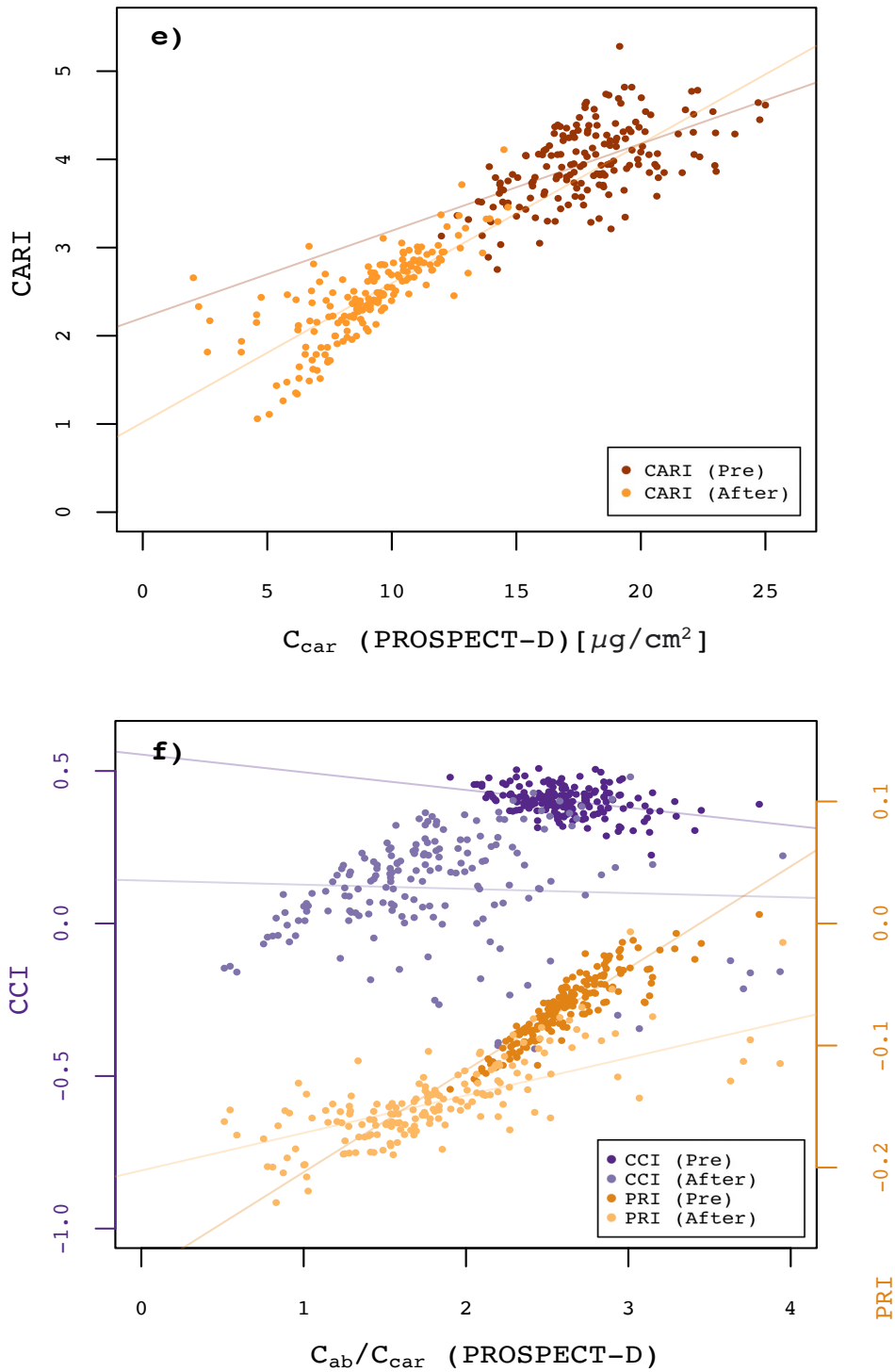


Figure 3.17: (Continued). e) Carotenoid related index (CARI) from before and after the drought periods against C_{car} from PROSPECT-D. R^2 (CARI (Pre)) = 0.325, R^2 (CARI (After)) = 0.574. f) Carotenoid related indices (CCI, PRI) from before and after the drought periods against C_{ab}/C_{car} derived from PROSPECT-D. R^2 (CCI (Pre)) = 0.133, R^2 (CCI (After)) = 0.003, R^2 (PRI (Pre)) = 0.796, R^2 (PRI (After)) = 0.461.

3.6.2 Measured leaf traits have a moderate to strong relationship with leaf traits from PROSPECT-D inversion.

We conducted chromatographic separation for 20 leaf samples (Figure A.11) and we were able to identify main compounds based on retention time, standard spectra (Table A.4) and the decision tree proposed by Petibon and Wiesenberg (2022). However, we failed to retrieve anthocyanins due to either co-elution with unknown compounds or non-existence in all samples except for one case (Figure A.10). We also observed co-elution in α - and β -carotene due to unsuccessful separation for which we used α -carotene standard calibration to integrate.

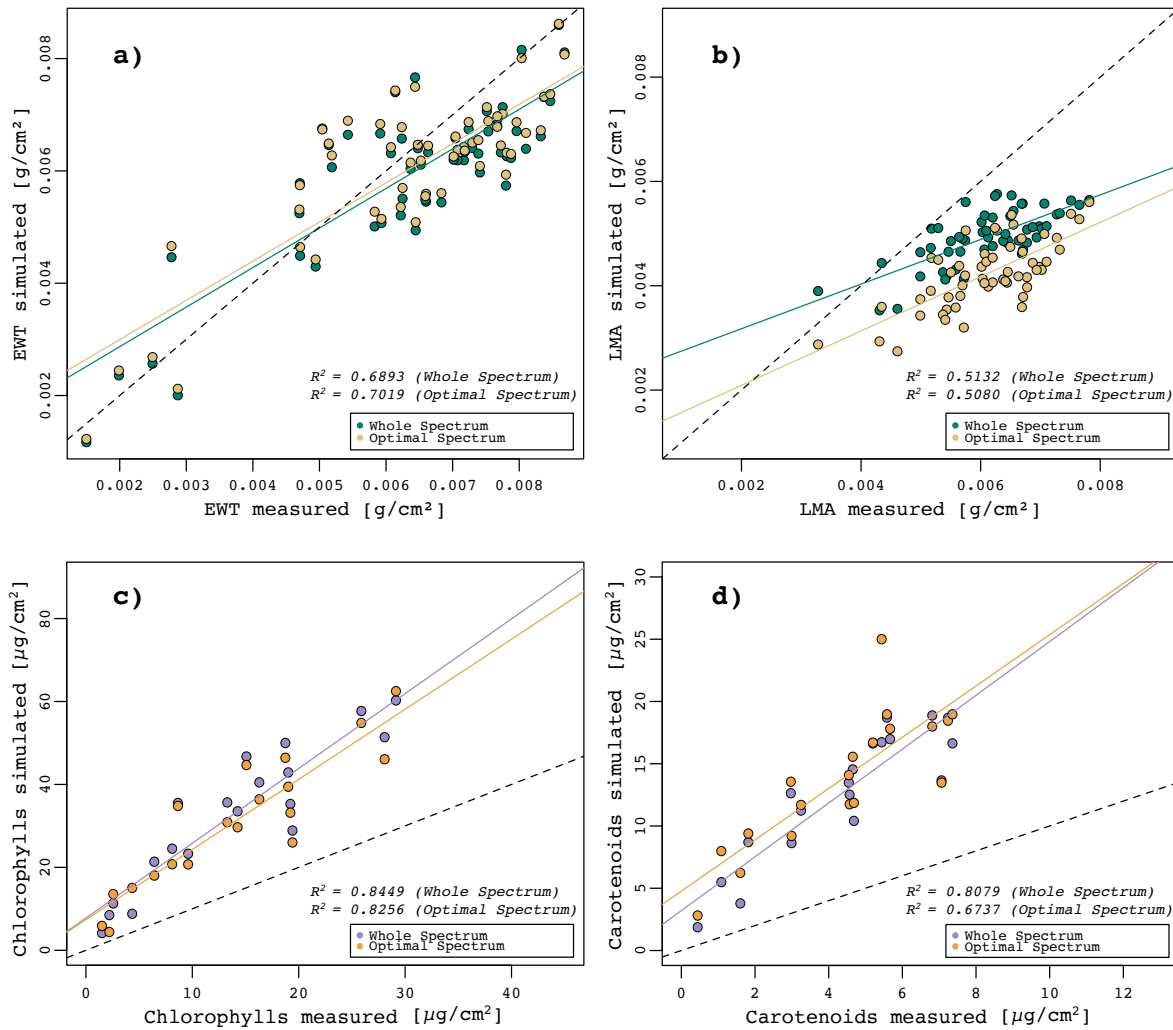


Figure 3.18: Linear regression of measured (a) EWT, (b) LMA, (c) C_{ab} , and (d) C_{car} against their simulated values from PROSPECT-D inversion over the whole and optimal spectrum.

Table 3.8: Summary of the measured (HPLC) and simulated (PROSPECT-D) leaf traits with each whole and optimal spectra input and corresponding accuracy parameters R^2 , RMSE, NRMSE. Sample size is n , intercept is β_0 and slope is β_1 . LMA and EWT are specified in $g.cm^{-2}$ while C_{ab} and C_{car} are specified in $\mu g.cm^{-2}$. Significance code is as followed: $p \leq 0.001$ '***', $p \leq 0.01$ '**', $p \leq 0.05$ '*'.

PROSPECT-D simulated data									
trait	spectra input	n	mean	β_0	β_1	R^2 (mult.)	mean	RMSE	NRMSE
EWT	whole	55	0.0064	0.0015**	0.7044***	0.6893	0.0060	0.00043	0.0954
	optimal	55	0.0064	0.0016***	0.6979***	0.7019	0.0061	0.00036	0.0798
LMA	whole	55	0.0061	0.0023***	0.4278***	0.5132	0.0049	0.00128	0.2823
	optimal	55	0.0061	0.0010*	0.5208***	0.5080	0.0042	0.00193	0.4246
C_{ab}	whole	18	13.781	7.7932*	1.8033***	0.8449	32.645	6.48371	0.1156
	optimal	18	13.781	7.3954*	1.6910***	0.8256	30.699	6.52164	0.1123
C_{car}	whole	18	4.3671	3.2030*	2.1610***	0.8079	12.640	2.17772	0.1281
	optimal	18	4.3671	4.7687*	2.0593***	0.6737	13.769	2.96171	0.1335

All of the estimated traits showed moderate to high correlation accuracy ($R^2 = 0.5080 - 0.8849$). C_{ab} whole spectrum showed the highest and LMA optimal spectrum the lowest (Table 3.8). Out of both the whole spectrum and optimal spectrum input, the whole spectrum performed better in the estimation of LMA ($R^2 = 0.5132$), C_{ab} ($R^2 = 0.8449$) and C_{car} ($R^2 = 0.8079$). EWT was better estimated with the optimal spectrum ($R^2 = 0.7019$). NRMSE for all spectral inputs and estimated traits varied between 7.98% and 42.4% and were therefore high. However, only estimated LMA exhibited a high NRMSE for whole spectrum (42.4%) and optimal input (28.2%), whereas C_{ab} (NRMSE = 11.2-11.4%) and C_{car} (NRMSE = 12.8-13.3%) showed high accuracy for both spectral inputs. EWT exhibited the highest accuracy for optimal input (NRMSE = 7.98%) and for whole input (NRMSE = 9.54%). Furthermore, there were systemic underestimation in both simulated EWT and LMA ($\beta_1 < 1$) and overestimation in both simulated C_{ab} and C_{car} ($\beta_1 > 1$). We did not include any derivatives into the peak area integration because of the lack of their standard spectra. This may have either led to a underestimation of the absolute pigment concentration in the leaves or an overestimation in the simulated leaf traits.

Chapter 4

Discussion

4.1 Drought stress impact on leaf traits

F. sylvatica seedlings from various provenances were grouped into treatment and control group and were monitored during the first drought simulation. We quantified the variation in their spectral response with spectral indices and simulated leaf traits (PROSPECT-D inversion) at the end of the drought period.

Drought conditions altered the relative abundance of photosynthetically-active pigments. We observed a significant decrease in chlorophyll related indices (NDSR, ChINDI, CIRE) corresponding to a decrease in PROSPECT-D simulated C_{ab} in drought-treated seedlings (Table 3.2). Previous studies found a similar decrease in chlorophyll content per area in drought-stressed *F. sylvatica* with HPLC or SPAD measurements (Arend et al., 2016; Gallé & Feller, 2007; Tognetti et al., 1995). Gallé and Feller (2007), for instance, found that the activity of PSII during drought stress is down-regulated, which is supported by the reduction of chlorophyll in severely drought stressed leaves. Leaf chlorophyll content is well known to be positively correlated with photosynthetic rate (Emerson, 1929; Fleischer, 1935). However, C_{chl} as measured with SPAD in our experiment did not exhibit a decrease in chlorophyll content in spite of the observed decrease in the respective indices and C_{ab} . A major limitation of the SPAD chlorophyll meter is the need for empirical calibration methods, which can be linear, exponential or polynomial models to convert unitless data to chlorophyll concentration (Coste et al., 2010). The calibration method for our data, however, is independent from species at a cost of accuracy (Brown et al., 2022; Maxwell & Johnson, 2000). Richardson et al. (2002) found that spectral indices consistently outperformed SPAD measurements, which agrees with our findings (Figure 3.18a). SPAD further only detects chlorophyll concentration at one point of the leaf, which also varies within the leaf (Sun et al., 2018a). The observed results are unlikely to be attributed to the calibration method, as it is generally applicable to *F. sylvatica*, and we have taken into consideration the placement of the SPAD device. Our heterogeneous block design consisted of representative seedlings from all

provenances. Hereby, the variance in C_{chl} means was explained by provenance rather than their treatment (Table 3.1). The SPAD method could detect the dark green leaf color of the Italian provenances (ITx), but not the change in pigmentation driven by drought stress.

Carotenoid content as quantified by the CARI index and C_{car} was significantly decreased in drought-treated seedlings, compared to the control group (Table 3.3). This is in line with previous findings (Gallé & Feller, 2007; Junaid et al., 2023). However, to compensate for water stress, the photosynthetic apparatus is known to change rather carotenoid composition than total content. One may observe an increased ratio of xanthophyll cycle pigments (VAZ), which are a division of the carotenoids, to chlorophyll content during water limitation (Biswal, 1995; Demmig-Adams & Adams, 1992; Merzlyak et al., 1999). VAZ contribute to dissipate excess energy in the apparatus during drought situations and are thus regarded as key pigments for photo-protection in *F. sylvatica* (Munné-Bosch & Alegre, 2000). This is consistent with our findings where the PROSPECT-D modelled ratio C_{chl}/C_{car} declines in drought-treated seedlings. Based on these observations, we infer that when plants are water stressed, the content of both chlorophylls and carotenoids decline correspondingly. However, the proportion between them changes differently, with chlorophylls tending to degrade faster than carotenoids. In agreement, we found a decline in PRI and CCI, which are spectral indices related to the chlorophyll and carotenoid ratio (Figure 3.17f) and correlated to photosynthetic capacity (Filella et al., 2009). PRI and CCI both use the 531 nm, which is indicative of the xanthophyll cycle epoxidation state transition (Gamon et al., 1992). Both were significantly decreased in drought-treated seedlings (Table 3.3).

Anthocyanins are expected to accumulate in the leaves upon exposure to water limitation (Gould, 2004). Their main protective contributions are the mediation of stressors (i.e., ROS) by antioxidant activity and light attenuation reducing excess energy similar to carotenoids (Feild et al., 2001; Landi et al., 2015; Steyn et al., 2002), and are proposed to be key regulators of drought stress tolerance (Landi et al., 2015). However, their role upon exposure to different environmental stressors is still under debate (Chalker-Scott, 1999; Steyn et al., 2002). We found a significant increase of the anthocyanin related indices RGR and ARI in drought-treated seedlings. However, we found contradictory information with PROSPECT-D modelled C_{ant} , which did not show significant differences between the control and the treatment group. This discrepancy can be partially explained by the simplistic empirical approach of spectral ratios. RGR is the result of red band divided by green bands (Table 2.2) by (Gamon & Surfus, 1999), where the red bands is solely dependent on chlorophyll absorption while the green bands depends on chlorophyll, carotenoid and anthocyanin absorption. This could potentially explain why RGR is not only influenced by anthocyanins but also by pigment composition particularly when increased chlorophyll and carotenoid concentrations influence the anthocyanin signal regardless of the actual anthocyanin concentration. Furthermore, the absorption of anthocyanin is dependent on several factors such as species, co-pigmentation and pH (Gitelson et al., 2001). As for ARI, Gitelson et al. (2001) tested the index on maple and dogwood and concluded that the applicability

of ARI on other plant species still needs to be verified. The modelled C_{ant} also showed only a minuscule amount C_{ant} compared to the range of variation in PROSPECT-D (Table 2.3) indicating a generally low signal in anthocyanins in *F. sylvatica*. This claim is backed-up by our HPLC analysis on drought-treated and control seedlings, where we did not succeed in the retrieval of anthocyanins potentially due to co-elution with unknown compounds and miniscule amount of anthocyanins. We found anthocyanins only in one specific variety of *F. sylvatica* namely *Long red* (Figure A.10), which suggests that the method is suitable to extract anthocyanins. We thus presume, that anthocyanin content was relatively low in our samples during the first drought period and its change cannot be adequately quantified. We also underline that the performed indices to retrieve anthocyanin show a dependency on the measurement period before and after the drought period, which possibly indicates a dependency on phenology (Figure 3.17d).

Moisture stress was captured with MSI, which was observed to be higher in drought-treated seedlings as expected. Many studies concerning hydraulic function in leaves observed a similar increase in MSI suggesting MSI to be a good indicator of altered plant water status (Kim et al., 2015; Zhang & Zhou, 2019). Conversely, water content related indices WI and NDWI did not change in seedlings undergoing drought stress implying no water content changes in the leaf (Table 3.5). One of the most crucial counteracting mechanisms of plants to water deficiency is the rapid regulation of stomatal conductance to prevent plant dehydration. The closure of stomata pores allow a decrease of gas-exchange through reduced water vapor transpiration and thus preserve water resources (Agurla et al., 2018; Aranda et al., 2015; Wankmüller & Carminati, 2022). *F. sylvatica*, as moderate anisohydric species, optimizes stomatal conductance under drought conditions (Peuke et al., 2002; Tardieu & Simonneau, 1998). We suspect that water content was preserved in our leaf samples through stomatal regulation and we thus could not pick up a variation in the spectral response. This view is supported by the PROSPECT-D EWT outputs which was found to be identical in drought-treated seedlings and (Table 3.7). Another measure for hydraulic functioning and water dynamics throughout a drought is the leaf water potential (Ψ), the energy state of water in a system reflecting the water's ability to move. Throughout studies, Ψ varies a lot due to different climate and soil conditions and it is strongly influenced by seasonal and diurnal changes (Bartlett et al., 2012; Czajkowski & Bolte, 2006; Dietrich et al., 2019), which resembles the anisohydric behaviour of *F. sylvatica* (Roman et al., 2015). In our experiment, we showed that WABI to be significantly decreased in the drought-treated seedlings (Table 3.5). WABI relates independent changes in photoprotective pigments involved in non-photochemical quenching (NPQ) (531 nm) and water content reflectances (around 1500 nm) which indicate stress-induced changes by Ψ (Rapaport et al., 2015). Thus, we infer that Ψ was indeed decreased in drought-treated seedlings due to the quick reactivity of NPQ by limited water availability. Conclusively, the discrepancy between changes in Ψ and no changes in water content suggests that the seedlings may be able to maintain relatively stable water content through rapid adjustments such as stomatal regulations while simultaneously varying their Ψ .

LMA can be understood as the leaf-level cost of light interception (Gutschick, 1999) and it is

a key indicator for plant strategies (Grime, 2001). An alternative way to define LMA is the accumulation of different classes of compounds such as lignin or proteins per area (Poorter & Villar, 1997). We derived LMA from reflectance data via an LMA related index (NDLMA) and via PROSPECT-D inversion and found no differences in drought-treated seedlings, implying that leaf structure hardly had time to acclimatize to our induced drought (Poorter et al., 2009). Furthermore, there is generally considerable variation within individual seedlings (Shipley, 1995), following for instance light-gradients (Anten & Hirose, 1999) or gravity gradients (Niinemets, 1997), which we did not consider during the measurements. We thus question the suitability of such measurements in our framework as we also did not find any drought induced differences in cellulose, nitrogen and lignin related indices such as CAI, NDNI and NDLI respectively (Table 3.6). We expected increased accumulation of nitrogen (He et al., 2022) and lignin (Brinkmann et al., 2003; Hu et al., 2009; Liu et al., 2018), while we expected cellulose to decrease (Hu et al., 2022).

Epicuticular waxes are located on the leaf surface and serve as protective barrier against ultraviolet light exposure and uncontrolled water diffusion (Speckert et al., 2023). As they are directly exposed to the environment, leaf waxes are expected to adjust to abiotic stressors such as drought with the aim to conserve water and resist cellular dehydration in leaves (Shepherd & Wynne Griffiths, 2006). Studies across various species such as sorghum (*Sorghum bicolor*) (Jordan et al., 1983), maize (*Zea mays*) (Premachandra et al., 1991) and tomato (*Lycopersicon esculentum*) (Xu et al., 1995) found increased quantity of wax causing a decrease in transpiration when water is limited. Deposition of wax as a response to water stress was observed to occur swiftly within a few days (Bengtson et al., 1978; Premachandra et al., 1991). Along with our expectations, we observed a slight increase of EWI in drought-treated seedlings, albeit not a significant one (Table 3.6). This can be potentially explained by alternative water conservation mechanisms such as the aforementioned stomatal regulation to cope with the imposed water stress in *F. sylvatica* or by changing the composition of the waxes rather than varying the amount (Sachse et al., 2009).

As a major effect of our experimental conditions, we found that longer seedlings tended to have lower soil moisture in both control and treatment group (Figure 3.4), potentially due to larger biomass and increased water needs. We thus cannot exclude the possibility that taller seedlings on average experienced a more severe drought due to their higher demand for water. We addressed this limitation by controlling for tree lengths within our block design and by excluding moderately wilting seedlings in the data analysis so that only visually healthy seedlings are considered in the analysis. A significant association between length and traits would indicate that the responses to drought depend on length, which we found in some cases. However, all cases tended to have a weak relationship as well as no specific direction. Along with the experimental conditions, we would like to point out that foliar water uptake through permeable cuticles in *F. sylvatica* may have been an influence on the actual drought conditions of the seedlings (Schreel et al., 2020).

4.2 Using field spectroscopy to capture leaf trait variation

Leaf spectroscopy allow the detection of species trait variation but it is governed by uncertainties depending on the measurement methods (Cavender-Bares et al., 2016; Li et al., 2023; Petibon et al., 2021). We contribute to understand this by comparing the biological variation V_b of drought-treated with control seedlings and throughout the growing season. We found that the spectral variation V_s was governed by both phenology and the simulated drought. Throughout the measurement period, the mean standard deviation was lower than the treatment group exhibited indicating that the treatment may have caused a higher variation in the seedlings' spectral fingerprints. This was particularly noticeable as V_b in the measurement period with a maximum of 65.75% in September as compared to the maximum of 128.11% in the treatment groups. We thus infer that the variation during different measurement time-points is smaller than the variation of drought-stressed seedlings. This is also evident when comparing V_b which was substantially different in control and treatment groups as well (e.g. 20.37% (680 nm) in control compared to 128.11% (680 nm) in treatment group). The relative uncertainties U_r of V_s never exceeded 13% in all datasets while the mean ranged from 0.45-2.34%. Therefore, the relative uncertainties associated with leaf reflectance across the measurement period and the treatment groups only represented a small portion of the spectral variation and thus remained negligible compared to the total variation. This finding aligns with the results of Petibon et al. (2021), who employed identical measurement devices. In light with this finding, we suggest to consider phenology when researching stressors-dependent leaf traits and to isolate its signal from the object of study.

Hyperspectral leaf spectroscopy offers a non-destructive, repeatable, and rapid measurement method of leaf traits at the intraspecific level as opposed to traditional methods and is thus a promising method in ecological research (Helsen et al., 2021; Messier et al., 2010; Siefert et al., 2015). We demonstrated that applying spectral indices to hyperspectral data is a simple method for deriving leaf trait variation, making it a valuable tool in remote sensing. However, it is crucial to note that spectral indices do not necessarily provide mechanistic explanations: Spectral indices hardly disclose the leaf physiological processes and metabolic systems underpinning the drought responses (Rapaport et al., 2015). A different approach is the inclusion of relevant physical processes. The inversion of the PROSPECT RTM simulates leaf traits based on the physical processes of light interaction with leaves (Jacquemoud & Ustin, 2019). We performed a subsequent extraction and HPLC analysis proposed by (Petibon & Wiesenberg, 2022) to establish a chromatographic profile of complex photosynthetic pigments of drought-treated and control seedlings to estimate C_{ab} and C_{car} . Our validation data between the simulated and extracted trait show a strong relationship for C_{ab} and C_{car} and a moderate relationship for EWT and LMA. This finding aligns with Spafford et al. (2021), who found similar NRMSE in their dataset when N is estimated and only R is used. The relationships of the leaf traits only vary slightly between whole and optimal spectrum except for LMA. In this case, the use

of optical subdomains or whole spectrum for the inversion depended on the performance of the validated samples as opposed to the decision tree by Spafford et al. (2021). The robustness of the retrieval of leaf traits may also depend on the availability of transmittance T data, which can be retrieved with an integrating sphere measurement device for instance (Petibon et al., 2021). Both R and T combined carry the most information for PROSPECT inversion (Spafford et al., 2021).

4.3 Intraspecific variation in drought stress responses

The experiment demonstrated a variety of physiological responses to decreased water availability. We hypothesized that there is intraspecific variation in such drought responses depending on the seedling's provenance. We tested the interaction provenance x treatment during the first drought period for each spectral index and modelled leaf trait. Against expectations, our results reveal that drought-treated seedlings did not exhibit responses depending on their provenance indicating a homogeneous response in the measured traits across all provenances. And yet, some studies on intraspecific variation found small performances differences in varying populations of *F. sylvatica* in ecophysiological stress relevant to water stress such as photosynthetic rate and stomatal conductance (Cocozza et al., 2016; González De Andrés et al., 2021), but the variation in traits across species do not reflect a pattern at the intraspecific level (Sánchez-Gómez et al., 2013). This is in agreement with our log response ratios (LRR), which do not show a gradient based on mean annual precipitation at the site of origin (Figure 3.8, Figure 3.9, Figure 3.10 and Figure 3.13). Notably, we found variation in LRRs in terms of the magnitude and the direction of the different responses of leaf traits to the simulated drought. Across all leaf traits, the Serbian provenance (RSF) responded generally with a greater magnitude in both directions. However, we included outlier responses and therefore heavily wilting seedlings into the LRR analysis. These outliers did not show a clear pattern across the provenances (Figure A.4). We found variation between provenances in a few cases independently from the treatment. Indices related to lignin, nitrogen and epicuticular wax were significantly different across the provenances, and in particular, Italian provenances (ITx) showed the highest and the lowest lignin content. However, the reliability of the statistics is impaired due to varying sample sizes of the provenances. Despite evidence of intraspecific variation in stomatal conductance (Leverenz et al., 1999), there is limited evidence for photosynthetic activity among populations for *F. sylvatica* (Bresson et al., 2011; Cocozza et al., 2016; Leverenz et al., 1999; Tognetti et al., 1995). This suggests that *F. sylvatica* populations across the species' range possess the ability for phenotypic adjustments. However, such studies as well as ours do not incorporate variation among individuals of the same population. We focused on phenotypic differences by comparing population means, which may have masked variation within a given population. Schmeddes et al. (2023) showed that at the lowest intraspecific level, which is the progeny of the mother tree, the variations are the highest, which suggests a high potential for acclimation towards climatic

variability already at the individual level. Despite cross-species assessment of leaf traits (i.e., EWT, LMA) (Asner et al., 2014), it remains unclear whether spectrally-derived traits models at the leaf level are accurate enough to reliably capture trait differences at the intraspecific level (Feilhauer et al., 2018; Girard et al., 2020).

Sustainable forest management practices are required for European beech to persist. In light of our results, we suggest to shift the focus towards well-performing individual trees in the progeny of the mother trees as they exhibit high phenotypic variation rather than on a population level (Schmeddes et al., 2023). Phenotypic plasticity is a key factor for the adaptation and persistence, and is suggested to be high in *F. sylvatica* due to their extensive distribution range and exposition to different environmental constraints exemplified in the geographical distribution of our seedlings' provenance (Bussotti et al., 2015). A management practice is actively assisted migration of pre-adapted species, which is in this case drought adapted phenotypes, towards future climatic conditions and is recently advocated in forest management (Aitken & Bemmels, 2016). It can be a systematic tool of introducing new variants (i.e., new populations of the same species) rather than replacing it with a different species (Hällfors et al., 2014). This entails, however, ecological risks related to invasiveness of external species in an ecological continuum (Winder et al., 2011). We further emphasize the importance of forest compositions for drought tolerance and resilience. Mixed stands, thus higher tree species biodiversity, are on average more resistant and resilience to drought than pure stands (Pardos et al., 2021). Our common garden experiment did not simulate a forest environment, where seedlings grow in the shade of larger canopies, influencing ecophysiological traits such as photosynthetic productivity (Masarovicová & Štefančík, 1990), and compete for resources (Wilkins & Wagner, 2021). When studying the persistence of a species, it is also key to take interspecific competition into consideration. For instance, evidence from dendroclimatological research suggests that changes in environmental conditions such as warmer climate may favour thermophilous species such as oak (*Quercus petraea*) or maple (*Acer campestre*) over *F. sylvatica* populations (Kunz et al., 2018). Furthermore, a deeper understanding of phenotypic variation and intraspecific diversity is needed. It is achievable by incorporating population structure and genetic information coupled with data about seed source climate and environmental conditions. Regarding further research, we recommend to consider other drought-tolerance relevant factors such as legacy effects, "ecological stress memory" (Walter et al., 2013), root-systems or temperature tolerance with individuals beyond the juvenile stage and at different phenological periods.

Chapter 5

Conclusion

Due to increasing duration of drought-periods, there is growing concern that *F. sylvatica* may no longer be adapted to the set of environmental conditions, challenging the persistence of European beech forests. Thus, understanding intraspecific variation in ecophysiological processes that happen in response to increased drought stress is key. Hyperspectral spectroscopy offers a rapid and non-destructive way to collect spectral information of individual leaves. We demonstrated the potential of using hyperspectral spectroscopy to study intraspecific drought responses with empirical and physically-based approaches. Slight changes in leaf traits such as photosynthetically-active pigments and water potential were detectable in drought-treated seedlings. However, we did not detect changes in water content and leaf biomass. We found that the biological variation between individuals is larger in drought-treated seedlings than control seedlings and also larger than the variation throughout the experiment. Notably, the relative uncertainty of our spectral measurements were negligible. The inversion of PROSPECT-D is a robust physically-based approach to quantify leaf traits and was shown to be accurate for this approach. Finally, we hypothesized that there is intraspecific variation in drought responses depending on the seedling's provenances, but our study revealed that there was no significant variation in the drought responses based on the provenance, which could be due to the large variation already on the population and individual level. Consequently, we suggest that sustainable forest management should focus on well-performing individual trees and on forest composition to mitigate the effects of global warming in the near future.

Bibliography

- Agurla, S., Gahir, S., Munemasa, S., Murata, Y., & Raghavendra, A. S. (2018). Mechanism of Stomatal Closure in Plants Exposed to Drought and Cold Stress [Series Title: Advances in Experimental Medicine and Biology]. In M. Iwaya-Inoue, M. Sakurai, & M. Uemura (Eds.), *Survival Strategies in Extreme Cold and Desiccation* (pp. 215–232, Vol. 1081). Springer Singapore. https://doi.org/10.1007/978-981-13-1244-1_12
- Aitken, S. N., & Bemmels, J. B. (2016). Time to get moving: Assisted gene flow of forest trees. *Evolutionary Applications*, *9*(1), 271–290. <https://doi.org/10.1111/eva.12293>
- Allen, C. D., Macalady, A. K., Chenchouni, H., Bachelet, D., McDowell, N., Vennetier, M., Kitzberger, T., Rigling, A., Breshears, D. D., Hogg, E., Gonzalez, P., Fensham, R., Zhang, Z., Castro, J., Demidova, N., Lim, J.-H., Allard, G., Running, S. W., Semerci, A., & Cobb, N. (2010). A global overview of drought and heat-induced tree mortality reveals emerging climate change risks for forests. *Forest Ecology and Management*, *259*(4), 660–684. <https://doi.org/10.1016/j.foreco.2009.09.001>
- Allen, W. A., Gausman, H. W., Richardson, A. J., & Thomas, J. R. (1969). Interaction of Isotropic Light with a Compact Plant Leaf [Publisher: Optica Publishing Group]. *J. Opt. Soc. Am.*, *59*(10), 1376–1379. <https://doi.org/10.1364/JOSA.59.001376>
- Alvarez-Maldini, C., Acevedo, M., Dumroese, R. K., González, M., & Cartes, E. (2020). Intraspecific Variation in Drought Response of Three Populations of *Cryptocarya alba* and *Persea lingue*, Two Native Species From Mediterranean Central Chile. *Frontiers in Plant Science*, *11*, 1042. <https://doi.org/10.3389/fpls.2020.01042>
- Anten, N. P. R., & Hirose, T. (1999). Interspecific differences in above-ground growth patterns result in spatial and temporal partitioning of light among species in a tall-grass meadow. *Journal of Ecology*, *87*(4), 583–597. <https://doi.org/10.1046/j.1365-2745.1999.00365.x>
- Aranda, I., Cano, F. J., Gasco, A., Cochard, H., Nardini, A., Mancha, J. A., Lopez, R., & Sanchez-Gomez, D. (2015). Variation in photosynthetic performance and hydraulic architecture across European beech (*Fagus sylvatica* L.) populations supports the case for local adaptation to water stress. *Tree Physiology*, *35*(1), 34–46. <https://doi.org/10.1093/treephys/tpu101>
- Arend, M., Sever, K., Pflug, E., Gessler, A., & Schaub, M. (2016). Seasonal photosynthetic response of European beech to severe summer drought: Limitation, recovery and post-

- drought stimulation. *Agricultural and Forest Meteorology*, *220*, 83–89. <https://doi.org/10.1016/j.agrformet.2016.01.011>
- Arnold, P. A., Kruuk, L. E. B., & Nicotra, A. B. (2019). How to analyse plant phenotypic plasticity in response to a changing climate. *New Phytologist*, *222*(3), 1235–1241. <https://doi.org/10.1111/nph.15656>
- Asner, G. P., Martin, R. E., Carranza-Jiménez, L., Sinca, F., Tupayachi, R., Anderson, C. B., & Martinez, P. (2014). Functional and biological diversity of foliar spectra in tree canopies throughout the Andes to Amazon region. *New Phytologist*, *204*(1), 127–139. <https://doi.org/10.1111/nph.12895>
- Baccari, S., Elloumi, O., Chaari-Rkhis, A., Fenollosa, E., Morales, M., Drira, N., Ben Abdallah, F., Fki, L., & Munné-Bosch, S. (2020). Linking Leaf Water Potential, Photosynthesis and Chlorophyll Loss With Mechanisms of Photo- and Antioxidant Protection in Juvenile Olive Trees Subjected to Severe Drought. *Frontiers in Plant Science*, *11*, 614144. <https://doi.org/10.3389/fpls.2020.614144>
- Bacelar, E. A., Santos, D. L., Moutinho-Pereira, J. M., Lopes, J. I., Gonçalves, B. C., Ferreira, T. C., & Correia, C. M. (2007). Physiological behaviour, oxidative damage and antioxidant protection of olive trees grown under different irrigation regimes. *Plant and Soil*, *292*(1-2), 1–12. <https://doi.org/10.1007/s11104-006-9088-1>
- Bakbergenuly, I., Hoaglin, D. C., & Kulinskaya, E. (2020). Estimation in meta-analyses of response ratios. *BMC Medical Research Methodology*, *20*(1), 263. <https://doi.org/10.1186/s12874-020-01137-1>
- Bartlett, M. K., Scoffoni, C., & Sack, L. (2012). The determinants of leaf turgor loss point and prediction of drought tolerance of species and biomes: A global meta-analysis. *Ecology Letters*, *15*(5), 393–405. <https://doi.org/10.1111/j.1461-0248.2012.01751.x>
- Baudis, M., Ellerbrock, R. H., Felsmann, K., Gessler, A., Gimbel, K., Kayler, Z., Puhlmann, H., Ulrich, A., Weiler, M., Welk, E., & Bruelheide, H. (2014). Intraspecific differences in responses to rainshelter-induced drought and competition of *Fagus sylvatica* L. across Germany. *Forest Ecology and Management*, *330*, 283–293. <https://doi.org/10.1016/j.foreco.2014.07.012>
- Ben Abdallah, M., Methenni, K., Nouairi, I., Zarrouk, M., & Youssef, N. B. (2017). Drought priming improves subsequent more severe drought in a drought-sensitive cultivar of olive cv. Chétoui. *Scientia Horticulturae*, *221*, 43–52. <https://doi.org/10.1016/j.scienta.2017.04.021>
- Bengtson, C., Larsson, S., & Liljenberg, C. (1978). Effects of Water Stress on Cuticular Transpiration Rate and Amount and Composition of Epicuticular Wax in Seedlings of Six Oat Varieties. *Physiologia Plantarum*, *44*(4), 319–324. <https://doi.org/10.1111/j.1399-3054.1978.tb01630.x>
- Benito Garzón, M., Robson, T. M., & Hampe, A. (2019). Trait SDMs: Species distribution models that account for local adaptation and phenotypic plasticity. *New Phytologist*, *222*(4), 1757–1765. <https://doi.org/10.1111/nph.15716>

- Betsch, P., Bonal, D., Breda, N., Montpied, P., Peiffer, M., Tuzet, A., & Granier, A. (2011). Drought effects on water relations in beech: The contribution of exchangeable water reservoirs. *Agricultural and Forest Meteorology*, *151*(5), 531–543. <https://doi.org/10.1016/j.agrformet.2010.12.008>
- Biswal, B. (1995). Carotenoid catabolism during leaf senescence and its control by light. *Journal of Photochemistry and Photobiology B: Biology*, *30*(1), 3–13. [https://doi.org/10.1016/1011-1344\(95\)07197-A](https://doi.org/10.1016/1011-1344(95)07197-A)
- Boren, E. J., Boschetti, L., & Johnson, D. M. (2019). Characterizing the Variability of the Structure Parameter in the PROSPECT Leaf Optical Properties Model. *Remote Sensing*, *11*(10), 1236. <https://doi.org/10.3390/rs11101236>
- Bresson, C. C., Vitasse, Y., Kremer, A., & Delzon, S. (2011). To what extent is altitudinal variation of functional traits driven by genetic adaptation in European oak and beech? *Tree Physiology*, *31*(11), 1164–1174. <https://doi.org/10.1093/treephys/tpr084>
- Brinkmann, K., Blaschke, L., & Polle, A. (2003). Comparison of Different Methods for Lignin Determination as a Basis for Calibration of Near-Infrared Reflectance Spectroscopy and Implications of Lignoproteins. *Journal of chemical ecology*, *28*, 2483–501. <https://doi.org/10.1023/A:1021484002582>
- Brown, L. A., Williams, O., & Dash, J. (2022). Calibration and characterisation of four chlorophyll meters and transmittance spectroscopy for non-destructive estimation of forest leaf chlorophyll concentration. *Agricultural and Forest Meteorology*, *323*, 109059. <https://doi.org/10.1016/j.agrformet.2022.109059>
- Buddenbaum, H., Stern, O., Stellmes, M., Stoffels, J., Poeschel, P., Hill, J., & Werner, W. (2012). Field Imaging Spectroscopy of Beech Seedlings under Dryness Stress. *Remote Sensing*, *4*(12), 3721–3740. <https://doi.org/10.3390/rs4123721>
- Buras, A., Rammig, A., & Zang, C. S. (2020). Quantifying impacts of the 2018 drought on European ecosystems in comparison to 2003. *Biogeosciences*, *17*(6), 1655–1672. <https://doi.org/10.5194/bg-17-1655-2020>
- Burnett, A. C., Anderson, J., Davidson, K. J., Ely, K. S., Lamour, J., Li, Q., Morrison, B. D., Yang, D., Rogers, A., & Serbin, S. P. (2021a). A best-practice guide to predicting plant traits from leaf-level hyperspectral data using partial least squares regression (T. Lawson, Ed.). *Journal of Experimental Botany*, *72*(18), 6175–6189. <https://doi.org/10.1093/jxb/erab295>
- Burnett, A. C., Serbin, S. P., Davidson, K. J., Ely, K. S., & Rogers, A. (2021b). Detection of the metabolic response to drought stress using hyperspectral reflectance (R. Gleadow, Ed.). *Journal of Experimental Botany*, *72*(18), 6474–6489. <https://doi.org/10.1093/jxb/erab255>
- Buschmann, C., & Nagel, E. (1993). In vivo spectroscopy and internal optics of leaves as basis for remote sensing of vegetation. *International Journal of Remote Sensing*, *14*(4), 711–722. <https://doi.org/10.1080/01431169308904370>

- Bussotti, F., Pollastrini, M., Holland, V., & Brüggemann, W. (2015). Functional traits and adaptive capacity of European forests to climate change. *Environmental and Experimental Botany*, *111*, 91–113. <https://doi.org/10.1016/j.envexpbot.2014.11.006>
- Camarillo-Castillo, F., Huggins, T. D., Mondal, S., Reynolds, M. P., Tilley, M., & Hays, D. B. (2021). High-resolution spectral information enables phenotyping of leaf epicuticular wax in wheat. *Plant Methods*, *17*(1), 58. <https://doi.org/10.1186/s13007-021-00759-w>
- Carsjens, C., Nguyen Ngoc, Q., Guzy, J., Knutzen, F., Meier, I. C., Muller, M., Finkeldey, R., Leuschner, C., & Polle, A. (2014). Intra-specific variations in expression of stress-related genes in beech progenies are stronger than drought-induced responses. *Tree Physiology*, *34*(12), 1348–1361. <https://doi.org/10.1093/treephys/tpu093>
- Caudullo, G., Welk, E., & San-Miguel-Ayanz, J. (2017). Chorological maps for the main European woody species. *Data in Brief*, *12*, 662–666. <https://doi.org/10.1016/j.dib.2017.05.007>
- Cavender-Bares, J., Gamon, J. A., Hobbie, S. E., Madritch, M. D., Meireles, J. E., Schweiger, A. K., & Townsend, P. A. (2017). Harnessing plant spectra to integrate the biodiversity sciences across biological and spatial scales. *American Journal of Botany*, *104*(7), 966–969. <https://doi.org/10.3732/ajb.1700061>
- Cavender-Bares, J., Meireles, J., Couture, J., Kaproth, M., Kingdon, C., Singh, A., Serbin, S., Center, A., Zuniga, E., Pilz, G., & Townsend, P. (2016). Associations of Leaf Spectra with Genetic and Phylogenetic Variation in Oaks: Prospects for Remote Detection of Biodiversity. *Remote Sensing*, *8*(3), 221. <https://doi.org/10.3390/rs8030221>
- Chalker-Scott, L. (1999). Environmental Significance of Anthocyanins in Plant Stress Responses. *Photochemistry and Photobiology*, *70*(1), 1–9. <https://doi.org/10.1111/j.1751-1097.1999.tb01944.x>
- Cocozza, C., De Miguel, M., Pšidová, E., Ditmarová, L., Marino, S., Maiuro, L., Alvino, A., Czajkowski, T., Bolte, A., & Tognetti, R. (2016). Variation in Ecophysiological Traits and Drought Tolerance of Beech (*Fagus sylvatica* L.) Seedlings from Different Populations. *Frontiers in Plant Science*, *7*. <https://doi.org/10.3389/fpls.2016.00886>
- Cook, J., Oreskes, N., Doran, P. T., Anderegg, W. R. L., Verheggen, B., Maibach, E. W., Carlton, J. S., Lewandowsky, S., Skuce, A. G., Green, S. A., Nuccitelli, D., Jacobs, P., Richardson, M., Winkler, B., Painting, R., & Rice, K. (2016). Consensus on consensus: A synthesis of consensus estimates on human-caused global warming. *Environmental Research Letters*, *11*(4), 048002. <https://doi.org/10.1088/1748-9326/11/4/048002>
- Coste, S., Baraloto, C., Leroy, C., Marcon, É., Renaud, A., Richardson, A. D., Roggy, J.-C., Schimann, H., Uddling, J., & Hérault, B. (2010). Assessing foliar chlorophyll contents with the SPAD-502 chlorophyll meter: A calibration test with thirteen tree species of tropical rainforest in French Guiana. *Annals of Forest Science*, *67*(6), 607–607. <https://doi.org/10.1051/forest/2010020>
- Creux, N., & Harmer, S. (2019). Circadian Rhythms in Plants. *Cold Spring Harbor Perspectives in Biology*, *11*(9), a034611. <https://doi.org/10.1101/cshperspect.a034611>

- Czajkowski, T., & Bolte, A. (2006). Unterschiedliche Reaktion deutscher und polnischer Herkünfte der Buche (*Fagus sylvatica* L.) auf Trockenheit.
- Czyż, E. A., Guillén Escribà, C., Wulf, H., Tedder, A., Schuman, M. C., Schneider, F. D., & Schaepman, M. E. (2020). Intraspecific genetic variation of a *Fagus sylvatica* population in a temperate forest derived from airborne imaging spectroscopy time series. *Ecology and Evolution*, *10*(14), 7419–7430. <https://doi.org/10.1002/ece3.6469>
- Danner, M., Locherer, M., Hank, T., & Richter, K. (2015). Spectral Sampling with the ASD FIELDSPEC 4 [Publisher: GFZ Data Services]. *EnMAP Field Guides Technical Report*; <https://doi.org/10.2312/ENMAP.2015.008>
- Datt, B. (1999). Remote Sensing of Water Content in Eucalyptus Leaves. *Australian Journal of Botany*, *47*(6), 909. <https://doi.org/10.1071/BT98042>
- Daughtry, C., Hunt, E., & McMurtrey, J. (2004). Assessing crop residue cover using shortwave infrared reflectance. *Remote Sensing of Environment*, *90*(1), 126–134. <https://doi.org/10.1016/j.rse.2003.10.023>
- De La Riva, E. G., Olmo, M., Poorter, H., Ubera, J. L., & Villar, R. (2016). Leaf Mass per Area (LMA) and Its Relationship with Leaf Structure and Anatomy in 34 Mediterranean Woody Species along a Water Availability Gradient (C. Armas, Ed.). *PLOS ONE*, *11*(2), e0148788. <https://doi.org/10.1371/journal.pone.0148788>
- de La Harpe, M., & Schuman, M. C. (2021). Protocol for seeds handling of *Fagus sylvatica*. *Fagus sylvatica* sampling campaign 2020-2021. [Unpublished Protocol].
- Demmig-Adams, B., & Adams, W. W. (1992). Photoprotection and Other Responses of Plants to High Light Stress. *Annual Review of Plant Physiology and Plant Molecular Biology*, *43*(1), 599–626. <https://doi.org/10.1146/annurev.pp.43.060192.003123>
- Dietrich, L., Delzon, S., Hoch, G., & Kahmen, A. (2019). No role for xylem embolism or carbohydrate shortage in temperate trees during the severe 2015 drought (G. Battipaglia, Ed.). *Journal of Ecology*, *107*(1), 334–349. <https://doi.org/10.1111/1365-2745.13051>
- Dittmar, C., Zech, W., & Elling, W. (2003). Growth variations of Common beech (*Fagus sylvatica* L.) under different climatic and environmental conditions in Europe—a dendroecological study. *Forest Ecology and Management*, *173*(1-3), 63–78. [https://doi.org/10.1016/S0378-1127\(01\)00816-7](https://doi.org/10.1016/S0378-1127(01)00816-7)
- D’Odorico, P., Schuman, M. C., Kurz, M., & Csilléry, K. (2023). Discerning Oriental from European beech by leaf spectroscopy: Operational and physiological implications. *Forest Ecology and Management*, *541*, 121056. <https://doi.org/10.1016/j.foreco.2023.121056>
- Dounavi, A., Netzer, F., Celepirovic, N., Ivanković, M., Burger, J., Figueroa, A., Schön, S., Simon, J., Cremer, E., Fussi, B., Konnert, M., & Rennenberg, H. (2016). Genetic and physiological differences of European beech provenances (*F. sylvatica* L.) exposed to drought stress. *Forest Ecology and Management*, *361*, 226–236. <https://doi.org/10.1016/j.foreco.2015.11.014>
- Drobyshev, I., Övergaard, R., Saygin, I., Niklasson, M., Hickler, T., Karlsson, M., & Sykes, M. T. (2010). Mastling behaviour and dendrochronology of European beech (*Fagus sylvatica*

- L.) in southern Sweden. *Forest Ecology and Management*, 259(11), 2160–2171. <https://doi.org/10.1016/j.foreco.2010.01.037>
- Durrant, T., de Rigo, D., & Caudullo, G. (2016, March). *Fagus sylvatica* in Europe: Distribution, habitat, usage and threats.
- Emerson, R. (1929). Chlorophyll content and rate of photosynthesis. *Proceedings of the National Academy of Sciences*, 15(3), 281–284. <https://doi.org/10.1073/pnas.15.3.281>
- ESRI Inc. (2023). ArcGIS Pro. <https://www.esri.com/en-us/arcgis/products/arcgis-pro/overview>
- Feild, T. S., Lee, D. W., & Holbrook, N. M. (2001). Why Leaves Turn Red in Autumn. The Role of Anthocyanins in Senescing Leaves of Red-Osier Dogwood. *Plant Physiology*, 127(2), 566–574. <https://doi.org/10.1104/pp.010063>
- Feilhauer, H., Schmid, T., Faude, U., Sánchez-Carrillo, S., & Cirujano, S. (2018). Are remotely sensed traits suitable for ecological analysis? A case study of long-term drought effects on leaf mass per area of wetland vegetation. *Ecological Indicators*, 88, 232–240. <https://doi.org/10.1016/j.ecolind.2018.01.012>
- Felipe de Mendiburu & Muhammad Yaseen. (2020). *Agricolae: Statistical Procedures for Agricultural Research*.
- Feret, J.-B., François, C., Asner, G. P., Gitelson, A. A., Martin, R. E., Bidel, L. P., Ustin, S. L., Le Maire, G., & Jacquemoud, S. (2008). PROSPECT-4 and 5: Advances in the leaf optical properties model separating photosynthetic pigments. *Remote Sensing of Environment*, 112(6), 3030–3043. <https://doi.org/10.1016/j.rse.2008.02.012>
- Féret, J.-B., Gitelson, A., Noble, S., & Jacquemoud, S. (2017). PROSPECT-D: Towards modeling leaf optical properties through a complete lifecycle. *Remote Sensing of Environment*, 193, 204–215. <https://doi.org/10.1016/j.rse.2017.03.004>
- Féret, J.-B., Le Maire, G., Jay, S., Berveiller, D., Bendoula, R., Hmimina, G., Cheraïet, A., Oliveira, J., Ponzoni, F., Solanki, T., De Boissieu, F., Chave, J., Nouvellon, Y., Porcar-Castell, A., Proisy, C., Soudani, K., Gastellu-Etchegorry, J.-P., & Lefèvre-Fonollosa, M.-J. (2019). Estimating leaf mass per area and equivalent water thickness based on leaf optical properties: Potential and limitations of physical modeling and machine learning. *Remote Sensing of Environment*, 231, 110959. <https://doi.org/10.1016/j.rse.2018.11.002>
- Féret, J.-B., François, C., Gitelson, A., Asner, G. P., Barry, K. M., Panigada, C., Richardson, A. D., & Jacquemoud, S. (2011). Optimizing spectral indices and chemometric analysis of leaf chemical properties using radiative transfer modeling. *Remote Sensing of Environment*, 115(10), 2742–2750. <https://doi.org/10.1016/j.rse.2011.06.016>
- Filella, I., Porcar-Castell, A., Munné-Bosch, S., Bäck, J., Garbulska, M. F., & Peñuelas, J. (2009). PRI assessment of long-term changes in carotenoids/chlorophyll ratio and short-term changes in de-epoxidation state of the xanthophyll cycle. *International Journal of Remote Sensing*, 30(17), 4443–4455. <https://doi.org/10.1080/01431160802575661>
- Fleischer, W. E. (1935). The relation between chlorophyll content and rate of photosynthesis. *Journal of General Physiology*, 18(4), 573–597. <https://doi.org/10.1085/jgp.18.4.573>

- Gai, J., Wang, J., Xie, S., Xiang, L., & Wang, Z. (2023). Spectroscopic determination of chlorophyll content in sugarcane leaves for drought stress detection. *Precision Agriculture*. <https://doi.org/10.1007/s11119-023-10082-0>
- Gallé, A., & Feller, U. (2007). Changes of photosynthetic traits in beech saplings (*Fagus sylvatica*) under severe drought stress and during recovery. *Physiologia Plantarum*, *131*(3), 412–421. <https://doi.org/10.1111/j.1399-3054.2007.00972.x>
- Gamon, J. A., & Surfus, J. S. (1999). Assessing leaf pigment content and activity with a reflectometer. *New Phytologist*, *143*(1), 105–117. <https://doi.org/10.1046/j.1469-8137.1999.00424.x>
- Gamon, J., Peñuelas, J., & Field, C. (1992). A narrow-waveband spectral index that tracks diurnal changes in photosynthetic efficiency. *Remote Sensing of Environment*, *41*(1), 35–44. [https://doi.org/10.1016/0034-4257\(92\)90059-S](https://doi.org/10.1016/0034-4257(92)90059-S)
- Gamon, J. A., Huemmrich, K. F., Wong, C. Y. S., Ensminger, I., Garrity, S., Hollinger, D. Y., Noormets, A., & Peñuelas, J. (2016). A remotely sensed pigment index reveals photosynthetic phenology in evergreen conifers. *Proceedings of the National Academy of Sciences*, *113*(46), 13087–13092. <https://doi.org/10.1073/pnas.1606162113>
- Gao, B.-c. (1996). NDWI—A normalized difference water index for remote sensing of vegetation liquid water from space. *Remote Sensing of Environment*, *58*(3), 257–266. [https://doi.org/10.1016/S0034-4257\(96\)00067-3](https://doi.org/10.1016/S0034-4257(96)00067-3)
- García-Plazaola, J., & Becerril, J. (2000). Effects of drought on photoprotective mechanisms in European beech (*Fagus sylvatica* L.) seedlings from different provenances. *Trees*, *14*(8), 485–490. <https://doi.org/10.1007/s004680000068>
- Garonna, I., de Jong, R., & Schaepman, M. E. (2016). Variability and evolution of global land surface phenology over the past three decades (1982-2012) [Publisher: Wiley-Blackwell Publishing, Inc.]. <https://doi.org/10.5167/UZH-116954>
- Geßler, A., Keitel, C., Kreuzwieser, J., Matyssek, R., Seiler, W., & Rennenberg, H. (2006). Potential risks for European beech (*Fagus sylvatica* L.) in a changing climate. *Trees*, *21*(1), 1–11. <https://doi.org/10.1007/s00468-006-0107-x>
- Girard, A., Schweiger, A. K., Carteron, A., Kalacska, M., & Laliberté, E. (2020). Foliar Spectra and Traits of Bog Plants across Nitrogen Deposition Gradients. *Remote Sensing*, *12*(15), 2448. <https://doi.org/10.3390/rs12152448>
- Gitelson, A., & Merzlyak, M. N. (1994). Spectral Reflectance Changes Associated with Autumn Senescence of *Aesculus hippocastanum* L. and *Acer platanoides* L. Leaves. Spectral Features and Relation to Chlorophyll Estimation. *Journal of Plant Physiology*, *143*(3), 286–292. [https://doi.org/10.1016/S0176-1617\(11\)81633-0](https://doi.org/10.1016/S0176-1617(11)81633-0)
- Gitelson, A. A. (2005). Remote estimation of canopy chlorophyll content in crops. *Geophysical Research Letters*, *32*(8), L08403. <https://doi.org/10.1029/2005GL022688>
- Gitelson, A. A., Merzlyak, M. N., & Chivkunova, O. B. (2001). Optical Properties and Non-destructive Estimation of Anthocyanin Content in Plant Leaves. *Photochemistry and*

- Photobiology*, 74(1), 38. [https://doi.org/10.1562/0031-8655\(2001\)074<0038:OPANEO>2.0.CO;2](https://doi.org/10.1562/0031-8655(2001)074<0038:OPANEO>2.0.CO;2)
- González De Andrés, E., Rosas, T., Camarero, J. J., & Martínez-Vilalta, J. (2021). The intraspecific variation of functional traits modulates drought resilience of European beech and pubescent oak. *Journal of Ecology*, 109(10), 3652–3669. <https://doi.org/10.1111/1365-2745.13743>
- Gould, K. S. (2004). Nature's Swiss Army Knife: The Diverse Protective Roles of Anthocyanins in Leaves. *Journal of Biomedicine and Biotechnology*, 2004(5), 314–320. <https://doi.org/10.1155/S1110724304406147>
- Green, B. R., & Durnford, D. G. (1996). The chlorophyll-carotenoid proteins of oxygenic photosynthesis. *Annual Review of Plant Physiology and Plant Molecular Biology*, 47(1), 685–714. <https://doi.org/10.1146/annurev.arplant.47.1.685>
- Grime, J. (2001, January). Plant Strategies, Vegetation Processes, and Ecosystem Properties [Journal Abbreviation: Biological Conservation - BIOL CONSERV]. In *Biological Conservation - BIOL CONSERV* (Vol. 107). [https://doi.org/10.1016/S0006-3207\(02\)00055-1](https://doi.org/10.1016/S0006-3207(02)00055-1)
- Guo, J., Xu, W., Yu, X., Shen, H., Li, H., Cheng, D., Liu, A., Liu, J., Liu, C., Zhao, S., & Song, J. (2016). Cuticular Wax Accumulation Is Associated with Drought Tolerance in Wheat Near-Isogenic Lines. *Frontiers in Plant Science*, 7. <https://doi.org/10.3389/fpls.2016.01809>
- Gutschick, V. P. (1999). Research Reviews: Biotic and Abiotic Consequences of Differences in Leaf Structure [Publisher: [Wiley, New Phytologist Trust]]. *The New Phytologist*, 143(1), 3–18. Retrieved January 19, 2024, from <http://www.jstor.org/stable/2588510>
- Hällfors, M. H., Vaara, E. M., Hyvärinen, M., Oksanen, M., Schulman, L. E., Siipi, H., & Lehvävirta, S. (2014). Coming to Terms with the Concept of Moving Species Threatened by Climate Change – A Systematic Review of the Terminology and Definitions (P. Hohenlohe, Ed.). *PLoS ONE*, 9(7), e102979. <https://doi.org/10.1371/journal.pone.0102979>
- Havaux, M. (2014). Carotenoid oxidation products as stress signals in plants. *The Plant Journal*, 79(4), 597–606. <https://doi.org/10.1111/tpj.12386>
- He, J., Hu, W., Li, Y., Zhu, H., Zou, J., Wang, Y., Meng, Y., Chen, B., Zhao, W., Wang, S., & Zhou, Z. (2022). Prolonged drought affects the interaction of carbon and nitrogen metabolism in root and shoot of cotton. *Environmental and Experimental Botany*, 197, 104839. <https://doi.org/10.1016/j.envexpbot.2022.104839>
- Hedges, L. V., Gurevitch, J., & Curtis, P. S. (1999). The meta-analysis of response rations in experimental ecology. *Ecology*, 80(4), 1150–1156. [https://doi.org/10.1890/0012-9658\(1999\)080\[1150:TMAORR\]2.0.CO;2](https://doi.org/10.1890/0012-9658(1999)080[1150:TMAORR]2.0.CO;2)
- Helsen, K., Bassi, L., Feilhauer, H., Kattenborn, T., Matsushima, H., Van Cleemput, E., Somers, B., & Honnay, O. (2021). Evaluating different methods for retrieving intraspecific leaf trait variation from hyperspectral leaf reflectance. *Ecological Indicators*, 130, 108111. <https://doi.org/10.1016/j.ecolind.2021.108111>

- Hermann, M., Röthlisberger, M., Gessler, A., Rigling, A., Senf, C., Wohlgemuth, T., & Wernli, H. (2023). Meteorological history of low-forest-greenness events in Europe in 2002–2022. *Biogeosciences*, *20*(6), 1155–1180. <https://doi.org/10.5194/bg-20-1155-2023>
- Hijmans, R. J., Cameron, S. E., Parra, J. L., Jones, P. G., & Jarvis, A. (2005). Very high resolution interpolated climate surfaces for global land areas. *International Journal of Climatology*, *25*(15), 1965–1978. <https://doi.org/10.1002/joc.1276>
- Hu, F., Zhang, Y., & Guo, J. (2023). Effects of drought stress on photosynthetic physiological characteristics, leaf microstructure, and related gene expression of yellow horn. *Plant Signaling & Behavior*, *18*(1), 2215025. <https://doi.org/10.1080/15592324.2023.2215025>
- Hu, W., Gao, M., Xu, B., Wang, S., Wang, Y., & Zhou, Z. (2022). Co-occurring elevated temperature and drought stresses during cotton fiber thickening stage inhibit fiber biomass accumulation and cellulose synthesis. *Industrial Crops and Products*, *187*, 115348. <https://doi.org/10.1016/j.indcrop.2022.115348>
- Hu, Y., Li, W. C., Xu, Y. Q., Li, G. J., Liao, Y., & Fu, F. (2009). Differential expression of candidate genes for lignin biosynthesis under drought stress in maize leaves. *Journal of Applied Genetics*, *50*(3), 213–223. <https://doi.org/10.1007/BF03195675>
- Hueni, A., & Bialek, A. (2017). Cause, Effect, and Correction of Field Spectroradiometer Inter-channel Radiometric Steps. *IEEE Journal of Selected Topics in Applied Earth Observations and Remote Sensing*, *10*(4), 1542–1551. <https://doi.org/10.1109/JSTARS.2016.2625043>
- Hunt Jr., E., & Rock, B. (1989). Detection of changes in leaf water content using Near- and Middle-Infrared reflectances. *Remote Sensing of Environment*, *30*(1), 43–54. [https://doi.org/10.1016/0034-4257\(89\)90046-1](https://doi.org/10.1016/0034-4257(89)90046-1)
- ICL-SF. (2023, February). Osmocote Exact Standard. https://icl-sf.com/de-de/products/ornamental_horticulture/osmocote-exact-standard-12-14m/
- IPCC. (2023, June). *Climate Change 2022 – Impacts, Adaptation and Vulnerability: Working Group II Contribution to the Sixth Assessment Report of the Intergovernmental Panel on Climate Change* (1st ed.). Cambridge University Press. <https://doi.org/10.1017/9781009325844>
- Jacquemoud, S., & Baret, F. (1990). PROSPECT: A model of leaf optical properties spectra. *Remote Sensing of Environment*, *34*(2), 75–91. [https://doi.org/10.1016/0034-4257\(90\)90100-Z](https://doi.org/10.1016/0034-4257(90)90100-Z)
- Jacquemoud, S., Ustin, S., Verdebout, J., Schmuck, G., Andreoli, G., & Hosgood, B. (1996). Estimating leaf biochemistry using the PROSPECT leaf optical properties model. *Remote Sensing of Environment*, *56*(3), 194–202. [https://doi.org/10.1016/0034-4257\(95\)00238-3](https://doi.org/10.1016/0034-4257(95)00238-3)
- Jacquemoud, S., & Ustin, S. (2019, September). *Leaf Optical Properties* (1st ed.). Cambridge University Press. <https://doi.org/10.1017/9781108686457>
- Jordan, W. R., Monk, R. L., Miller, F. R., Rosenow, D. T., Clark, L. E., & Shouse, P. J. (1983). Environmental Physiology of Sorghum. I. Environmental and Genetic Control

- of Epicuticular Wax Load ¹. *Crop Science*, 23(3), 552–558. <https://doi.org/10.2135/cropsci1983.0011183X002300030025x>
- Joshi, H., Duttand, S., Choudhary, P., & Mundra, S. (2019). Role of Effective Microorganisms (EM) in Sustainable Agriculture. *International Journal of Current Microbiology and Applied Sciences*, 8(03), 172–181. <https://doi.org/10.20546/ijcmas.2019.803.024>
- Junaid, M. D., Öztürk, Z. N., & Gökçe, A. F. (2023). Drought stress effects on morphophysiological and quality characteristics of commercial carrot cultivars. *Turkish Journal of Botany*, 47(2), 111–126. <https://doi.org/10.55730/1300-008X.2750>
- Kim, D. M., Zhang, H., Zhou, H., Du, T., Wu, Q., Mockler, T. C., & Berezin, M. Y. (2015). Highly sensitive image-derived indices of water-stressed plants using hyperspectral imaging in SWIR and histogram analysis. *Scientific Reports*, 5, 15919. <https://doi.org/10.1038/srep15919>
- Kothari, S., & Schweiger, A. K. (2022). Plant spectra as integrative measures of plant phenotypes. *Journal of Ecology*, 110(11), 2536–2554. <https://doi.org/10.1111/1365-2745.13972>
- Kreyling, J., Buhk, C., Backhaus, S., Hallinger, M., Huber, G., Huber, L., Jentsch, A., Konnert, M., Thiel, D., Wilmking, M., & Beierkuhnlein, C. (2014). Local adaptations to frost in marginal and central populations of the dominant forest tree *Fagus sylvatica* L. as affected by temperature and extreme drought in common garden experiments. *Ecology and Evolution*, 4(5), 594–605. <https://doi.org/10.1002/ece3.971>
- Kunz, J., Löffler, G., & Bauhus, J. (2018). Minor European broadleaved tree species are more drought-tolerant than *Fagus sylvatica* but not more tolerant than *Quercus petraea*. *Forest Ecology and Management*, 414, 15–27. <https://doi.org/10.1016/j.foreco.2018.02.016>
- Lajeunesse, M. J. (2016). Bias and correction for the log response ratio in ecological meta-analysis [Publisher: Figshare]. <https://doi.org/10.6084/M9.FIGSHARE.C.3307854.V1>
- Landi, M., Tattini, M., & Gould, K. S. (2015). Multiple functional roles of anthocyanins in plant-environment interactions. *Environmental and Experimental Botany*, 119, 4–17. <https://doi.org/10.1016/j.envexpbot.2015.05.012>
- Lawlor, D. W., & Cornic, G. (2002). Photosynthetic carbon assimilation and associated metabolism in relation to water deficits in higher plants. *Plant, Cell & Environment*, 25(2), 275–294. <https://doi.org/10.1046/j.0016-8025.2001.00814.x>
- Lemaire, G., Francois, C., Soudani, K., Berveiller, D., Pontailier, J., Breda, N., Genet, H., Davi, H., & Dufrene, E. (2008). Calibration and validation of hyperspectral indices for the estimation of broadleaved forest leaf chlorophyll content, leaf mass per area, leaf area index and leaf canopy biomass. *Remote Sensing of Environment*, 112(10), 3846–3864. <https://doi.org/10.1016/j.rse.2008.06.005>
- Leuschner, C. (2020). Drought response of European beech (*Fagus sylvatica* L.)—A review. *Perspectives in Plant Ecology, Evolution and Systematics*, 47, 125576. <https://doi.org/10.1016/j.ppees.2020.125576>

- Leuzinger, S., Zott, G., Asshoff, R., & Korner, C. (2005). Responses of deciduous forest trees to severe drought in Central Europe. *Tree Physiology*, *25*(6), 641–650. <https://doi.org/10.1093/treephys/25.6.641>
- Leverenz, J. W., Bruhn, D., & Saxe, H. (1999). Responses of two provenances of *Fagus sylvatica* seedlings to a combination of four temperature and two CO₂ treatments during their first growing season: Gas exchange of leaves and roots. *New Phytologist*, *144*(3), 437–454. <https://doi.org/10.1046/j.1469-8137.1999.00541.x>
- Li, C., Czyż, E. A., Halitschke, R., Baldwin, I. T., Schaepman, M. E., & Schuman, M. C. (2023). Evaluating potential of leaf reflectance spectra to monitor plant genetic variation. *Plant Methods*, *19*(1), 108. <https://doi.org/10.1186/s13007-023-01089-9>
- Li, Z., & Ahammed, G. J. (2023). Plant stress response and adaptation via anthocyanins: A review. *Plant Stress*, *10*, 100230. <https://doi.org/10.1016/j.stress.2023.100230>
- Lichtenthaler, H. K., Gitelson, A., & Lang, M. (1996). Non-Destructive Determination of Chlorophyll Content of Leaves of a Green and an Aurea Mutant of Tobacco by Reflectance Measurements. *Journal of Plant Physiology*, *148*(3-4), 483–493. [https://doi.org/10.1016/S0176-1617\(96\)80283-5](https://doi.org/10.1016/S0176-1617(96)80283-5)
- Liu, Q., Luo, L., & Zheng, L. (2018). Lignins: Biosynthesis and Biological Functions in Plants. *International Journal of Molecular Sciences*, *19*(2), 335. <https://doi.org/10.3390/ijms19020335>
- Mafakheri, A., Siosemardeh, A., Bahramnejad, B., Struik, P., & Sohrabi, Y. (2010). Effect of Drought Stress on Yield, Proline and Chlorophyll Contents in Three Chickpea Cultivars [Place: Lismore, N.S.W. Publisher: Southern Cross Publishers]. *Australian Journal of Crop Science*, *4*(8), 580–585. Retrieved January 4, 2024, from <https://search.informit.org/doi/10.3316/informit.857341254680658>
- Markwell, J., Osterman, J. C., & Mitchell, J. L. (1995). Calibration of the Minolta SPAD-502 leaf chlorophyll meter. *Photosynthesis Research*, *46*(3), 467–472. <https://doi.org/10.1007/BF00032301>
- Martinez del Castillo, E., Zang, C. S., Buras, A., Hacket-Pain, A., Esper, J., Serrano-Notivoli, R., Hartl, C., Weigel, R., Klesse, S., Resco de Dios, V., Scharnweber, T., Dorado-Liñán, I., van der Maaten-Theunissen, M., van der Maaten, E., Jump, A., Mikac, S., Banzragch, B.-E., Beck, W., Cavin, L., . . . de Luis, M. (2022). Climate-change-driven growth decline of European beech forests. *Communications Biology*, *5*(1), 163. <https://doi.org/10.1038/s42003-022-03107-3>
- Masarovicová, E., & Štefančík, L. (1990). Some ecophysiological features in sun and shade leaves of tall beech trees. *Biologia Plantarum*, *32*(5), 374–387. <https://doi.org/10.1007/BF02898503>
- Maxwell, K., & Johnson, G. N. (2000). Chlorophyll fluorescence—a practical guide. *Journal of Experimental Botany*, *51*(345), 659–668. <https://doi.org/10.1093/jexbot/51.345.659>
- Meireles, J. E., & Schweiger, A. (2020, July). Meireles/spectrolab: CRAN-v0.0.9. <https://doi.org/10.5281/ZENODO.3934575>

- Merzlyak, M. N., Gitelson, A. A., Chivkunova, O. B., & Rakitin, V. Y. (1999). Non-destructive optical detection of pigment changes during leaf senescence and fruit ripening. *Physiologia Plantarum*, *106*(1), 135–141. <https://doi.org/10.1034/j.1399-3054.1999.106119.x>
- Messier, J., McGill, B. J., & Lechowicz, M. J. (2010). How do traits vary across ecological scales? A case for trait-based ecology. *Ecology Letters*, *13*(7), 838–848. <https://doi.org/10.1111/j.1461-0248.2010.01476.x>
- Millán, M. M. (2014). Extreme hydrometeorological events and climate change predictions in Europe. *Journal of Hydrology*, *518*, 206–224. <https://doi.org/10.1016/j.jhydrol.2013.12.041>
- Miller, J. R., Steven, M. D., & Demetriades-Shah, T. H. (1992). Reflection of layered bean leaves over different soil backgrounds: Measured and simulated spectra. *International Journal of Remote Sensing*, *13*(17), 3273–3286. <https://doi.org/10.1080/01431169208904118>
- Minolta. (1989). Chlorophyll meter SPAD-502. Instruction manual.
- Munné-Bosch, S., & Alegre, L. (2000). Changes in carotenoids, tocopherols and diterpenes during drought and recovery, and the biological significance of chlorophyll loss in *Rosmarinus officinalis* plants. *Planta*, *210*(6), 925–931. <https://doi.org/10.1007/s004250050699>
- NCCS. (2018). CH2018 - Klimaszenarien für die Schweiz.
- Niinemets, Ü. (1997). Energy requirement for foliage construction depends on tree size in young *Picea abies* trees. *Trees*, *11*(7), 420–431. <https://doi.org/10.1007/PL00009684>
- Pardos, M., Del Río, M., Pretzsch, H., Jactel, H., Bielak, K., Bravo, F., Brazaitis, G., Defosse, E., Engel, M., Godvod, K., Jacobs, K., Jansone, L., Jansons, A., Morin, X., Nothdurft, A., Oreti, L., Ponette, Q., Pach, M., Riofrío, J., ... Calama, R. (2021). The greater resilience of mixed forests to drought mainly depends on their composition: Analysis along a climate gradient across Europe. *Forest Ecology and Management*, *481*, 118687. <https://doi.org/10.1016/j.foreco.2020.118687>
- Pedregosa, F., Varoquaux, G., Gramfort, A., Michel, V., Thirion, B., Grisel, O., Blondel, M., Prettenhofer, P., Weiss, R., Dubourg, V., Vanderplas, J., Passos, A., Cournapeau, D., Brucher, M., Perrot, M., Duchesnay, E., & Louppe, G. (2012). Scikit-learn: Machine Learning in Python. *Journal of Machine Learning Research*, *12*.
- Petibon, F., Czyż, E. A., Ghielmetti, G., Hueni, A., Kneubühler, M., Schaepman, M. E., & Schuman, M. C. (2021). Uncertainties in measurements of leaf optical properties are small compared to the biological variation within and between individuals of European beech. *Remote Sensing of Environment*, *264*, 112601. <https://doi.org/10.1016/j.rse.2021.112601>
- Petibon, F., & Wiesenberg, G. L. B. (2022). Characterization of complex photosynthetic pigment profiles in European deciduous tree leaves by sequential extraction and reversed-phase high-performance liquid chromatography. *Frontiers in Plant Science*, *13*, 957606. <https://doi.org/10.3389/fpls.2022.957606>
- Petrovic, S., Zvezdanović, J., Anelković, T., & Marković, D. (2012). The identification of chlorophyll and its derivatives in the pigment mixtures: HPLC-chromatography, visible and mass spectroscopy studies. *Savremene tehnologije*, *1*, 16–24.

- Peuke, A. D., Schraml, C., Hartung, W., & Rennenberg, H. (2002). Identification of drought-sensitive beech ecotypes by physiological parameters. *New Phytologist*, *154*(2), 373–387. <https://doi.org/10.1046/j.1469-8137.2002.00400.x>
- Pflug, E. E., Buchmann, N., Siegwolf, R. T. W., Schaub, M., Rigling, A., & Arend, M. (2018). Resilient Leaf Physiological Response of European Beech (*Fagus sylvatica* L.) to Summer Drought and Drought Release. *Frontiers in Plant Science*, *9*, 187. <https://doi.org/10.3389/fpls.2018.00187>
- Pluess, A. R., Frank, A., Heiri, C., Lalagüe, H., Vendramin, G. G., & Oddou-Muratorio, S. (2016). Genome–environment association study suggests local adaptation to climate at the regional scale in *Fagus sylvatica*. *New Phytologist*, *210*(2), 589–601. <https://doi.org/10.1111/nph.13809>
- Poorter, H., Niinemets, Ü., Poorter, L., Wright, I. J., & Villar, R. (2009). Causes and consequences of variation in leaf mass per area (LMA): A meta-analysis. *New Phytologist*, *182*(3), 565–588. <https://doi.org/10.1111/j.1469-8137.2009.02830.x>
- Poorter, H., & Villar, R. (1997). The fate of acquired carbon in plants: Chemical composition and construction costs. <https://api.semanticscholar.org/CorpusID:194329>
- Premachandra, G. S., SANEOKA, H., KANAYA, M., & OGATA, S. (1991). Cell Membrane Stability and Leaf Surface Wax Content as Affected by Increasing Water Deficits in Maize [Publisher: Oxford University Press]. *Journal of Experimental Botany*, *42*(235), 167–171. Retrieved January 19, 2024, from <http://www.jstor.org/stable/23693345>
- Quero, J. L., Villar, R., Marañón, T., & Zamora, R. (2006). Interactions of drought and shade effects on seedlings of four *Quercus* species: Physiological and structural leaf responses. *New Phytologist*, *170*(4), 819–834. <https://doi.org/10.1111/j.1469-8137.2006.01713.x>
- R Core Team. (2023). R: A Language and Environment for Statistical Computing. <https://www.R-project.org/>
- Ramírez-Valiente, J. A., Santos Del Blanco, L., Alía, R., Robledo-Arnuncio, J. J., & Climent, J. (2022). Adaptation of Mediterranean forest species to climate: Lessons from common garden experiments. *Journal of Ecology*, *110*(5), 1022–1042. <https://doi.org/10.1111/1365-2745.13730>
- Rapaport, T., Hochberg, U., Cochavi, A., Karnieli, A., & Rachmilevitch, S. (2017). The potential of the spectral ‘water balance index’ (WABI) for crop irrigation scheduling. *New Phytologist*, *216*(3), 741–757. <https://doi.org/10.1111/nph.14718>
- Rapaport, T., Hochberg, U., Shoshany, M., Karnieli, A., & Rachmilevitch, S. (2015). Combining leaf physiology, hyperspectral imaging and partial least squares-regression (PLS-R) for grapevine water status assessment. *ISPRS Journal of Photogrammetry and Remote Sensing*, *109*, 88–97. <https://doi.org/10.1016/j.isprsjprs.2015.09.003>
- Richardson, A. D., Duigan, S. P., & Berlyn, G. P. (2002). An evaluation of noninvasive methods to estimate foliar chlorophyll content. *New Phytologist*, *153*(1), 185–194. <https://doi.org/10.1046/j.0028-646X.2001.00289.x>

- Rigling, A., Etzold, S., Bebi, P., Brang, P., Ferretti, M., Forrester, D., Gärtner, H., Gessler, A., Ginzler, C., Moser, B., Schaub, M., Stroheker, S., Trotsiuk, V., Walthert, L., Zweifel, R., & Wohlgemuth, T. (2019). Wie viel Trockenheit ertragen unsere Wälder? Lehren aus extremen Trockenjahren. *Lernen aus Extremereignissen*, 39–51. <https://doi.org/10.55419/wsl:19983>
- Rodriguez-Dominguez, C. M., Forner, A., Martorell, S., Choat, B., Lopez, R., Peters, J. M. R., Pfautsch, S., Mayr, S., Carins-Murphy, M. R., McAdam, S. A. M., Richardson, F., Diaz-Espejo, A., Hernandez-Santana, V., Menezes-Silva, P. E., Torres-Ruiz, J. M., Batz, T. A., & Sack, L. (2022). Leaf water potential measurements using the pressure chamber: Synthetic testing of assumptions towards best practices for precision and accuracy. *Plant, Cell & Environment*, 45(7), 2037–2061. <https://doi.org/10.1111/pce.14330>
- Roman, D. T., Novick, K. A., Brzostek, E. R., Dragoni, D., Rahman, F., & Phillips, R. P. (2015). The role of isohydric and anisohydric species in determining ecosystem-scale response to severe drought. *Oecologia*, 179(3), 641–654. <https://doi.org/10.1007/s00442-015-3380-9>
- Rose, L., Leuschner, C., Köckemann, B., & Buschmann, H. (2009). Are marginal beech (*Fagus sylvatica* L.) provenances a source for drought tolerant ecotypes? *European Journal of Forest Research*, 128(4), 335–343. <https://doi.org/10.1007/s10342-009-0268-4>
- Rukh, S., Sanders, T. G. M., Krüger, I., Schad, T., & Bolte, A. (2023). Distinct Responses of European Beech (*Fagus sylvatica* L.) to Drought Intensity and Length—A Review of the Impacts of the 2003 and 2018–2019 Drought Events in Central Europe. *Forests*, 14(2), 248. <https://doi.org/10.3390/f14020248>
- Saathoff, A. J., & Welles, J. (2021). Gas exchange measurements in the unsteady state. *Plant, Cell & Environment*, 44(11), 3509–3523. <https://doi.org/10.1111/pce.14178>
- Sachse, D., Kahmen, A., & Gleixner, G. (2009). Significant seasonal variation in the hydrogen isotopic composition of leaf-wax lipids for two deciduous tree ecosystems (*Fagus sylvatica* and *Acerpseudoplatanus*). *Organic Geochemistry*, 40(6), 732–742. <https://doi.org/10.1016/j.orggeochem.2009.02.008>
- Sánchez-Gómez, D., Robson, T. M., Gascó, A., Gil-Pelegrín, E., & Aranda, I. (2013). Differences in the leaf functional traits of six beech (*Fagus sylvatica* L.) populations are reflected in their response to water limitation. *Environmental and Experimental Botany*, 87, 110–119. <https://doi.org/10.1016/j.envexpbot.2012.09.011>
- Sasagawa, T., Akitsu, T. K., Ide, R., Takagi, K., Takanashi, S., Nakaji, T., & Nasahara, K. N. (2022). Accuracy Assessment of Photochemical Reflectance Index (PRI) and Chlorophyll Carotenoid Index (CCI) Derived from GCOM-C/SGLI with In Situ Data. *Remote Sensing*, 14(21), 5352. <https://doi.org/10.3390/rs14215352>
- Schaepman-Strub, G., Schaepman, M., Painter, T., Dangel, S., & Martonchik, J. (2006). Reflectance quantities in optical remote sensing—definitions and case studies. *Remote Sensing of Environment*, 103(1), 27–42. <https://doi.org/10.1016/j.rse.2006.03.002>
- Schmeddes, J., Muffler, L., Barbeta, A., Beil, I., Bolte, A., Holm, S., Karitter, P., Klisz, M., Löff, M., Nicolas, M., Peñuelas, J., Vitasse, Y., Weigel, R., & Kreyling, J. (2023). High

- phenotypic variation found within the offspring of each mother tree in *Fagus sylvatica* regardless of the environment or source population. *Global Ecology and Biogeography*, geb.13794. <https://doi.org/10.1111/geb.13794>
- Schmied, G., Pretzsch, H., Ambs, D., Uhl, E., Schmucker, J., Fäth, J., Biber, P., Hoffmann, Y.-D., Šeho, M., Mellert, K. H., & Hilmers, T. (2023). Rapid beech decline under recurrent drought stress: Individual neighborhood structure and soil properties matter. *Forest Ecology and Management*, 545, 121305. <https://doi.org/10.1016/j.foreco.2023.121305>
- Schneider, C. A., Rasband, W. S., & Eliceiri, K. W. (2012). NIH Image to ImageJ: 25 years of image analysis. *Nature Methods*, 9(7), 671–675. <https://doi.org/10.1038/nmeth.2089>
- Scholander, P. F., Bradstreet, E. D., Hemmingsen, E. A., & Hammel, H. T. (1965). Sap Pressure in Vascular Plants: Negative hydrostatic pressure can be measured in plants. *Science*, 148(3668), 339–346. <https://doi.org/10.1126/science.148.3668.339>
- Schreel, J. D. M., Leroux, O., Goossens, W., Brodersen, C., Rubinstein, A., & Steppe, K. (2020). Identifying the pathways for foliar water uptake in beech (*Fagus sylvatica* L.): A major role for trichomes. *The Plant Journal*, 103(2), 769–780. <https://doi.org/10.1111/tpj.14770>
- Schwinning, S., Lortie, C. J., Esque, T. C., & DeFalco, L. A. (2022). What common-garden experiments tell us about climate responses in plants. *Journal of Ecology*, 110(5), 986–996. <https://doi.org/10.1111/1365-2745.13887>
- Serbin, S. P., Singh, A., McNeil, B. E., Kingdon, C. C., & Townsend, P. A. (2014). Spectroscopic determination of leaf morphological and biochemical traits for northern temperate and boreal tree species. *Ecological Applications*, 24(7), 1651–1669. <https://doi.org/10.1890/13-2110.1>
- Serrano, L., Peñuelas, J., & Ustin, S. L. (2002). Remote sensing of nitrogen and lignin in Mediterranean vegetation from AVIRIS data. *Remote Sensing of Environment*, 81(2-3), 355–364. [https://doi.org/10.1016/S0034-4257\(02\)00011-1](https://doi.org/10.1016/S0034-4257(02)00011-1)
- Shepherd, T., & Wynne Griffiths, D. (2006). The effects of stress on plant cuticular waxes. *New Phytologist*, 171(3), 469–499. <https://doi.org/10.1111/j.1469-8137.2006.01826.x>
- Shipley, B. (1995). Structured Interspecific Determinants of Specific Leaf Area in 34 Species of Herbaceous Angiosperms. *Functional Ecology*, 9(2), 312. <https://doi.org/10.2307/2390579>
- Siefert, A., Violle, C., Chalmandrier, L., Albert, C. H., Taudiere, A., Fajardo, A., Aarssen, L. W., Baraloto, C., Carlucci, M. B., Cianciaruso, M. V., De L. Dantas, V., De Bello, F., Duarte, L. D. S., Fonseca, C. R., Freschet, G. T., Gaucherand, S., Gross, N., Hikosaka, K., Jackson, B., ... Wardle, D. A. (2015). A global meta-analysis of the relative extent of intraspecific trait variation in plant communities (J. Chase, Ed.). *Ecology Letters*, 18(12), 1406–1419. <https://doi.org/10.1111/ele.12508>
- Sims, D. A., & Gamon, J. A. (2002). Relationships between leaf pigment content and spectral reflectance across a wide range of species, leaf structures and developmental stages.

- Remote Sensing of Environment*, 81(2-3), 337–354. [https://doi.org/10.1016/S0034-4257\(02\)00010-X](https://doi.org/10.1016/S0034-4257(02)00010-X)
- Spafford, L., Le Maire, G., MacDougall, A., De Boissieu, F., & Féret, J.-B. (2021). Spectral subdomains and prior estimation of leaf structure improves PROSPECT inversion on reflectance or transmittance alone. *Remote Sensing of Environment*, 252, 112176. <https://doi.org/10.1016/j.rse.2020.112176>
- Speckert, T. C., Petibon, F., & Wiesenberg, G. L. B. (2023). Late-season biosynthesis of leaf fatty acids and n-alkanes of a mature beech (*Fagus sylvatica*) tree traced via ^{13}C pulse-chase labelling and compound-specific isotope analysis. *Frontiers in Plant Science*, 13, 1029026. <https://doi.org/10.3389/fpls.2022.1029026>
- Steyn, W. J., Wand, S. J. E., Holcroft, D. M., & Jacobs, G. (2002). Anthocyanins in vegetative tissues: A proposed unified function in photoprotection. *New Phytologist*, 155(3), 349–361. <https://doi.org/10.1046/j.1469-8137.2002.00482.x>
- Stojnić, S., Orlović, S., Ballian, D., Ivankovic, M., Šijačić-Nikolić, M., Pilipović, A., Bogdan, S., Kvesić, S., Mataruga, M., Daničić, V., Cvjetković, B., Miljković, D., & Wuehlisch, G. V. (2015). Provenance by site interaction and stability analysis of European beech (*Fagus sylvatica* L.) provenances grown in common garden experiments. *Silvae Genetica*, 64(1-6), 133–147. <https://doi.org/10.1515/sg-2015-0013>
- Stokes, G. G. (1860). On the Intensity of the Light Reflected from or Transmitted through a Pile of Plates [Publisher: The Royal Society]. *Proceedings of the Royal Society of London*, 11, 545–556. Retrieved January 6, 2024, from <http://www.jstor.org/stable/111970>
- Sturm, J., Santos, M. J., Schmid, B., & Damm, A. (2022). Satellite data reveal differential responses of Swiss forests to unprecedented 2018 drought. *Global Change Biology*, 28(9), 2956–2978. <https://doi.org/10.1111/gcb.16136>
- Sun, H., Zheng, T., Liu, N., Cheng, M., Li, M., & Zhang, Q. (2018a). Vertical distribution of chlorophyll in potato plants based on hyperspectral imaging. *Nongye Gongcheng Xuebao/Transactions of the Chinese Society of Agricultural Engineering*, 34, 149–156. <https://doi.org/10.11975/j.issn.1002-6819.2018.01.020>
- Sun, J., Shi, S., Yang, J., Du, L., Gong, W., Chen, B., & Song, S. (2018b). Analyzing the performance of PROSPECT model inversion based on different spectral information for leaf biochemical properties retrieval. *ISPRS Journal of Photogrammetry and Remote Sensing*, 135, 74–83. <https://doi.org/10.1016/j.isprsjprs.2017.11.010>
- Sun, T., Rao, S., Zhou, X., & Li, L. (2022). Plant carotenoids: Recent advances and future perspectives. *Molecular Horticulture*, 2(1), 3. <https://doi.org/10.1186/s43897-022-00023-2>
- Tarantola, A. (2005). *Inverse problem theory and methods for model parameter estimation* [OCLC: ocm56672375]. Society for Industrial; Applied Mathematics.
- Tardieu, F., & Simonneau, T. (1998). Variability among species of stomatal control under fluctuating soil water status and evaporative demand: Modelling isohydric and anisohydric

- behaviours. *Journal of Experimental Botany*, 49(Special), 419–432. https://doi.org/10.1093/jxb/49.Special_Issue.419
- Thom, D., Buras, A., Heym, M., Klemmt, H.-J., & Wauer, A. (2023). Varying growth response of Central European tree species to the extraordinary drought period of 2018 – 2020. *Agricultural and Forest Meteorology*, 338, 109506. <https://doi.org/10.1016/j.agrformet.2023.109506>
- Tognetti, R., Johnson, J., & Michelozzi, M. (1995). The response of European beech (*Fagus sylvatica* L.) seedlings from two Italian populations to drought and recovery. *Trees*, 9(6). <https://doi.org/10.1007/BF00202499>
- Verrelst, J., Camps-Valls, G., Muñoz-Marí, J., Rivera, J. P., Veroustraete, F., Clevers, J. G., & Moreno, J. (2015). Optical remote sensing and the retrieval of terrestrial vegetation bio-geophysical properties – A review. *ISPRS Journal of Photogrammetry and Remote Sensing*, 108, 273–290. <https://doi.org/10.1016/j.isprsjprs.2015.05.005>
- Walter, J., Jentsch, A., Beierkuhnlein, C., & Kreyling, J. (2013). Ecological stress memory and cross stress tolerance in plants in the face of climate extremes. *Environmental and Experimental Botany*, 94, 3–8. <https://doi.org/10.1016/j.envexpbot.2012.02.009>
- Walthert, L., Ganthaler, A., Mayr, S., Saurer, M., Waldner, P., Walser, M., Zweifel, R., & Von Arx, G. (2021). From the comfort zone to crown dieback: Sequence of physiological stress thresholds in mature European beech trees across progressive drought. *Science of The Total Environment*, 753, 141792. <https://doi.org/10.1016/j.scitotenv.2020.141792>
- Wang, F., Israel, D., Ramírez-Valiente, J.-A., Sánchez-Gómez, D., Aranda, I., Aphalo, P. J., & Robson, T. M. (2021). Seedlings from marginal and core populations of European beech (*Fagus sylvatica* L.) respond differently to imposed drought and shade. *Trees*, 35(1), 53–67. <https://doi.org/10.1007/s00468-020-02011-9>
- Wankmüller, F. J. P., & Carminati, A. (2022). Stomatal regulation prevents plants from critical water potentials during drought: Result of a model linking soil–plant hydraulics to abscisic acid dynamics. *Ecohydrology*, 15(5), e2386. <https://doi.org/10.1002/eco.2386>
- Wellstein, C., Poschlod, P., Gohlke, A., Chelli, S., Campetella, G., Rosbakh, S., Canullo, R., Kreyling, J., Jentsch, A., & Beierkuhnlein, C. (2017). Effects of extreme drought on specific leaf area of grassland species: A meta-analysis of experimental studies in temperate and sub-Mediterranean systems. *Global Change Biology*, 23(6), 2473–2481. <https://doi.org/10.1111/gcb.13662>
- Whitman, D., & Ananthakrishnan, T. (Eds.). (2009, January). *Phenotypic Plasticity of Insects: Mechanisms and Consequences*. Science Publishers. <https://doi.org/10.1201/b10201>
- Wild, J., Kopecký, M., Macek, M., Šanda, M., Jankovec, J., & Haase, T. (2019). Climate at ecologically relevant scales: A new temperature and soil moisture logger for long-term microclimate measurement. *Agricultural and Forest Meteorology*, 268, 40–47. <https://doi.org/10.1016/j.agrformet.2018.12.018>
- Wilkens, J. F., & Wagner, S. (2021). Empirical survival model for European beech (*Fagus sylvatica* L.) seedlings in response to interactive resource gradients and (a-) biotic conditions

- within an experimental canopy gap study. *Forest Ecology and Management*, 499, 119627. <https://doi.org/10.1016/j.foreco.2021.119627>
- Winder, R., Nelson, E., & Beardmore, T. (2011). Ecological implications for assisted migration in Canadian forests. *The Forestry Chronicle*, 87(06), 731–744. <https://doi.org/10.5558/tfc2011-090>
- Wright, I. J., Reich, P. B., Westoby, M., Ackerly, D. D., Baruch, Z., Bongers, F., Cavender-Bares, J., Chapin, T., Cornelissen, J. H. C., Diemer, M., Flexas, J., Garnier, E., Groom, P. K., Gulias, J., Hikosaka, K., Lamont, B. B., Lee, T., Lee, W., Lusk, C., . . . Villar, R. (2004). The worldwide leaf economics spectrum. *Nature*, 428(6985), 821–827. <https://doi.org/10.1038/nature02403>
- Wu, X., Yuan, J., Luo, A., Chen, Y., & Fan, Y. (2016). Drought stress and re-watering increase secondary metabolites and enzyme activity in dendrobium moniliforme. *Industrial Crops and Products*, 94, 385–393. <https://doi.org/10.1016/j.indcrop.2016.08.041>
- Xu, H. (2006). Modification of normalised difference water index (NDWI) to enhance open water features in remotely sensed imagery. *International Journal of Remote Sensing*, 27(14), 3025–3033. <https://doi.org/10.1080/01431160600589179>
- Xu, H.-l., Gauthier, L., & Gosselin, A. (1995). Stomatal and Cuticular Transpiration of Greenhouse Tomato Plants in Response to High Solution Electrical Conductivity and Low Soil Water Content. *Journal of the American Society for Horticultural Science*, 120(3), 417–422. <https://doi.org/10.21273/JASHS.120.3.417>
- Zhang, F., & Zhou, G. (2019). Estimation of vegetation water content using hyperspectral vegetation indices: A comparison of crop water indicators in response to water stress treatments for summer maize. *BMC Ecology*, 19(1), 18. <https://doi.org/10.1186/s12898-019-0233-0>
- Zhao, F., Guo, Y., Huang, Y., Reddy, K. N., Lee, M. A., Fletcher, R. S., & Thomson, S. J. (2014). Early detection of crop injury from herbicide glyphosate by leaf biochemical parameter inversion. *International Journal of Applied Earth Observation and Geoinformation*, 31, 78–85. <https://doi.org/10.1016/j.jag.2014.03.010>
- Zhou, X., Huang, W., Kong, W., Ye, H., Dong, Y., & Casa, R. (2017). Assessment of leaf carotenoids content with a new carotenoid index: Development and validation on experimental and model data. *International Journal of Applied Earth Observation and Geoinformation*, 57, 24–35. <https://doi.org/10.1016/j.jag.2016.12.005>

Appendix A

Supplementary Materials

A.1 Common garden experiment block design

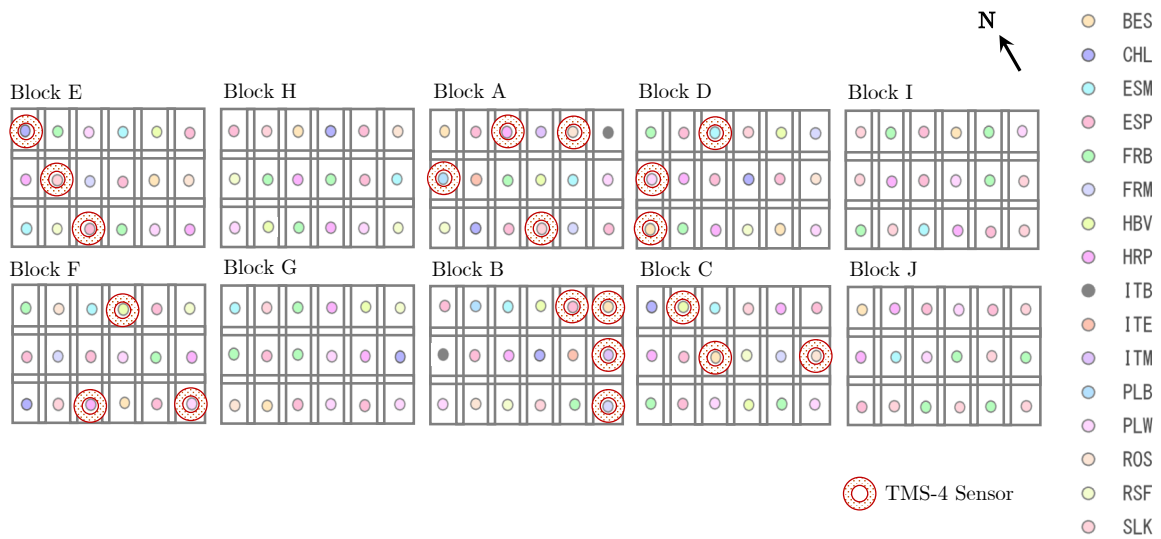


Figure A.1: Randomized representative block design with provenances for the common garden experiment and location of TMS-4 sensors. North arrow indicates north direction.

A.2 Instrument configurations

Table A.1: Instrument configurations for ASD FieldSpec 4 during spectra acquisition.

Type	Configuration	Type	Configuration
Foreoptic	Bare Fiber	Integration Time	8.5 ms
Spectrum	10	SWIR1 Gain	500
Dark Current	100	SWIR1 Offset	2048
White Reference	10	SWIR2 Gain	500
Scan Type	AB Even	SWIR2 Offset	2048

A.3 Drought simulation



Figure A.2: Photos of visual drought symptoms photographed during the first drought period. Such symptoms include wilting and bleaching of the leaves.



Figure A.3: Side view and bird's-eye view of the seedling with rain cover used to simulate the drought.

A.4 Wilting depending on length and provenance during the first drought period

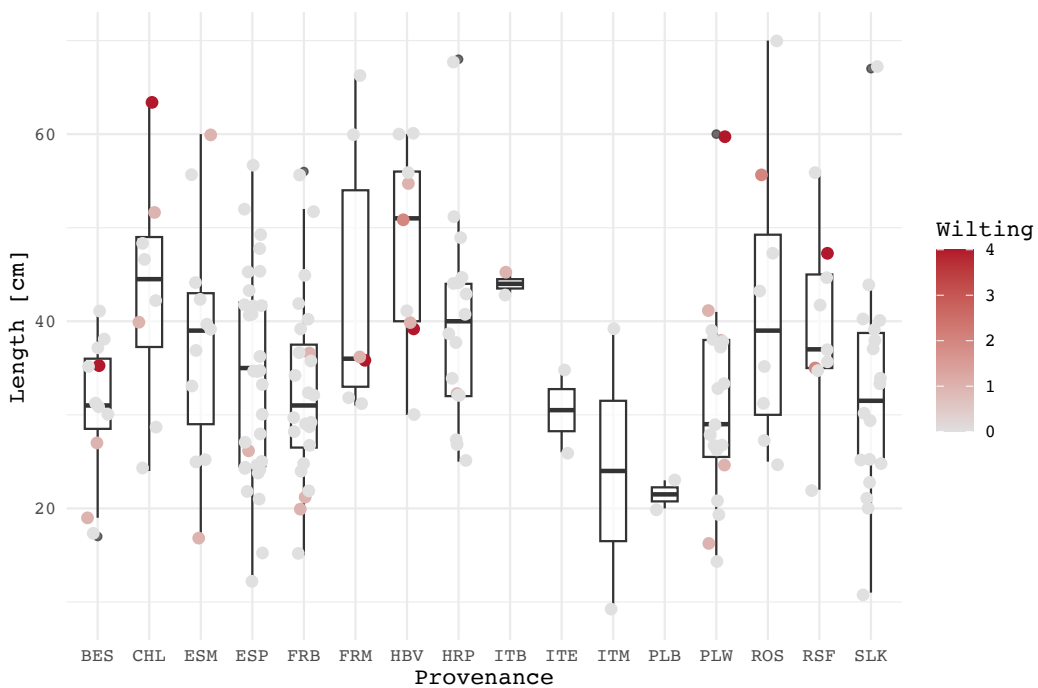


Figure A.4: The length distribution of the seedlings (n=180) depending on provenances. Scatter points display the length value coloured by their corresponding wilting index value. The wilting indices do not show a specific pattern across the provenances and across lengths.

A.5 Post hoc analysis

Table A.2: Post-hoc Tukey’s honest significance difference (HSD) test performed for C_{chl} (SPAD), NDLI and NDNI (spectral indices), and EWT (PROSPECT-D), which showed significant differences in their provenances based on ANOVA. Letters (a, ab, b) represent grouping of means and same letters are not significantly different from each other. Sample size is provided in brackets.

C_{chl} (SPAD)			NDLI			NDNI			EWT (PROSPECT-D)		
provenance	value	groups	provenance	value	groups	provenance	value	groups	provenance	value	group
ITE (2)	36.08	a	ITE (2)	0.032	a	ITE (2)	0.112	a	ITE (2)	0.0067	a
ROS (7)	30.88	ab	PLB (2)	0.031	ab	ITM (2)	0.109	a	PLB (2)	0.0065	a
ESP (31)	29.99	ab	ESM (10)	0.030	ab	PLB (2)	0.107	a	ITM (2)	0.0064	a
HRP (18)	29.75	ab	ITM (2)	0.030	ab	ESM (10)	0.107	a	HBV (6)	0.0064	a
SLK (18)	29.58	ab	HRP (18)	0.030	ab	FRB (24)	0.107	a	FRB (24)	0.0062	a
FRB (24)	29.44	ab	FRB (24)	0.030	ab	HBV (6)	0.104	ab	ESM (10)	0.0062	a
PLB (2)	29.38	ab	ESP (31)	0.030	ab	ESP (31)	0.104	ab	SLK (18)	0.0061	a
ITM (2)	29.15	ab	HBV (6)	0.029	ab	RSF (6)	0.104	ab	HRP (18)	0.0061	a
RSF (6)	28.90	ab	RSF (6)	0.029	ab	HRP (18)	0.103	ab	ESP (31)	0.0061	a
PLW (18)	28.20	ab	FRM (5)	0.029	ab	SLK (18)	0.103	ab	FRM (5)	0.0060	ab
HBV (6)	27.84	ab	ROS (7)	0.029	ab	FRM (5)	0.103	ab	RSF (6)	0.0060	ab
FRM (5)	27.67	ab	SLK (18)	0.029	ab	ROS (7)	0.101	ab	CHL (7)	0.0058	ab
CHL (7)	27.52	ab	CHL (7)	0.028	ab	CHL (7)	0.100	ab	ROS (7)	0.0058	ab
ESM (10)	27.23	b	PLW (18)	0.028	ab	BES (10)	0.099	ab	PLW (18)	0.0057	ab
BES (10)	26.79	b	BES (10)	0.028	ab	PLW (18)	0.099	ab	BES (10)	0.0057	ab
ITB (2)	24.50	b	ITB (2)	0.022	b	ITB (2)	0.080	ab	ITB (2)	0.0040	ab

A.6 Validation data from pigment extraction and HPLC

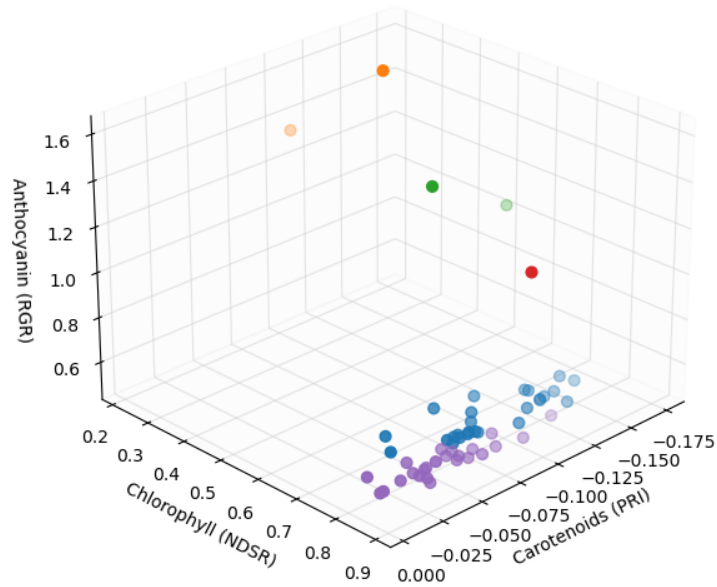


Figure A.5: 3D-cube plot depicting indices related to anthocyanin (RGR), chlorophyll (NDSR) and carotenoids (PRI), which were used for the selection of validation samples. Each color illustrates samples belonging to one of the five k-means clusters. The opaqueness of the data points display depth.



Figure A.6: Leaf area estimation in ImageJ using the point tool and a known distance scale.

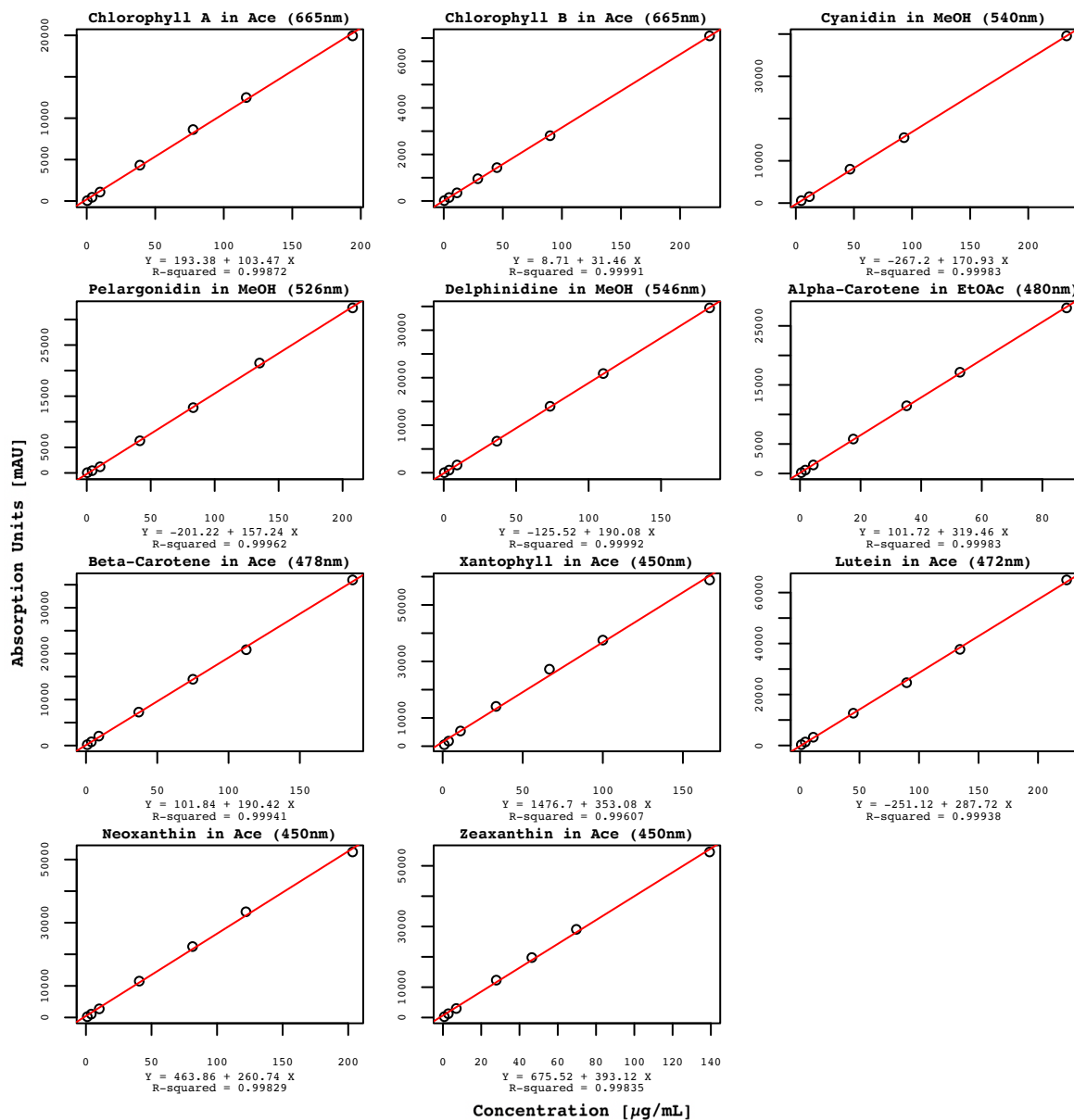


Figure A.7: Calibration curves from standards for the determination of pigment concentration including regression function and accuracy.

Table A.3: Method gradient for both eluents in the HPLC analysis.

Run time (min)	Eluent A (%)	Eluent B (%)
0	20	80
15	10	90
20	0	100
41	20	80
44	20	80

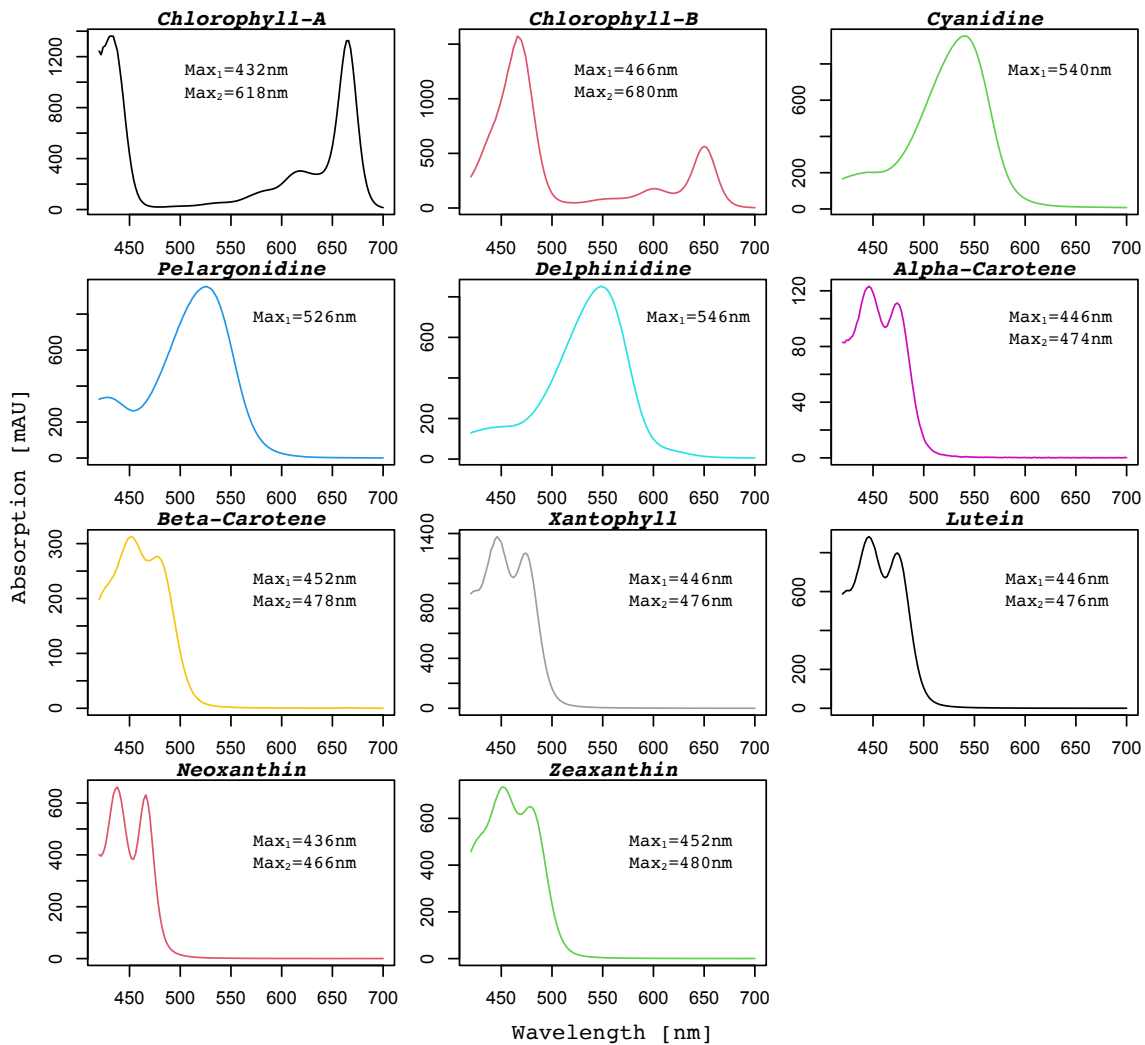


Figure A.8: Pigment standards spectra with absorption maxima used for the identification of pigments. Note that lutein and xantophyll are the same compound. Our xantophyll standard was extracted from marigold and lutein was synthesized.

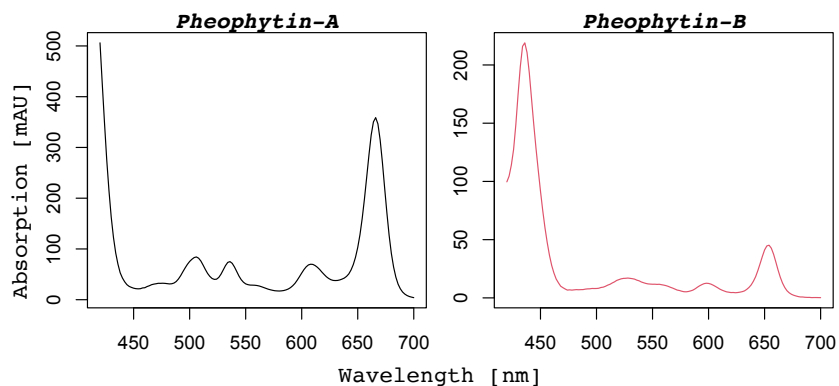


Figure A.9: Spectra of pheophytin a and b sampled from a chromatogram when identifying unknown pigments.

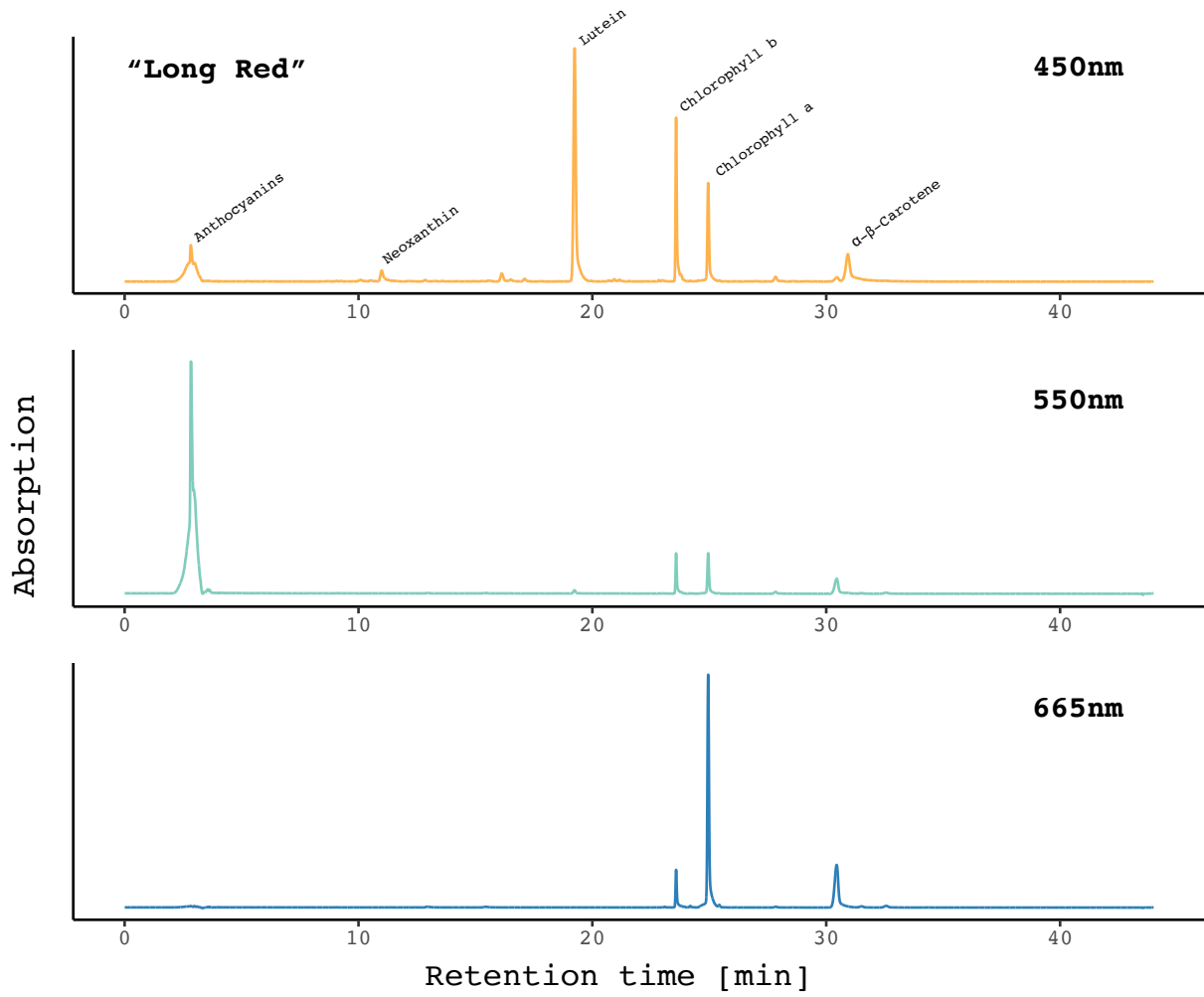


Figure A.10: Chromatogram of *Long red* special variety with corresponding wavelengths: 450 nm, 550 nm and 665 nm. *Long red* has seemingly high anthocyanin contents and are separable using the applied method.

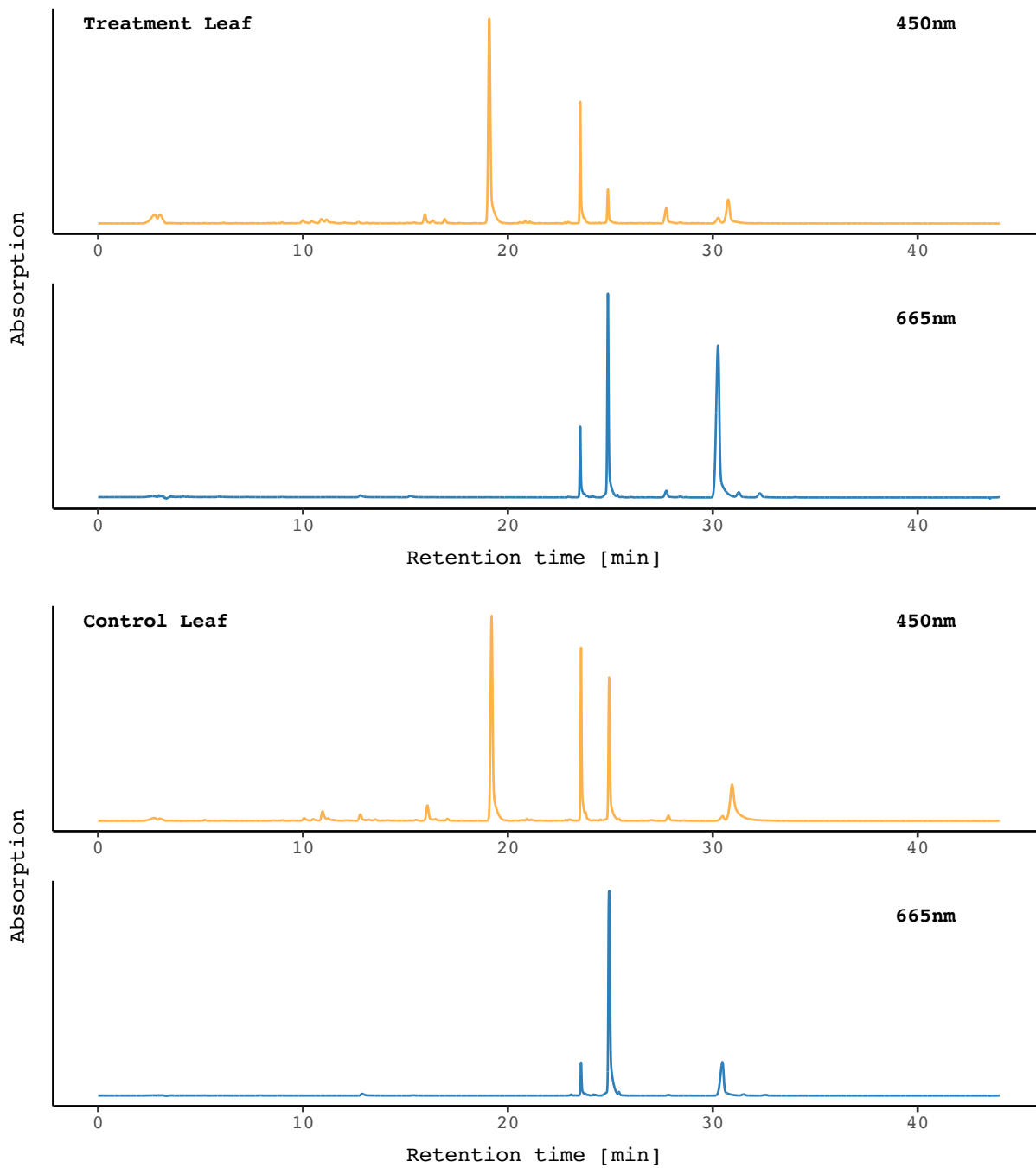


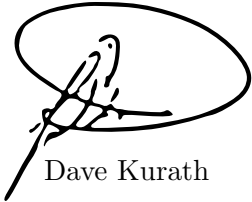
Figure A.11: Chromatogram of two leaf samples. Top: drought-treated leaf sample, bottom: control leaf sample. Y-axis depicts dimensionless absorption values and do not correspond to an absolute amount.

Table A.4: Retention times, estimated compound, and absorbance maxima of each peak, which were observed in a chromatogram of one sample. (*) indicates global absorption maximum.

peak #	retention time (min)	compound	absorption maxima (nm)
1	2.84	cyanidin	540*
2	2.98	pelargonidin	530*
3	3.05	unknown	-
4	3.70	unknown	-
5	4.41	unknown	-
6	5.21	chl dev	464*/650
7	6.12	car dev	442*/472
8	6.71	car dev	438*/470
9	8.29	car dev	426*/450
10	8.58	unknown	-
11	8.81	unknown	-
12	8.98	chl dev	436*/654
13	9.98	car dev	424*/451
14	10.43	car dev	424*/450
15	10.89	neo	439*/466
16	11.15	car dev	422*/450
17	12.04	car dev	446*/474
18	12.72	xan dev	437*/470/666
19	13.12	xan dev	423*/450/668
20	13.51	unknown	-
21	14.68	unknown	-
22	15.10	chl dev	450*/651
23	15.25	chl dev	424*/653
24	15.43	chl dev	450*/652
25	15.95	α -car dev	446*/473
26	16.34	car dev	430*/455
27	16.92	car dev	426*/456
28	17.65	unknown	-
29	19.10	lut/xan	448*/474
30	20.31	unknown	-
31	20.58	car dev	442*/466
32	20.69	car dev	446*/475
33	20.84	car dev	440*/467
34	20.96	car dev	443*/465
35	21.07	car dev	445*/475
36	21.49	unknown	-
37	22.56	unknown	-
38	22.79	chl dev	456*/635
39	22.95	chl dev	466*/649
40	23.53	chl b	466*/602/656
41	23.75	chl b	466*/602/656
42	24.04	chl dev	428*/656
43	24.13	chl dev	426*/655
44	24.29	chl dev	450*/666
45	24.46	unknown	-
46	24.88	chl a	432*/618/665
47	25.35	chl dev	435*/665
48	26.00	chl dev	436*/660
49	27.73	pheo b	436*/528/598/654
50	28.43	chl dev	436*/601/651
51	30.26	pheo a	505/535/608/666*
52	30.75	α - β -car	452*/475/666
53	31.27	pheo dev	475/538/610/668*
54	32.30	chl dev	424*/604/652

Personal declaration: I hereby declare that the submitted thesis is the result of my own, independent work. All external sources are explicitly acknowledged in the thesis.

Zurich, January 29, 2024

A handwritten signature in black ink, consisting of several loops and a long tail stroke, enclosed within a hand-drawn oval. The signature is positioned above the printed name "Dave Kurath".

Dave Kurath